AN ABSTRACT OF THE THESIS OF

Michael E. Zimmerman for the degree of Master of Science in Civil Engineering presented on July 28, 1983.

Title: Nonlinear Dynamic Response of Bottom-Laid Deep Ocean Pipelines

Abstract approved: Redacted for Privacy

A finite element formulation is developed for the prediction of the large displacement response of pipelines which are placed upon irregularly contoured marine sediments and are subsequently subjected to episodic hydrodynamic loads. The equations of motion during each episode of extreme wave activity are obtained from a variational form of Hamiltons principle and this form of the equations of motion is integrated using the Newmark method of implicit integration. Within each time step a Newton-Raphson iteration scheme is used to achieve equilibrium while accurately tracking the nonlinear path-dependent response. An updated Lagrangian formulation shifts the pipeline reference configuration and separates rigid body movements from pipeline deformations. This provides a large deflection, small strain transient analysis of the pipeline response.

Nonlinear, elastic-plastic springs simulate transverse and axial bottom resistance from both cohesive and cohesionless sediments. Inclusion of a pressure differential across the pipe wall modifies

tensile stresses and influences the flexural stiffness of the finite element model through the geometric stiffness matrix. Hydrodynamic added mass and nonlinear, viscous drag forces are included by means of the relative-motion form of the Morison equation. The formulation results in a three-dimensional finite element model of a bottom-laid pipeline that is constrained to follow the irregularly contoured ocean bottom.

A finite element method computer model is developed and used to predict the pipeline response to both monochromatic and random wave loads. Numerical examples presented demonstrate the validity of the formulation and illustrate the results obtained from sample simulations. It is found that nonlinear structural behavior is a dominant factor in predicting pipeline response and that inclusion of nonlinear effects greatly reduces predicted pipeline displacements. It is further shown that both the directionality of wave attack and the wave length of incident waves significantly alters the magnitude and location of the maximum pipeline response. Computational times for the random wave simulations analyzed were substantial with an approximate ratio of CPU to real time ratio of 105 to 1 being typical for the finite element analysis of a prototype marine pipeline having 150 degrees of freedom.

Nonlinear Dynamic Response of Bottom-Land Deep Ocean Pipelines

by

Michael E. Zimmerman

A THESIS

submitted to

Oregon State University

in partial fulfillment of
the requirements for the
degree of

Master of Science

Completed July 28, 1983

Commencement June 1984

APPROVED:

Redacted for Privacy

Professor of Civil Engineering in charge of major

Redacted for Privacy

Head of department of Civil Engineering

Redacted for Privacy

Dean of Graduate School

Date thesis is presented July 28, 1983

Typed by Julie Womack and Nancy Platz for Michael E. Zimmerman

TABLE OF CONTENTS

LIST OF FIGURES

LIST OF FIGURES (continued)

LIST OF FIGURES (continued)

LIST OF TABLES

LIST OF SYMBOLS

a = contact area per unit length of pipe between pipeline and supporting sediment;

A = load bearing cross-sectional area of steel section;

b = width of sediment bearing below the pipe cross-section;

c = average sediment cohesion;

C_D, C_L, C_M = drag, lift and inertial coefficients, respectively;

$\mathbf{d_i}$ = the **local** generalized coordinates for an individual element;

$\{\mathbf{d}\}$ = the vector of **local** generalized coordinates for an individual element (12 x 1);

$\overline{\mathbf{d}}_i$ = the **local** generalized deformations for an individual element;

$\{\overline{\mathbf{d}}\}$ = the vector of **local** generalized deformations for an individual element (12 x 1);

D = total pipe section diameter;

$\mathbf{D_i}$ = the **global** generalized coordinates for an individual element;

$\{\mathbf{D}\}$ = the vector of **global** generalized coordinates for an individual element (12 x 1);

E = Youngs modulus of load bearing, steel section;

E_f = foundation modulus (load per unit length per unit deflection);

ETOL = energy tolerance for convergence;

f_d = maximum sediment bearing stress below pipe;

f_o = spectral peak wave frequency (hertz);

f_1 = first node vibration frequency (hertz);

$\{\mathbf{f}\}$ = vector of **local** internal **element** forces;

$\mathbf{F}$ = vector of **global** internal **pipeline** forces;

F_η, F_β = continuous fluid force per length of pipeline in the intrinsic eta (η) and beta (β) directions;

$F_{s\tau}$, $F_{s\eta}$ = continuous sediment force per length of pipeline in the intrinsic tau (τ) and eta (η) directions;

$\mathbf{F}_\tau$, $\mathbf{F}_\eta$, $\mathbf{F}_\beta$ = **local** generalized force components in τ, η, β directions;

$\mathbf{F}_X, \mathbf{F}_Y, \mathbf{F}_Z$ = **global** generalized components in X, Y, Z directions;

g = gravitational acceleration;

G = shear modulus;

h = water depth;

$\{\mathbf{h}\} = 0$ = vector equilibrium function;

H = wave height;

I = moment of inertial of the load bearing, steel pipe section;

J = torsional inertia of the load bearing, steel pipe section;

$\mathbf{k}_{ij}$ = component of the **local element** stiffness matrix (i = row, j = column);

$[\mathbf{k}]$ = **local element** stiffness matrix which includes both elastic and geometric stiffness (12 x 12);

$[\mathbf{k}_E]$ = elastic **local element** stiffness matrix (12 x 12);

$[\mathbf{k}_G]$ = geometric **local element** stiffness matrix (12 x 12);

$[\hat{\mathbf{k}}]$ = **nodal element** stiffness matrix (6 x 6);

$[\hat{\mathbf{K}}]$ = **nodal pipeline** stiffness matrix;

ℓ = span length;

ℓ_i = direction cosines between **global** X and **local** axes (i = 1, τ, i=2, η, i=3, β);

ℓ_{iI}, ℓ_{iJ} = direction cosines between **global** X and the i or j **nodal** axes of an element;

L, L_o, L_1 = current, reference and first finite element length, respectively;

m = pipeline mass per unit length;

m_i = direction cosines between **global** Y and **local** axes (i = 1, τ, i=2, η, i=3, β);

$[\mathbf{m}]$ = **local element** mass matrix (12 x 12);

$[\hat{\mathbf{m}}]$ = **nodal element** mass matrix (6 x 6);

m_{iI}, m_{iJ} = direction cosines between **global** Y and i or j **nodal** axes of an element;

n_i = direction cosines between **global** Z and **local** axes (i = 1, τ, i=2, η, i=3, β);

n_{iI}, n_{iJ} = direction cosines between **global** Z and the i or j **nodal** axes of an element;

N_c = bearing capacity factor;

N_σ = stress coefficient in cohesive sediment;

N_w = water surface profile;

$\{\mathbf{N}\}$ = vector of element shape functions;

p = axial force;

P = applied load (section 3.2);

PR = internal pipeline pressure;

q_d = bearing capacity of a cohesive sediment;

$\{\hat{q}\}$ = **nodal element** load vector;

$\{\hat{Q}\}$ = **nodal pipeline** load vector;

r_i = component of the continuous environmental loading per length of pipeline (i=1, axial; i=2, lateral; i=3, binormal; and i=4, torsional);

$\mathbf{r_i}$ = generalized components of the **local element** load vector;

$\{r\}$ = **local element** load vector (12 x 1);

$\mathbf{R}$ = vector of **global pipeline** forces;

RTOL = force tolerance for convergence;

s = depth of pipeline settlement;

S_A = sediment spring constant for axial resistance;

S_L = sediment spring constant for lateral resistance;

SC_i = sediment resistance capacity per unit length of pipeline (i=1, axial; i=2, lateral);

$S(\omega,\Theta)$ = directional wave spectrum;

t = time;

t_0 = initial time;

t_1 = arbitrary final time;

$[\mathbf{t_i}]$ = **nodal** tangent stiffness contribution of an **element**;

T = total kinetic energy due to conservative forces;

$[\mathbf{T_l}]$ = transformation matrix for an element between **global** and **local** coordinate systems (12 x 12);

Nonlinear Dynamic Response of Bottom-Laid Deep Ocean Pipelines

1.0 Introduction

1.1 Motivation

Traditional design practices for offshore pipelines attempt to ensure stability along the entire pipeline system. In shallow water, the standard practice requires the burial of pipeline systems resulting in increased construction costs from trenching operations. Uncertainties regarding the effectiveness of trenching operations, coupled with a desire to minimize construction costs, has generated an increased interest in analyzing the dynamic response of bottom supported pipeline systems in deeper water.

The design forces used to evaluate the stability of bottom supported pipelines include: hydrodynamic fluid pressures, resistive sediment forces, and the resistive stiffness of the pipeline. An analysis based on these criteria often results in a pipeline design which requires a weight coating to develop additional resistive forces necessary to maintain stability. However, even pipelines designed in this manner will experience significant motion when subjected to extreme wave events. The forces which determine the dynamic response of the pipeline during this extreme wave events are: 1) the hydroelastic fluid forces, 2) the resistive soil forces, and 3) the inertial and resistive forces of the pipeline.

Designing pipeline systems which are capable of responding dynamically during extreme wave loading provides an effective means for reducing both the deployment and material costs of deep ocean pipelines. The analysis described herein evaluates the nonlinear

dynamic response of marine pipeline systems in order to provide definitive design guidelines with respect to weight coatings and other statistical design parameters.

1.2 Previous Research

Increased usage of the ocean resources for commercial and military applications has promoted a great deal of interest in marine pipeline systems. Large scale environmental hazards which present a potential threat to ocean pipelines include seabed instabilities induced by soil liquification or sesmic activity [Demars, et al (1977) and Machemehl (1978)] and hydrodynamic fluid loadings induced by waves and currents. In addition to these large scale phenomenon, sections of pipeline may be exposed to localized stress concentrations that may result from scour-induced spanning [Ells (1975)].

A preliminary route selection process serves as a practical means of avoiding potential pipeline failures due to seabed instabilities. Sediment loading models which aide design engineers in unstable regions where facilities mandate the use of marine pipelines have been proposed by Audibert, et al (1978) and Swanson and Jones (1982). These models provide a static analysis procedure for pipelines subjected to sediment flows.

The traditional design standard for pipelines subjected to hydrodynamic loading requires that the pipeline remain stable when subjected to a specified design wave. This type of static design typically involves balancing the resistive sediment forces and the maximum hydrodynamic forces. Early sediment resistance models for

bottom supported pipelines used a Coulomb friction model with estimated friction coefficients [Potynody (1961)]. More recent work [Lyons (1973) and Anard and Agarwal (1980)] supports the use of this type of sediment model for **cohesionless** sediments; however, other investigators such as Karal (1977) suggest that a Coulomb friction model is inappropriate for describing **cohesive** sediment resistance. Karal (1977) and Wantland et al. (1982) proposed sediment resistance models for cohesive materials that were based on a limit analysis of the plastic failure mechanism occurring during the rheological phenomenon. For long period loadings such as tidal currents, Karal (1983) further suggests that cohesive sediment resistance should be described as a function of loading rate to reflect the effects of pore water dissipation.

Computation of the hydrodynamic pressures which load the pipeline during the design wave is typically performed using the Morison equation. Investigative efforts by Brown (1967), Sarpkaya (1975), Yamamoto et al (1973) and others have served to quantify the force coefficients used in the Morison equation and has aided in the prediction of the fluid forces which cause pipeline instabilities. In regions where high fluid pressures threaten pipeline stability, design options include attachment of additional weight coating, placement of anchor blocks along the pipeline route, and burial of the pipeline in sub-sea trenches. General procedures for evaluating the stability of ocean pipeline systems in shallow water have been presented by Huang and Hudspeth (1982) and Jones (1976).

Recent investigations by Lambrokos (1982) and Karal and Halvorsen (1982) suggest that the no-motion design criteria for deep-ocean pipelines subjected to fluid loadings may be relaxed in order to allow pipeline motions to occur during these extreme wave episodes that have long return periods. These investigators examined the nonlinear, fluid-soil-pipe interaction problem using finite difference algorithms. These algorithms employed nonlinear sediment models and computed the time domain response of the pipeline to a hydroelastic fluid loading. Lambrokos (1982) and Karal and Halvorsen (1982) examined stochastic and monochromatic fluid loadings, respectively. The conclusions from both of these investigations indicate that displacements and dynamic stresses which resulted from peak wave loadings remained within acceptable design tolerances.

There is currently available not any published literature that provide either laboratory or prototype data for the dynamic response of a bottom-supported pipeline. The Morison force coefficients and the resistive sediment parameters used in these state-of-the-art dynamic analyses have been adopted from commonly accepted values that are used in static-equivalent pipeline stability analyses.

1.3 **Objectives**

Present design methodologies for marine pipeline systems generally require only a static-equivalent stability analysis using hydrodynamic pipe loadings computed from a design wave. Pipelines which are subsequently exposed to an extreme wave event that

that exceeds the design wave load may then be subjected to dynamic stresses and motions which could endanger the pipe system or surrounding sub-sea facilities. Numerical computations for the linear pipeline responses during peak wave loadings have been performed [Lambrakos (1982) and Karal and Halvorsen (1982)] using finite difference techniques. These linear responses to nonlinear loads provide useful information regarding pipeline behavior during episodes of dynamic pipeline response; however, further evaluation of the nonlinear behavior in a directional, random wave environment seems warranted.

The purpose of this analysis is to develop a finite element method (FEM) formulation which can be utilized for a detailed study of the evolution of pipeline configurations under random wave attack from directional seas. The primary features of the FEM algorithm developed include: 1) the ability to predict the large deflection response of the pipeline; 2) the ability to model nonlinear hydroelastic fluid forces; 3) the ability to independently model cohesive and cohesionless sediment loads; and 4) the ability to adopt irregular bottom contours. Additional features provided by the finite element method include: 1) flexibility in discretizing the pipeline system; and 2) the ability to model features such as a missing weight coating along any arbitrary portion of the pipeline.

1.4 **Scope of Study**

The formulation presented is directed toward predicting the dynamic stresses and displacements which develop in a pipeline

subjected to a peak wave episode. This analyses is concerned primarily with the environmental loadings and the dynamic responses of the pipeline system. The solution algorithm has been constructed in a format which allows the specification of stochastic sediment characteristics and wave kinematics that are required to define the environment surrounding the pipeline system.

In Chapter 2 the finite element formulation is developed from the governing differential equations for a beam-column using well-known variational techniques. Extension of the finite element formulation to large deflection analysis is achieved through the adoption of a convected coordinate system. Chapter 2 also provides a description of the environmental loadings to which the pipeline is subjected. Numerical approximations for these environmental loadings are used in conjunction with the finite element algorithm. Numerical examples which illustrate test problems and the computed pipeline behavior during peak wave episodes are presented in Chapter 3. Chapter 4 provides a summary of the analyses, as well as conclusions and an evaluation of the limitations of the methodology.

A flow diagram for the computer algorithm that was used to compute the example responses given in Chapter 3 is illustrated at the conclusion of Chapter 2. Documentation for this algorithm is given in **AppendiX A.** Because of the large amount of CPU required to compute the nonlinear dynamic response by FEM, the algorithm is presently limited to large modern main frame computer facilities.

2.0 Formulation Of Problem

2.1 Methodology

In this chapter, the governing differential equations for a continuous pipeline system subjected to nonlinear environmental loads are presented. These equations predict, for small deflections, the biaxial bending, the axial displacements, and the twisting motions of the pipeline. The nonlinear environmental loads to which the pipeline is subjected include hydrodynamic viscous drag and a materially nonlinear sediment stiffness. Application of the governing equations to finite deflection analysis is made possible by adopting a convective coordinate system which tracks with the pipeline motions.

The governing dimensional equations of motion are nondimensionalized in order to avoid numerical instabilities. Variational techniques are applied to the nondimensional equations of motion in order to establish a general energy principle which can be applied to the pipeline system. A finite element method (FEM) formulation of the problem is employed that permits the continuous pipeline system to be discretized for numerical computations. An incremental iterative solution technique (Newton-Raphson) is introduced in order to accomodate the nonlinear terms in the equations.

Development of the FEM formulation begins with the evaluation of the response of a single element to an arbitrary static loading. The tangent stiffness of an element, that includes a preexisting axial force, is derived using an energy principle. This stiffness, coupled with a convective coordinate system and an

incremental iterative solution technique, extends analysis capability to static large deflections. Introduction of inertial effects and a time integration scheme allows finite deflection dynamic analysis for arbitrary dynamic loadings.

The restriction of the pipeline response to certain modes (viz., sliding of the pipeline along the seafloor) imposes constraints on pipeline movements. Coordinate system transformations are introduced in order to couple the element responses that have been restricted to sliding only along the ocean floor. Optional end restraints are introduced to provide greater flexibility in describing boundary conditions at the pipeline terminations.

Environmental load descriptions are developed by replacing the arbitrary loadings on an element with approximate representations of applied environmental forces. Fluid loads on each element are computed from both hydrostatic and hydrodynamic pressures. The hydrodynamic pressures are represented by a relative-motion form of the Morison equation. Within the incremental iterative procedure, a first-order Taylor series expansion of the hydrodynamic loading couples the dynamic fluid forces to the pipeline responses. Sediment loads on the pipeline elements are defined by linearly-elastic, perfectly-plastic springs. The **lateral** and **axial** characteristics of these sediment springs are determined independently for **cohesive** and for **cohesionless** soils by evaluating the sediment resistance capacities.

Coupling the individual element responses will simulate the response of the entire continuous pipeline system. An algorithm is

introduced in which individual elements are combined to model the pipeline; and the Newton-Raphson iteration technique is employed within a discrete time step to determine the pipeline configuration and stresses required to place the system in dynamic equilibrium. A Newmark-beta numerical integration scheme is then used to proceed through those sequential time steps which constitute an environmental episode.

2.2 Equations of Motion

The equations of motion apply to the continuous pipeline depicted in Fig. 2.1. that also specifies both the global (X,Y,Z) and local (τ,η,β) coordinate systems. The local tangential direction (τ), as shown in Fig. 2.1, coincides with the longitudinal axis of the pipe, and the binormal direction (β) is locally perpendicular to the ocean floor. The normal direction (η) is orthogonal to both the tangential and binormal axes.

2.2.1 Partial Differential Equations Controlling Pipeline Response

The partial differential equations for the small deflection response of a pipeline [Clough and Penzien (1975), pp. 297-306 and Chajes (1974), pp. 196-201] are as follows:

$$\frac{\partial^2}{\partial x^{*2}}\left(E^*I^*\frac{\partial^2 u_i^*}{\partial x^{*2}}\right) + p^*\frac{\partial^2 u_i^*}{\partial x^{*2}} + m^*\frac{\partial^2 u_i^*}{\partial t^{*2}} = r_i^*(x^*, t^*, u_2^*);\ i = 2, 3 \qquad (2.2\text{-}1a)$$

$$m^*\frac{\partial^2 u_i^*}{\partial t^{*2}} - \frac{\partial}{\partial x^*}\left(E^*A^*\frac{\partial u_i^*}{\partial x^*}\right) = r_i^*(x^*, t^*, u_i^*);\ i = 1 \qquad (2.2\text{-}1b)$$

Figure 2.1 Definition sketch of global (X,Y,Z) and local (τ,η,β) coordinate axes.

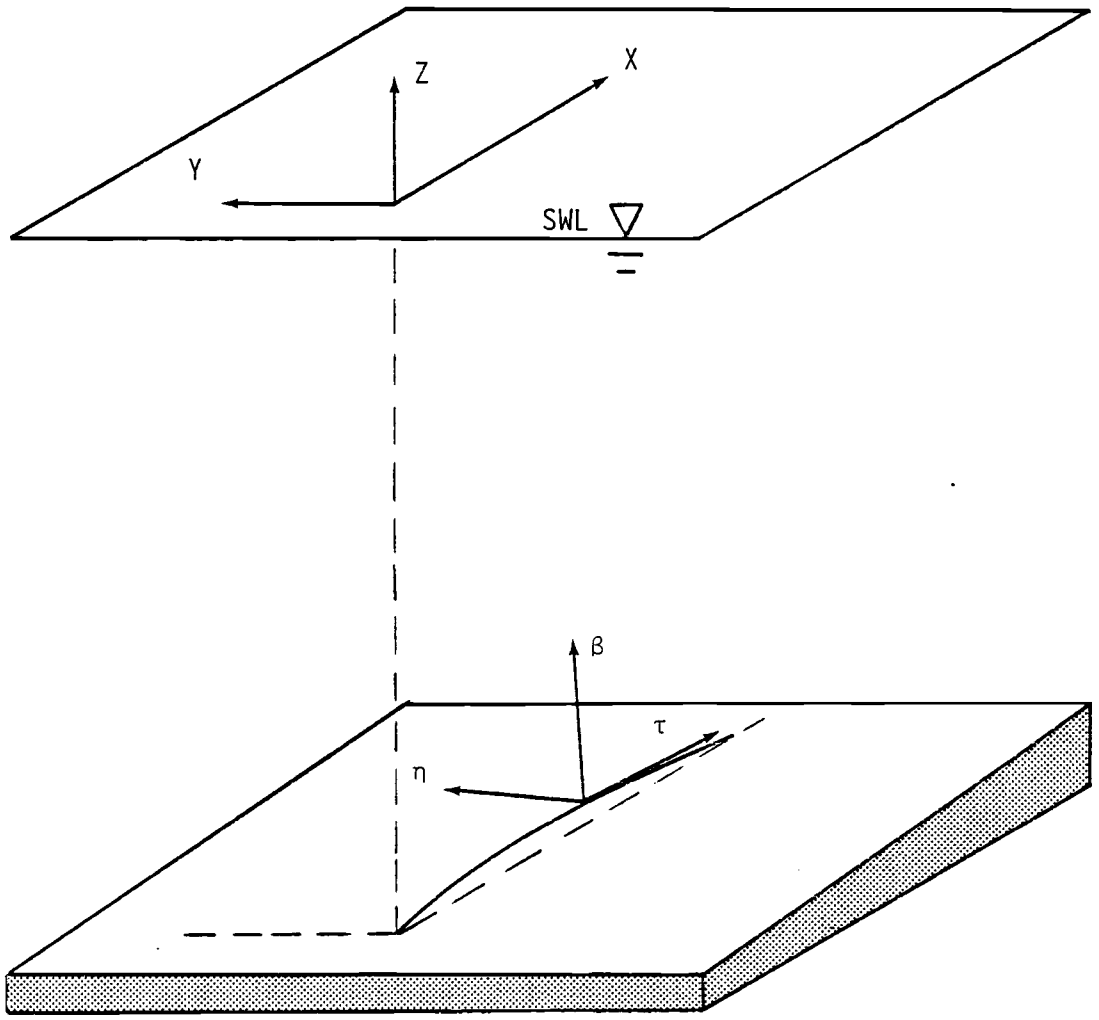

and

$$G^* J^* \frac{\partial^2 u_i^*}{\partial x^{*2}} = r_i^*; \; i = 4 \qquad (2.2\text{-}1c)$$

in which m^* = mass per unit length; x^* = position along the pipe segment; t^* = time; E^* = elastic modulus; I^* = cross-sectional moment of inertia; A^* = cross-sectional area; G^* = shear modulus; J^* = torsional inertia; p^* = axial tensile load; u_i^* = i^{th} component of displacement, where u_i^* is defined in Fig. 2.2; and r_i^* = i^{th} component of applied load per unit length. Equations (2.2-1) describe biaxial bending, axial deformation, and torsional response, repectively.

The effect of structural damping, shear deformation, and rotational inertia are neglected in Eqs. (2.2-1). Simplification of the general load representations and the imposition of constraints on the pipeline motions that will be introduced later will eliminate Eq. (2.2-1c). However, torsional rigidity will be retained at this time in order to obtain a fully three-dimensional formulation for the pipeline response.

The equations for flexural and axial reponses will be shown to be nonlinear (even for small deflections) because the applied environmental loads are nonlinear functions of either the pipeline displacement or its derivatives. Extending Eqs. (2.2-1) to include finite deflections introduces geometric nonlinearities which may be treated by adopting a convected coordinate system.

Figure 2.2 Applied pipeline loadings and displacement fields.

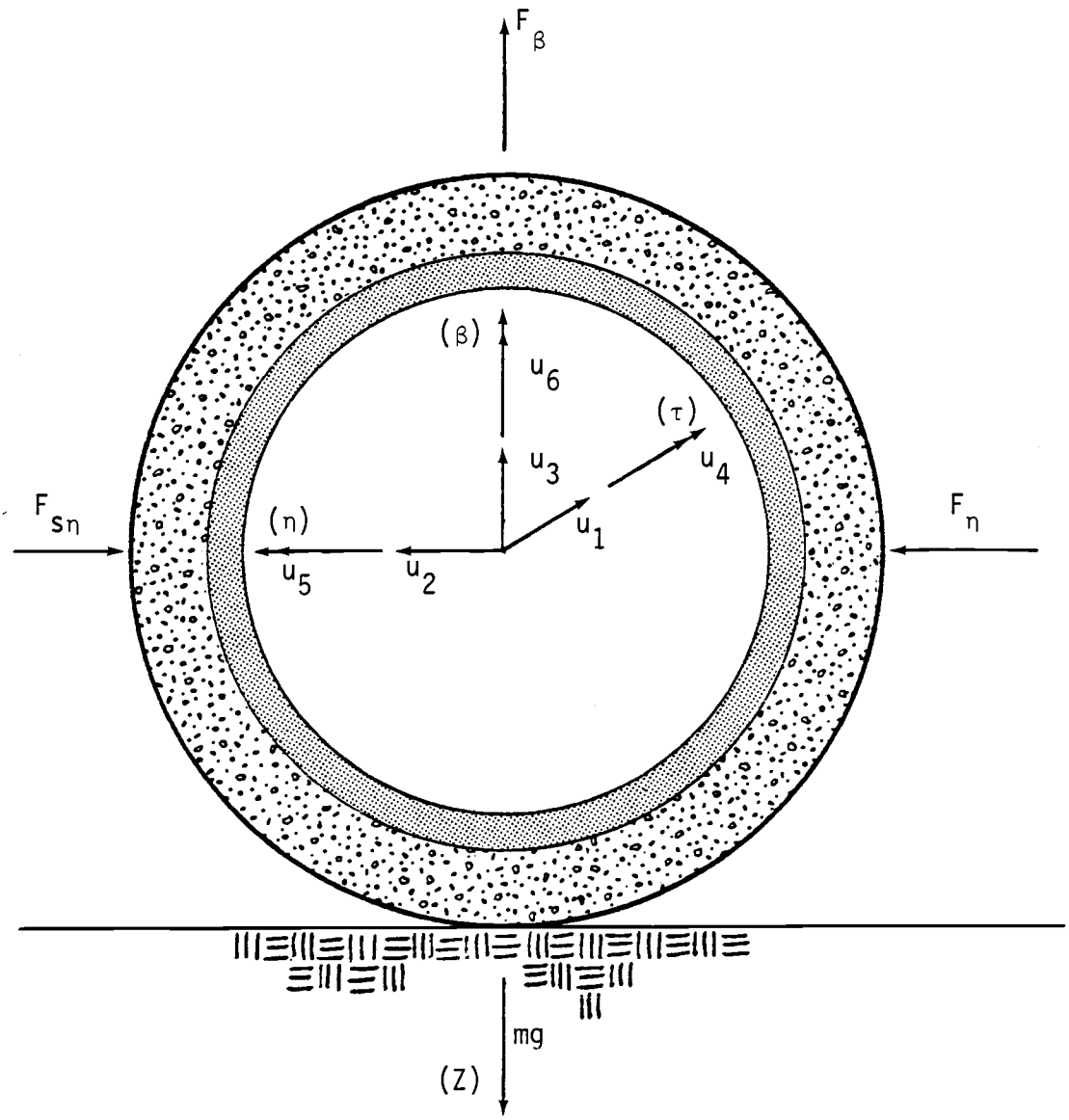

2.2.2 Nondimensionalization of Controlling Equations

Numerical techniques to be employed in the solution of Eqs. (2.2-1) require manipulations and decompositions of the systems of equations. To assure numerical accuracy in the solution algorithms, the controlling equations are nondimensionalized. The nondimensionalizing parameters chosen are the following: the peak spectral wave frequency, f_o; the mass density of the fluid medium, ρ_o; and length of the first pipeline element used in the finite element discretization, L_1. Typical relationships between dimensional (denoted by superscript asterisks *) and nondimensional quantities (denoted without superscripts) are represented by the following expressions:

$$(X,Y,Z,u_i) = \left(X^*,Y^*,Z^*,u_i^*\right)\frac{1}{L_1} \; ; \; i = i = 1,2,3 \tag{2.2-2a}$$

$$(t,\Delta t) = \left(t^*,\Delta t^*\right)f_o \tag{2.2-2b}$$

$$(m) = \left(m^*\right)\frac{1}{\rho_o L_1^2} \tag{2.2-2c}$$

$$(r_i) = \left(r_i^*\right)\frac{1}{\rho_o L_1^3 f_o^2} \; ; \; i = 1,2,3 \tag{2.2-3d}$$

$$(r_i) = \left(r_i^*\right)\frac{1}{\rho_o L_1^4 f_o^2} \; ; \; i = 4 \tag{2.2-2e}$$

Replacing dimensional terms in Eqs. (2.2-1) with dimensionless terms from Eqs. (2.2-2) and eliminating common terms yields

$$\frac{\partial^2}{\partial x^2}\left(EI\frac{\partial^2 u_i}{\partial x^2}\right) + p\frac{\partial^2 u_i}{\partial x^2} + m\frac{\partial^2 u_i}{\partial t^2} = r_i(x,t,u_2);\ i = 2,3 \qquad (2.2\text{-}3a)$$

$$m\frac{\partial^2 u_i}{\partial t^2} - \frac{\partial}{\partial x}\left(EA\frac{\partial u_i}{\partial x}\right) = r_i(x,t,u_i)\ ;\ i = 1 \qquad (2.2\text{-}3b)$$

and

$$GJ\frac{\partial^2 u_i}{\partial x^2} = r_i;\ i = 4\ . \qquad (2.2\text{-}3c)$$

The common types of boundary conditions specified for these equations in practical ocean pipeline applications are the following:

$u = u' = 0$; fixed end (no displacement, no rotation)

$u = u'' = 0$; simply supported end (no displacement, no moment)

$u'' = u''' = 0$; free end (no moment, no shear)

in which the superscript prime (') denotes differentiation with respect to the longitudinal (axial) coordinate. These conditions are called **prescribed** boundary conditions if they specify displacements or rotations, or **natural** boundary conditions if they specify forces or moments.

2.3 Energy Concepts

The controlling equations presented in Section (2.2) pertain to a continuous system. An analytical solution of these equations is generally not possible when complicated environmental loadings or pipeline geometries are encountered. It is, therefore, necessary to evaluate the response of the pipeline numerically. The numerical techniques which will be employed to calculate the pipe-

line response will be introduced in the following sections of this chapter.

2.3.1 **Variational Principle**

The equilibrium Eqs. (2.2-3) have been shown to be equivalent to satisfying Hamilton's minimization principle [Hildebrand (1965)]. This minimization principle may be illustrated by Eq. (2.2-3a) for i = 2; i.e. for the flexural response of the pipe in the η-τ plane. Applying the principles from the calculus of variations, the scalar dot product between a small arbitrary displacement, δu_2 and Eq. (2.2-3a) may be integrated over the length of the pipe, L, to obtain the virtual work given by

$$\int^{L} \left[EI\frac{\partial^4 u_2}{\partial x^4} + p\frac{\partial^2 u_2}{\partial x^2} + m\frac{\partial^2 u_2}{\partial t^2} - r_2\right]\delta u_2 dx = 0 \qquad (2.3\text{-}1a)$$

in which all terms are nondimensional quantities. The first two terms in Eq. (2.3-1a) can be integrated by parts to obtain

$$\left[EI\frac{\partial^3 u_2}{\partial x^3}\,\delta u_2\right]_o^L - \left[EI\frac{\partial^2 u_2}{\partial x^2}\frac{\partial \delta u_2}{\partial x}\right]_o^L + \left[p\frac{\partial u_2}{\partial x}\,\delta u_2\right]_o^L +$$

$$+ \int^L EI\frac{\partial^2 \delta u_2}{\partial x^2}\frac{\partial^2 u_2}{\partial x^2}dx - \int^L p\frac{\partial u_2}{\partial x}\frac{\partial \delta u_2}{\partial x}dx +$$

$$+ \int m\frac{\partial^2 u_2}{\partial t^2}\,\delta u_2 dx - \int^L r_2 \delta u_2 dx = 0 \qquad (2.3\text{-}1b)$$

The first three terms in this equation vanish when evaluated using either the **prescribed** or **natural** boundary conditions previously given. The remaining terms are equivalent to the minimi-

zation of potential energy for the prescribed flexural response of the pipeline system [cf. Cook (1981) or Chajes (1979) for an in-depth discussion of the relevant energy principles].

Equation (2.3-1b) is an instantaneous equilibrium statement for the continuous pipeline. Integrating between an arbitrary initial time, t_o, and an arbitrary later time, t_1, gives

$$\int_{t_o}^{t_1} \left[\int_0^L m\frac{\partial^2 u_2}{\partial t^2}\,\delta u_2 dx + \left(\int_0^L EI\frac{\partial^2 u_2}{\partial x^2}\frac{\partial^2 \delta u_2}{\partial x^2}\,dx + \int_0^L p\,\frac{\partial u_2}{\partial x}\frac{\partial \delta u_2}{\partial x}\,dx \right) \right] dt$$

$$- \int_{t_o}^{t_1} \left(\int_0^L r_2 \delta u_2 dx \right) dt = 0 \qquad (2.3\text{-}2a)$$

which is equivalent to Hamilton's principle [Clough and Penzien (1975)] given by

$$\int_{t_o}^{t_1} \delta(T - V)dt + \int_{t_o}^{t_1} \delta W_{nc}\,dt = 0 \qquad (2.3\text{-}2b)$$

in which δ = variation during the interval t_o to t_1; T = the total kinetic energy of the system given by

$$T = \frac{1}{2}\int_0^L m\left(\frac{\partial u_i}{\partial t}\right)^2 dx \quad i = 1,2,3,4 \;;$$

V = the potential energy of the system and of any conservative loads; and W_{nc} = the work done by nonconservative forces. For the illustrated example of the flexural response in the η-τ direction, the potential and conservative energy of the system are given by

$$V = \frac{1}{2}\int_0^L EI\left(\frac{\partial^2 u_2}{\partial x^2}\right)^2 dx - \frac{1}{2}\int_0^L p\left(\frac{\partial u_2}{\partial x}\right)^2 dx$$

and the work done by nonconservative forces is given by

$$W_{nc} = \int^{L} r_2 \delta u_2 dx.$$

The equivalence between the force Eqs. (2.2-3a) and the energy minimization expression given by Eqs. (2.3-2b) has been demonstrated only for the flexural response. However, similar analyses would also give equivalent minimum energy expressions for both the torsional and axial response modes (Eqs. 2.2-3 b & c).

This transformation of the controlling partial differential equations to a single energy principle equation is significant in the development of a finite element formulation. The finite element method (FEM) is a numerical solution technique that is based on the minimization of a discretized version of the energy in the system using discrete nodal equilibrium equations. Moreover, Hamilton's principle is applicable to a variety of dynamic systems and is not restricted solely to the dynamic beam equation.

2.3.2 **Discretization of the Continuous System**

For numerical analyses, it is convenient to discretize the pipeline system such that the displacement field within the system can be represented by the response of a set of generalized coordinates. The generalized coordinates for the pipeline under consideration consist of displacements and/or rotations at discrete points along the pipeline. If the displacement field of the pipeline is represented by a set of generalized coordinates, minimization of the total potential energy can be obtained by taking the derivatives of the total potential energy with respect to each of

the generalized coordinates. This numerical procedure is called the Rayleigh-Ritz method. A detailed presentation of this method can be found in Bathe (1982), Cook (1981) or in Clough and Penzien (1975).

In order to develop general numerical techniques, the dynamic response of the pipeline will be represented by the uncoupled responses in bending, in axial deformation, and in twisting. For each of these modes of response, equilibrium of the system requires that the energy of the system be minimized with respect to the displacement field associated with that mode of response.
The displacements and rotations for the entire pipeline may be approximated by the following relationship:

$$u_i(x,t) = d_i(t)\psi_i(x) \qquad ; i = 1,2,3,4 \qquad (2.3\text{-}3)$$

in which $u_i(x,t)$ = the spatial and temporal dependent displacement or rotation corresponding to the index i; $d_i(t)$ = the time varying generalized coordinate associated with the index i; and $\psi_i(x)$ = an admissible shape function for the given mode of response. The remaining rotation terms, u_5 and u_6, are defined for small deflections by the spatial derivatives of the transverse deflections with respect to position along the pipeline axis.

Substituting the separation of variables relationship given by Eqs. (2.3-3) into Hamilton's principle given by Eq. (2.3-2b) for determining the bending, axial, and twisting responses of the pipe system yields

$$\int_{t_o}^{t_1} \Big[\int^{L} \psi_i(x) m \psi_i(x) \ddot{d}_i(t) dx + \int^{L} \psi_i''(x) EI \psi_i''(x) d_i(t) dx$$

$$+ \int^{L} \psi_i'(x) p \psi_i'(x) d_i(t) dx - \int^{L} r_i \psi_i(x) dx \Big] \delta d_i dt = 0; \; i = 2,3 \qquad (2.3\text{-}4a)$$

$$\int_{t_o}^{t_1} \Big[\int^{L} \psi_1(x) m \psi_1(x) \ddot{d}_1(t) dx + \int^{L} \psi_1'(x) \; EA \psi_1'(x) d_1(t) dx$$

$$- \int^{L} r_1 \psi_1(x) dx \Big] \delta d_1 dt = 0 \qquad (2.3\text{-}4b)$$

$$\int_{t_o}^{t_1} \Big[\int^{L} \psi_4'(x) GJ \; \psi_4'(x) d_4(t) dx - \int^{L} r_4 \psi_4(x) dx \Big] \delta d_4 dt = 0 \qquad (2.3\text{-}4c)$$

in which the superscript primes (') = the spatial derivative along the pipeline axis and the overdots (••) = the second temporal derivative. If the temporal integration of these equations is performed numerically, the integrals in Eqs. (2.3-4) are minimized at each discrete time step. Because the components of the virtual motions of the corresponding generalized coordinates, d_i, are arbitrary, each of the bracketed terms in Eqs. (2.3-4) must be identically zero for each discrete time step within the time interval under consideration. •Evaluation of the bracketed terms in such a manner provides an expression for the equilibrium of forces for each mode of response at discrete time steps.

The finite element method utilizes the same principles which were applied to obtain Eqs. (2.3-4). However, rather than representing the modes of structural reponse by a single set of shape functions and generalized coordinates, the structure is modeled by a series of coupled elements. Proper coupling of the elements

allows simultaneous solution for the set of generalized coordinates which results in a force equilibrium within the finite element model. Changes in structural geometry due to dynamic responses can be easily modeled by the finite element method by adopting a local coordinate system for each element. Individual element effects can then be transformed to a mutual coordinate system in order to solve simultaneously for the unknown generalized coordinates. Because the basis of the finite element method is the individual elements used to model the structure, much of the effort in developing a solution algorithm for Eq. (2.2-3b) is directed toward formulating the equilibrium equations for a single element.

As an analogy to Eqs. (2.3-3) which represents a discretization of the entire pipeline, the displacment fields within an individual element only are represented by the matrix equation

$$u_i(x,t) = \{\mathbf{N}(x)\}_i^T \{\mathbf{d}(t)\}_i \qquad ; i = 1,2,3,4 \qquad (2.3\text{-}5)$$

in which $u_i(x,t)$ = the spatial and temporal components of displacement or rotation within the element which correspond to the index i; $\{\mathbf{d}(t)\}_i$ = the time varying vector of generalized coordinates associated with the i^{th} mode of response the element; $\{\mathbf{N}(x)\}_i$ = a vector of admissible shape functions for the i^{th} of response within the element; and the right superscript T = the transpose of a vector or matrix. Substituting Eq. (2.3-5) into the expression for Hamilton's principle given by Eq. (2.3-2b) gives a system of equations analogous to Eqs. (2.3-4). An important distinction between

these systems of equations, however, is that they now represent the dynamics of only a single element. The equilibrium equations for a single element only are now given by

$$[\mathbf{m}]^{t+\Delta t}\{\ddot{\mathbf{d}}\} + {}^{t+\Delta t}[\mathbf{k}]^{t+\Delta t}\{\mathbf{d}\} = {}^{t+\Delta t}\{\mathbf{r}\} \qquad (2.3\text{-}6)$$

in which the left superscript $^{t+\Delta t}$ represents an instantaneous point in time in the interval t_o to t_1; $[\mathbf{m}]$ = matrix representation of mass within the element; $^{t+\Delta t}\{\ddot{\mathbf{d}}\}$ = vector of the acceleration of an instantaneous generalized coordinate; $^{t+\Delta t}[\mathbf{k}]$ instantaneous matrix representation of element stiffness; $^{t+\Delta t}\{\mathbf{d}\}$ = vector of instantaneous generalized coordinates; and $^{t+\Delta t}\{\mathbf{r}\}$ = instantaneous vector representation of applied environmental loads. A detailed development of the individual terms in Eqs. (2.3-6) is presented in Section (2.4).

Equation (2.3-6) is a generalized force equilibrium statement. However, because the applied loads are nonlinear, the equation is nonlinear. To facilitate the evaluation of this equation and its extension to large deflections, a general solution technique for nonlinear systems of equations is presented.

2.3.3 **Nonlinear Solution Technique**

The Newton-Raphson iteration scheme, or modifications of it, provides a straight-forward algorithm for computing equilibrium solutions to nonlinear problems. The technique estimates the load-deflection response of an element that is caused by a change in position using a first-order approximation of the response evaluated at the current position [Bathe (1982), pp. 490-491]. To

apply this concept, consider the following generalization of Eq. (2.3-6) is considered:

$$\{\mathbf{h}^{t+\Delta t}(\mathbf{d}^k)\} = {}^{t+\Delta t}\{\mathbf{r}^k\} - {}^{t+\Delta t}([\mathbf{m}]\{\ddot{\mathbf{d}}^k\} + [\mathbf{k}]\{\mathbf{d}^k\}) = 0 \qquad (2.3\text{-}7a)$$

or

$$\{\mathbf{h}^{t+\Delta t}(\mathbf{d}^k)\} = \{\mathbf{r}^{t+\Delta t}(\mathbf{d}^k)\} - \{\mathbf{f}^{t+\Delta t}(\mathbf{d}^k)\} = 0 \qquad (2.3\text{-}7b)$$

in which the superscript ^{k} denotes iteration number; $\{\mathbf{d}^k\}$ = the generalized coordinates at the k^{th} iteration; $\{\mathbf{h}^{t+\Delta t}(\mathbf{d}^k)\}$ = equilibrium function at time $t+\Delta t$; $\{\mathbf{r}^{t+\Delta t}(\mathbf{d}^k)\}$ = the applied load function; and $\{\mathbf{f}^{t+\Delta t}(\mathbf{d}^k)\}$ = the structural resistance function which includes internal elements forces caused by both element deformations and inertial effects. The linear Taylor expansion of the equilibrium expression about the current postion $\{\mathbf{d}^{k-1}\}$ is

$${}^{t+\Delta t}\{\mathbf{h}(\mathbf{d}^{k-1} + \Delta\mathbf{d}^{k-1})\} = {}^{t+\Delta t}\{\mathbf{h}(\mathbf{d}^{k-1})\} + {}^{t+\Delta t}\left[\frac{\partial \mathbf{h}}{\partial \mathbf{d}}\right]_{\mathbf{d}^{k-1}} \{\Delta\mathbf{d}^{k-1}\} \qquad (2.3\text{-}8a)$$

where

$$\{\mathbf{d}^k\} = \{\mathbf{d}^{k-1}\} + \{\Delta\mathbf{d}^{k-1}\} \qquad (2.3\text{-}8b)$$

and in which $\Delta\mathbf{d}^0 = 0$ and $\mathbf{d}^0$ = the initial estimate for the pipeline nodal position at the beginning of a time step based on the kinematics from the previous time step. Substituting Eq. (2.3-7b) into Eq. (2.3-8a) gives the following iterative expression for an element at the discrete time $t+\Delta t$:

$$ {}^{t+\Delta t}\{\mathbf{r}^{k-1}\} - {}^{t+\Delta t}\{\mathbf{f}^{k-1}\} + {}^{t+\Delta t}\left[\frac{\partial \mathbf{r}}{\partial \mathbf{d}}\right]_{\mathbf{d}^{k-1}} \{\Delta \mathbf{d}^{k-1}\} - {}^{t+\Delta t}\left[\frac{\partial \mathbf{f}}{\partial \mathbf{d}}\right]_{\mathbf{d}^{k-1}} $$

$$ \{\Delta \mathbf{d}^{k-1}\} = 0 \qquad (2.3\text{-}9) $$

in which $\{\mathbf{d}^{k}\}$ has been expanded using Eq. (2.3-8b). Equation (2.3-9) is a general expression which will be used to iteratively solve for the pipeline response at time t+Δt. For a linear **structural** response such as that represented by Eq. (2.3-6), Eq. (2.3-9) can be rewritten as

$$ {}^{t+\Delta t}\{\mathbf{r}^{k-1}\} - [\mathbf{m}]\,{}^{t+\Delta t}\{\ddot{\mathbf{d}}^{k-1}\} - [\mathbf{k}]\,{}^{t+\Delta t}\{\mathbf{d}^{k-1}\} + \left[\frac{\partial \mathbf{r}}{\partial \mathbf{d}}\right]_{\mathbf{d}^{k-1}} \{\Delta \mathbf{d}^{k-1}\} $$

$$ - [\mathbf{m}]\left(\frac{\partial \ddot{\mathbf{d}}}{\partial \mathbf{d}}\right) \{\Delta \mathbf{d}^{k-1}\} - [\mathbf{k}]\{\Delta \mathbf{d}^{k-1}\} = 0 \qquad (2.3\text{-}10a) $$

in which

$$ {}^{t+\Delta t}\{\mathbf{f}^{k-1}\} = [\mathbf{m}]\,{}^{t+\Delta t}\{\ddot{\mathbf{d}}^{k-1}\} + [\mathbf{k}]\,{}^{t+\Delta t}\{\mathbf{d}^{k-1}\} \qquad (2.3\text{-}10b) $$

and

$$ \left[\frac{\partial \mathbf{f}}{\partial \mathbf{d}}\right]_{\mathbf{d}^{k-1}} = [\mathbf{m}]\left(\frac{\partial \ddot{\mathbf{d}}}{\partial \mathbf{d}}\right) + [\mathbf{k}] \qquad (2.3\text{-}10c) $$

The extension of Eqs. (2.3-10) to nonlinear structural responses requires that the internal structural forces, ${}^{t+\Delta t}\{\mathbf{f}^{k-1}\}$, be determined from element deformations rather than from total displacements or rotations, $\{\mathbf{d}^{k-1}\}$, as in Eq. (2.3-10b). It is further

necessary to evaluate the structural stiffness matrix, $[\mathbf{k}]$, iteratively in Eq. (2.3-10c) in terms of the axial loads which exist within the element at the $(k-1)^{th}$ iteration. An in-depth discussion of these procedures in presented in Section (2.4.1).

A graphical interpretation of the Newton-Raphson iteration scheme for a single degree of freedom system is presented in Fig. 2.3. This figure shows that the solution increment computed at each iteration is obtained by linearly projecting the previously computed slope of the load-displacement function using the previously computed displacement increment in order to satisfy the existing force imbalance. A more in-depth discussion of this solution technique is presented by either Bathe (1982) [pp 490-491] or Cook (1981) [pp. 357-382].

2.4 **Finite Element Method (FEM)**

The finite element method (FEM) described in sections 2.4 is directed toward predicting the large deflection dynamic response of a long slender beam subjected to specific environmental loads. The variational principle described in Section (2.3.1) is applied to develop the elastic and geometric stiffnesses of an element in terms of the generalized coordinates which determine the displacment fields of the elements. The introduction of a convected element coordinate system, coupled with the Newton-Raphson iteration scheme outlined in Section (2.3.3), permits extension of this formulation to static, large deflection analysis. A Newmark-beta temporal integration scheme is used in conjunction with the finite deflection model to predict dynamic stresses and displacements.

Figure 2.3 Graphical interpretation of the Newton-Raphson technique (Incrementally applied load to a softening system).

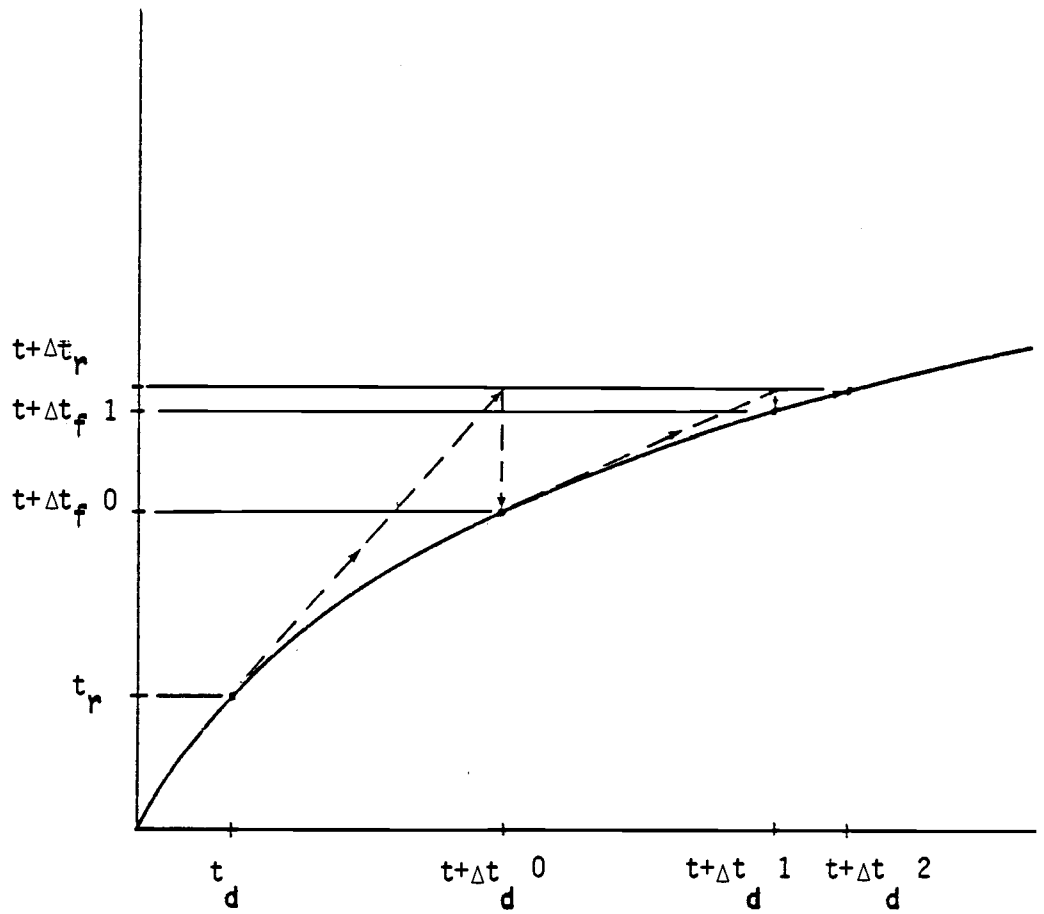

Application of the general dynamic model to the pipeline simulation requires specifying constraints on pipeline displacement [Section (2.4.2)], and then evaluating the applied environmental loads [Section (2.4.3)] consistent with the specified constraints. In Section (2.4.4) the pipeline dynamics are incorporated into an FEM algorithm for simulation of the pipeline response.

2.4.1 Structural Response for an Element

The pipe system is modeled by straight-lined segments using linear beam elements. Associated with each element are the displacement fields which are defined in terms of either generalized coordinates or various degrees of freedom. This concept has been discussed previously in Section (2.3.2) and was represented explicitly by Eq. (2.3-5). The generalized coordinates for an element are shown in Fig. 2.4 for a **local** coordinate system (τ, η, β). From Fig. 2.4 it is apparent that both the i and j ends of the member have six degrees of freedom.

Interpolation functions, together with the generalized coordinates define the displacement fields within an element, and are presented in Table 2.1. The displacement fields for flexural responses are approximated by cubic splines which utilize the slopes and ordinates of the element nodes as generalized coordinates. This type of scheme is termed **Hermitian** interpolation. The shape functions which define the axial and torsional response are associated with the longitudinal displacement and rotational degrees of freedom at the element ends. The splines that represent these displacement fields are linear and match the ordinate or τ rotation

Figure 2.4 Definition of local element degrees of freedom (double arrows denote rotation).

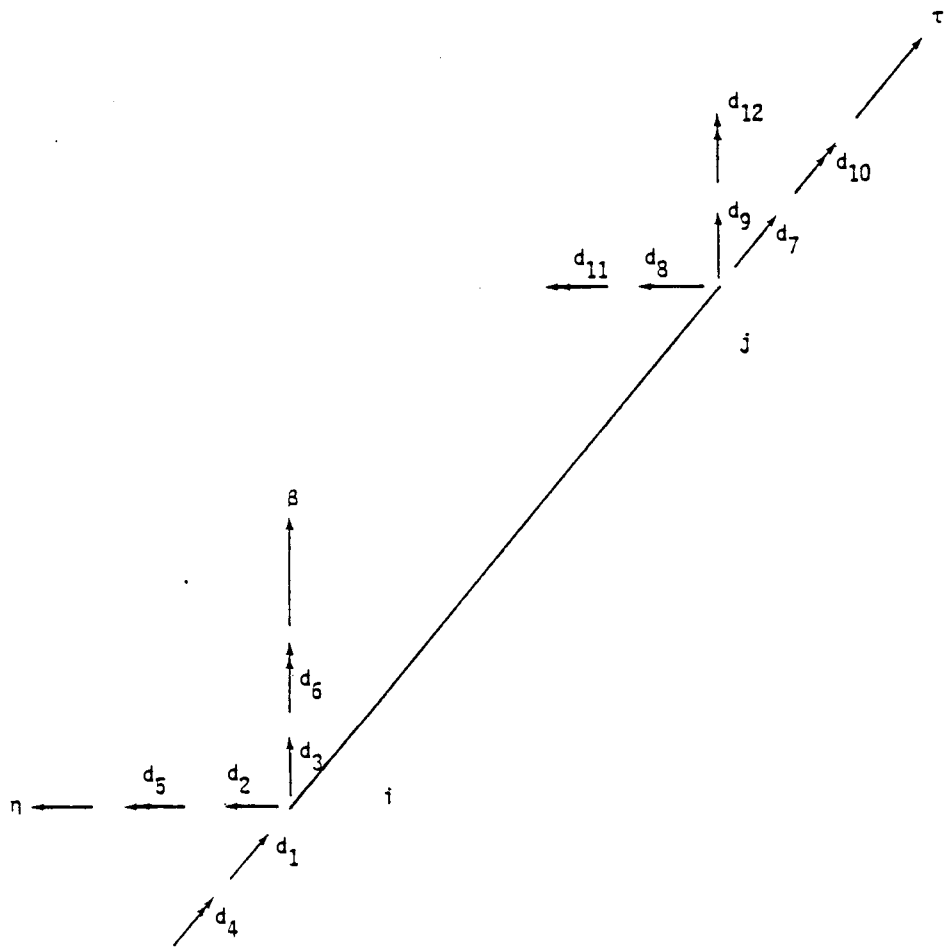

of the element ends. This type of formulation is based upon Lagrange's interpolation formula which defines a polynomial of order n-1 passing through n points. An in-depth discussion of interpolation schemes and higher-order elements is given by either Cook (1981) [pp. 77-102] or Bathe (1982) [pp. 114-186].

2.4.1a) **Static Linear Response**

The application of the Newton-Raphson iteration technique requires that the linear approximation of the structural stiffness be estimated at each given configuration. To demonstrate the development of the elastic and geometric stiffnesses, the element described in Fig. 2.4 is subjected to a preexisting tensile force, p, that is consistent with its current configuration. The stiffness can be derived by evaluating Eq. (2.3-2b) for static loading; i.e., by neglecting inertial effects. Substitution of the interpolation functions from Table 2.1 into Eq. (2.3-2b) and rearrangement to an equivalent static form yields

$$\left[\int^{L} \{\mathbf{N}''(x)\}_i EI \{\mathbf{N}''(x)\}_i^T dx\right]\{\mathbf{d}(t)\}_i + \left[\int^{L} \{\mathbf{N}'(x)\}_i p \{\mathbf{N}'(x)\}_i^T dx\right]\{\mathbf{d}(t)\}_i = \{\mathbf{r}(t)\}_i \; ; \; i = 2,3 \qquad (2.4\text{-}1a)$$

$$\left[\int^{L} \{\mathbf{N}'(x)\}_1 EA \{\mathbf{N}'(x)\}_1^T dx\right]\{\mathbf{d}(t)\}_1 = \{\mathbf{r}(t)\}_1 \qquad (2.4\text{-}1b)$$

$$\left[\int^{L} \{\mathbf{N}'(x)\}_4 GJ \{\mathbf{N}'(x)\}_4^T dx\right]\{\mathbf{d}(t)\}_4 = \{\mathbf{r}(t)\}_4 \qquad (2.4\text{-}1c)$$

Table 2.1. Interpolation splines and associated degrees of freedom.

Response	Shape Functions	Degrees of Freedom
$u_1(x,t)$ (axial)	$\{N(x)\}_1 = \begin{Bmatrix} 1 - \frac{x}{L} \\ \frac{x}{L} \end{Bmatrix}$	$\{d(t)\}_1 = \begin{Bmatrix} d_1 \\ d_7 \end{Bmatrix}$
$u_2(x,t)$ (eta,tau $\eta-\tau$ bending)	$\{N(x)\}_2 = \begin{Bmatrix} 1 - \frac{3x^2}{L^2} + \frac{2x^3}{L^3} \\ x - \frac{2x^2}{L} + \frac{x^3}{L^2} \\ \frac{3x^2}{L^2} - \frac{2x^3}{L^3} \\ -\frac{x^2}{L} + \frac{x^3}{L^2} \end{Bmatrix}$	$\{d(t)\}_2 = \begin{Bmatrix} d_2 \\ d_6 \\ d_8 \\ d_{12} \end{Bmatrix}$
$u_3(x,t)$ (beta, tau $\beta-\tau$ bending)	$\{N(x)\}_3 = \begin{Bmatrix} 1 - \frac{3x^2}{L^2} + \frac{2x^3}{L^3} \\ -x + \frac{2x^2}{L} - \frac{x^3}{L^2} \\ \frac{3x^2}{L^2} - \frac{2x^3}{L^3} \\ \frac{x^2}{L} - \frac{x^3}{L^2} \end{Bmatrix}$	$\{d(t)\}_3 = \begin{Bmatrix} d_3 \\ d_5 \\ d_9 \\ d_{11} \end{Bmatrix}$
$u_4(x,t)$ (torsion)	$\{N(x)\}_4 = \begin{Bmatrix} 1 - \frac{x}{L} \\ \frac{x}{L} \end{Bmatrix}$	$\{d(t)\}_4 = \begin{Bmatrix} d_4 \\ d_{10} \end{Bmatrix}$

in which $\{\mathbf{r}(t)\}_i$ = the vector of generalized applied nodal loads which represent the continuous loadings. The components of these vector loads correspond to the components of the generalized coordinate vector, $\{\mathbf{d}(t)\}_i$. For static analysis, the load vector is constant and evaluation of the integral terms in Eqs. (2.4-1) results in a set of simultaneous equations which can be solved to determine the generalized coordinates for which equilibrium exists. Evaluation of Eq. (2.4-1a) yields two sets of four simultaneous equations; and evaluation of Eqs. (2.4-1b & c) each yields two simultaneous equations. Combining all of these equations in matrix form gives

$$([\mathbf{k}_E] + [\mathbf{k}_G])\{\mathbf{d}\} = \{\mathbf{r}\} \tag{2.4-2a}$$

or

$$[\mathbf{k}]\{\mathbf{d}\} = \{\mathbf{r}\} \tag{2.4-2b}$$

in which $\{\mathbf{d}\}$ and $\{\mathbf{r}\}$ are the generalized displacement and load vectors, respectively, (the components of the vector $\{\mathbf{d}\}$ are shown in Figure 2.4) given by

$$\{\mathbf{d}\} = \begin{Bmatrix} d_1 \\ d_2 \\ d_3 \\ d_4 \\ d_5 \\ d_6 \\ d_7 \\ d_8 \\ d_9 \\ d_{10} \\ d_{11} \\ d_{12} \end{Bmatrix} \quad ; \{\mathbf{r}\} = \begin{Bmatrix} r_1 \\ r_2 \\ r_4 \\ r_5 \\ r_5 \\ r_6 \\ r_7 \\ r_8 \\ r_9 \\ r_{10} \\ r_{11} \\ r_{12} \end{Bmatrix} ; \tag{2.4-2c}$$

$[\mathbf{k}]$ = generalized structural stiffness matrix for a given tensile load p;

$$[\mathbf{k}] = [\mathbf{k}_E] + [\mathbf{k}_G] \tag{2.4-2d}$$

where $[\mathbf{k}_E]$ and $[\mathbf{k}_G]$ are defined in Figures 2.5 and 2.6, respectively.

The axial components of the geometric stiffness matrix, [i.e., $\mathbf{k}_{G11}$, $\mathbf{k}_{G17}$, $\mathbf{k}_{G71}$ and $\mathbf{k}_{G77}$ (subscripts denoting matrix location by row and column)] are not derived from Eq. (2.4-1b). These components were adopted from the element fomulations presented by Meek (1971) [pp. 543-588] or by Cook (1981) [pp. 331-337].

Equation (2.4-2b) is a linear equilibrium expression for the static response of a single element. A static equilibrium expression for the entire structure may be formed by summing contribu-

Figure 2.5 Elastic stiffness, $[k_E]$, in Eq. (2.4-2a) [Ref. McGuire and Gallagher (1979), p.91].

$$
\begin{bmatrix}
\frac{EA}{L} & 0 & 0 & 0 & 0 & 0 & \frac{-EA}{L} & 0 & 0 & 0 & 0 & 0 \\
 & \frac{12EI}{L^3} & 0 & 0 & 0 & \frac{6EI}{L^2} & 0 & \frac{-12EI}{L^3} & 0 & 0 & 0 & \frac{6EI}{L^2} \\
 & & \frac{12EI}{L^3} & 0 & \frac{-6EI}{L^2} & 0 & 0 & 0 & \frac{-12EI}{L^3} & 0 & \frac{-6EI}{L^2} & 0 \\
 & & & \frac{JG}{L} & 0 & 0 & 0 & 0 & 0 & \frac{-JG}{L} & 0 & 0 \\
 & & & & \frac{4EI}{L} & 0 & 0 & 0 & \frac{6EI}{L^2} & 0 & \frac{2EI}{L} & 0 \\
 & & & & & \frac{4EI}{L} & 0 & \frac{-6EI}{L^2} & 0 & 0 & 0 & \frac{2EI}{L} \\
\text{Symmetric} & & & & & & \frac{AE}{L} & 0 & 0 & 0 & 0 & 0 \\
 & & & & & & & \frac{12EI}{L^3} & 0 & 0 & 0 & \frac{-6EI}{L^2} \\
 & & & & & & & & \frac{12EI}{L^3} & 0 & \frac{6EI}{L^2} & 0 \\
 & & & & & & & & & \frac{JG}{L} & 0 & 0 \\
 & & & & & & & & & & \frac{4EI}{L} & 0 \\
 & & & & & & & & & & & \frac{4EI}{L}
\end{bmatrix}
$$

Figure 2.6 Geometric stiffness,$[k_E]$, for tensile load, p, in Eq. (2.4-2a) [Ref. Cook (1981), pp. 384-335 and Meek (1971), p.569].

$$
\begin{bmatrix}
\frac{p}{L} & 0 & 0 & 0 & 0 & 0 & \frac{-p}{L} & 0 & 0 & 0 & 0 & 0 \\
 & \frac{6p}{5L} & 0 & 0 & 0 & \frac{p}{10} & 0 & \frac{-6p}{5L} & 0 & 0 & 0 & \frac{p}{10} \\
 & & \frac{6p}{5L} & 0 & \frac{-p}{10} & 0 & 0 & 0 & \frac{-6p}{5L} & 0 & \frac{-p}{10} & 0 \\
 & & & 0 & 0 & 0 & 0 & 0 & 0 & 0 & 0 & 0 \\
 & & & & \frac{2pL}{15} & 0 & 0 & 0 & \frac{p}{10} & 0 & \frac{-pL}{30} & 0 \\
 & & & & & \frac{2pL}{15} & 0 & \frac{-p}{10} & 0 & 0 & 0 & \frac{-pL}{30} \\
\text{Symmetric} & & & & & & \frac{p}{L} & 0 & 0 & 0 & 0 & 0 \\
 & & & & & & & \frac{6p}{5L} & 0 & 0 & 0 & \frac{-pL}{30} \\
 & & & & & & & & \frac{6p}{5L} & 0 & \frac{p}{10} & 0 \\
 & & & & & & & & & 0 & 0 & 0 \\
 & & & & & & & & & & \frac{2pL}{15} & 0 \\
 & & & & & & & & & & & \frac{2pL}{15}
\end{bmatrix}
$$

tions from the active degrees of freedom from all of the elements. Combining element stiffnesses in this manner assures that the boundary conditions described in Section (2.2.2) will be satisfied.

2.4.1b) **Static Nonlinear Response**

In general, the displacements of a pipeline system during a peak forcing event may become significant. In such cases, the product of element stiffness and displacement does not yield the actual element forces. This is because large element motions involve both **rigid body movement** and actual **element deformation.** The **rigid body motion** of the system should produce no internal forces within an element for static analysis. In order to extend the concepts presented in Section (2.4.1a) to nonlinear static analysis, an updated Lagrangian formulation is adopted to define element displacements [Belytschko and Hsieh (1973) and Cook (1981), pp. 353-356] and is incorporated in the Newton-Raphson iteration scheme.

The concept of a convected coordinate system which moves with an element undergoing displacement may be readily demonstrated by the analogy of restricting the motion of an element in the η-τ plane to remain in the global X-Y plane. The result of such a constraint is an effective reduction of the three-dimensional element to a two-dimensional element. The reduction from a three-dimensional analysis to a two-dimensional analysis is for clarity of presentation and does not prohibit an extension of the concept to three-dimensional analyses.

Figure 2.7 depicts the constrained element before and after deformation. The global (X,Y,Z) degrees of freedom are denoted by $\mathbf{D}_i$, and the element deformations (not element degrees of freedom) are denoted by $\bar{\mathbf{d}}_i$. Because the element coordinate system tracks with the member and because the element is constrained to remain in the X-Y plane, the only deformations possible are $\bar{\mathbf{d}}_6$, $\bar{\mathbf{d}}_7$ and $\bar{\mathbf{d}}_{12}$. The element deformations may be computed from the following geometric relationships:

$$X_L = X_o + \mathbf{D}_7 - \mathbf{D}_1 \qquad (2.4\text{-}3a)$$

$$Y_L = Y_o + \mathbf{D}_8 - \mathbf{D}_2 \qquad (2.4\text{-}3b)$$

$$\theta_L = \mathrm{Tan}^{-1}(Y_L/X_L) \qquad (2.4\text{-}3c)$$

$$L = (X_L^2 + Y_L^2)^{1/2} \qquad (2.4\text{-}3d)$$

$$L_o = (X_o^2 + Y_o^2)^{1/2} \qquad (2.4\text{-}3e)$$

in which X_o, Y_o, L_o, X_L, Y_L, and L are defined in Fig. 2.7. Furthermore, Fig. 2.7 illustrates that

$$\bar{\mathbf{d}}_i = 0 \qquad ; i = 1\text{-}5,\ 8\text{-}11 \qquad (2.4\text{-}3f)$$

$$\bar{\mathbf{d}}_6 = \mathbf{D}_6 - (\theta_L - \theta_o) \qquad (2.4\text{-}3g)$$

Figure 2.7 Convected coordinates utilizing an updated Lagrangian formulation for a two dimensional example: (a) before deformation and (b) after deformation.

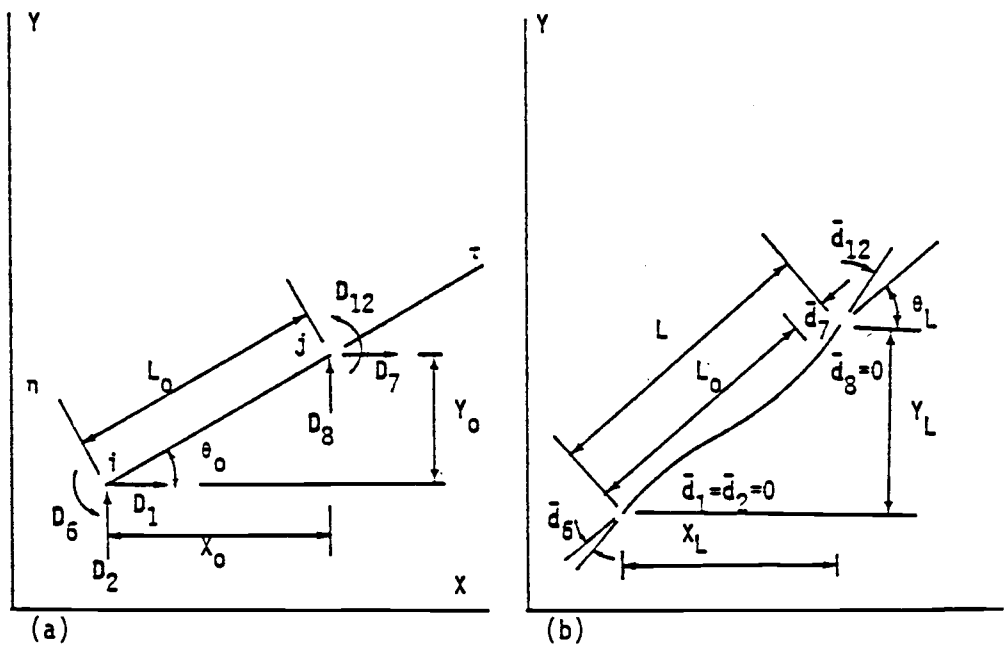

$$\bar{d}_7 = L - L_o \tag{2.4-3h}$$

and

$$\bar{d}_{12} = D_{12} - (\theta_L - \theta_o). \tag{2.4-3i}$$

From these computed deformations, the actual axial load within the element may be calculated by [Meek (1971), p. 557]

$$p = EA\left[\frac{\bar{d}_7}{L} + \frac{1}{30}\left(2\bar{d}_6^2 - \bar{d}_6\,\bar{d}_{12} + 2\bar{d}_{12}^2\right)\right] . \tag{2.4-4}$$

After evaluating the axial load within an element, the internal structural forces that result from these computed deformations may be evaluated using Eq. (2.4-2b). For an element in equilibrium, the resulting expression is

$$[k]\{\bar{d}\} = \{r\} \tag{2.4-5}$$

Because there is not a linear correspondence between element deformations and element displacements, the solutions to Eq. (2.4-5) must be obtained iteratively using the Newton-Raphson technique. Assuming that the load vector, $\{r\}$, is known for a given increment, $t+\Delta t$, Eq. (2.4-5) may be expanded in a linear Taylor series to give

$$^{t+\Delta t}\{r\} - [k]_{\bar{d}^{k-1}}\,{}^{t+\Delta t}\{\bar{d}^{k-1}\} - [k]_{\bar{d}^{k-1}}\,{}^{t+\Delta t}\{\Delta d^{k-1}\} = \{0\} \tag{2.4-6a}$$

in which

$$\{\mathbf{d}^{k}\} = \{\mathbf{d}^{k-1}\} + \{\Delta\mathbf{d}^{k-1}\} \; ; \tag{2.4-6b}$$

$$^{t+\Delta t}\{\mathbf{f}^{k-1}\} = [\mathbf{k}]_{\overline{\mathbf{d}}^{k-1}} \, ^{t+\Delta t}\{\overline{\mathbf{d}}^{k-1}\} \; ; \tag{2.4-6c}$$

and

$$[\frac{\partial \mathbf{f}}{\partial \mathbf{d}}]_{\overline{\mathbf{d}}^{k-1}} = [\mathbf{k}]_{\overline{\mathbf{d}}^{k-1}} \; . \tag{2.4-6d}$$

Equation (2.4-6a) provides an iterative procedure for evaluating the equilibrium configuration of an element subjected to an incrementally applied static load. The accuracy of this type of formulation is illustrated graphically in Fig. 2.8. This figure compares the analytical [Timoshenko (1972)] and finite element [Zimmerman (1982)] solutions for the large deflection response of a cantilever beam which has been subjected to an incrementally applied large point load at full span. The finite element model for this structure was comprised of four equal length elements.

Utilization of an updated Lagrangian formulation provides an accurate method of evaluating internal structural forces which occur during the three-dimensional dynamic simulation. The proper determination of these forces is fundamental to establishing the equilibrium configuration of the pipeline at each discrete time step during the simulation.

Figure 2.8 Comparisons between finite element and analytic solutions for the large deflection response of a cantilever beam.

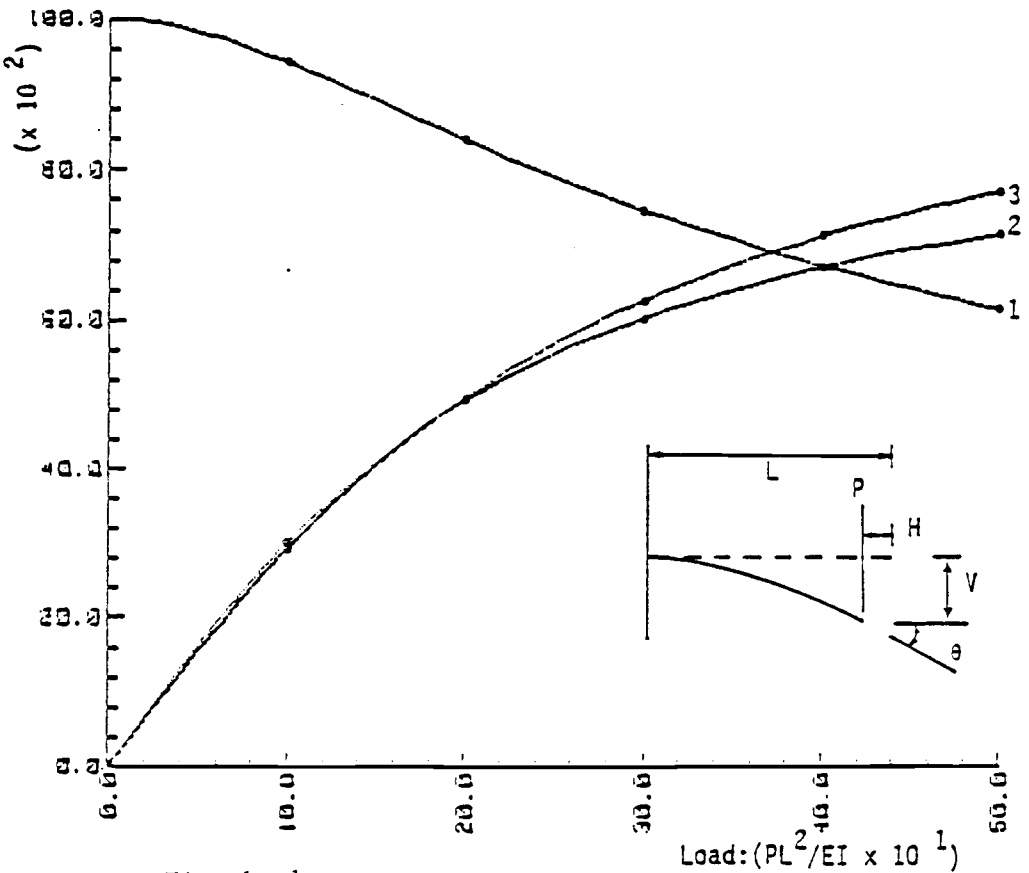

• - Timoshenko
——— - FEM results
1- 1-H/L
2- V/L
3- θ/(π/2)

Before extending the large deflection finite element formulation to include dynamic effects, it is prudent to examine a possible source of numerical error which may accompany this type of formulation. Consider again the linear beam element shown in Fig. 2.7. If $\theta_o = 0$ and if θ_L is defined by the FORTRAN function ATAN2(Y_L,X_L), then the rotation $\overline{d}_6$ is computed for either ± rotation. If $\theta_o = 180°$ and θ_L is computed by the FORTRAN function, then the rotation $\overline{d}_6$ will only be unambiguously computed for a rotation in a single direction. Similar difficulties exist for a more general three-dimensional formulation. Although it is possible to solve this problem in principle, it is more computationally efficient to avoid this source of error by defining the pipeline configuration as in Fig. 2.1. Figure 2.1 shows the longitudinal axis of the pipeline (τ direction) to be generally oriented in the positive X direction, and the β axis coincides approximately with the positive Z axis. The finite element algorithm employed to evaluate the pipeline response defines the i node of an element as the lower numbered node and the j node of the same element as the higher numbered node. Orienting individual elements such that their τ axis corresponds closely with the global X axis will assure that all practical displacements of the system may be accounted for without encountering numerical ambiguities. Favorable orientation of individual elements defined between successive nodes results from choosing a global coordinate system such that sequentially numbered pipe nodes have values which increase in the positive global X direction.

2.4.1c) **Dynamic Nonlinear Response**

The finite element formulations introduced thus far have neglected the effects of a time varying load-response relationship. Hamilton's principle as defined by Eqs. (2.3-4) can be applied to formulate the equations of motion for a single element. For arbitrary values of δd the interpolation functions from Table 2.1 may be substituted into Eq. (2.3.4) to yield

$$\int_{t_o}^{t_1} \left([\mathbf{m}]\{\ddot{\mathbf{d}}\} + [\mathbf{k}]\{\mathbf{d}\} - \{\mathbf{r}\}\right)dt = 0 \qquad (2.4\text{-}7a)$$

in which $[\mathbf{k}]$ has been defined in Figs. 2.5 and 2.6; $\{\mathbf{d}\}$ and $\{\mathbf{r}\}$ were defined in Eqs. (2.4-2c); and $[\mathbf{m}]$ = the element mass representation. A mass representation defined by

$$[\mathbf{m}] = \int_{o}^{L} \{\mathbf{N}\}\, m\, \{\mathbf{N}\}^{T}\, dx. \qquad (2.4\text{-}7b)$$

is termed a **consistent-mass** formulation because the shape functions utilized to construct the mass matrix are the same as those used to interpolate for the displacement fields. In contrast, the **lumped-mass** formulation assigns one-half of the element mass to each of the element nodes. Because all of the element mass is assigned to individual nodes, the lumped-mass formulation uncouples the inertial effects between opposite ends of an element and produces no direct moment contribution from inertial effects. For a well-discretized system, the lumped-mass formulation provides a more computationally efficient mass representation with no concurrent

loss in accuracy. Consequently, the lumped-mass representation will be employed in the current formulation. The lumped-mass matrix, $[\mathbf{m}]$, is depicted in Fig. 2.9.

Temporal integration of Eq. (2.4-7a) is performed numerically by the Newmark-beta method. This method is an extension of the linear acceleration method (Wilson θ). The Newmark-beta method is given [Bathe (1982)] by the following:

$$ {}^{t+\Delta t}\dot{\mathbf{d}} = {}^{t}\dot{\mathbf{d}} + \left[(1-\delta)\,{}^{t}\ddot{\mathbf{d}} + \delta\,{}^{t+\Delta t}\ddot{\mathbf{d}}\right]\Delta t \qquad (2.4\text{-}8a) $$

$$ {}^{t+\Delta t}\mathbf{d} = {}^{t}\mathbf{d} + {}^{t}\dot{\mathbf{d}}\Delta t + \left[(1/2 - \alpha)\,{}^{t}\ddot{\mathbf{d}} + \alpha\,{}^{t+\Delta t}\ddot{\mathbf{d}}\right]\Delta t^{2} \qquad (2.4\text{-}8b) $$

in which δ and α are the Newmark-beta integration parameters; superscripts $t+\Delta t$ and t denote increment number; and Δt = time step. For the commonly adopted values of $\delta = 1/2$ and $\alpha = 1/4$, this method integrates the kinematics over a time step assuming a constant average acceleration during the time step. This integration method is an **implicit** scheme. For **linear** structural systems, this technique has been demonstrated to be numerically stable regardless of the time step selected [Bathe (1982)].

Equations (2.4-8) can be rearranged and expanded in a form which is compatible with the Newton-Raphson iteration technique. This expansion yields:

$$ {}^{t+\Delta t}\ddot{\mathbf{d}}^{k} = \frac{1}{\alpha\Delta t^{2}}\left({}^{t+\Delta t}\mathbf{d}^{k} - {}^{t}\mathbf{d}\right) - \frac{1}{\alpha\Delta t}\,{}^{t}\dot{\mathbf{d}} - \left(\frac{1}{2\alpha} - 1\right){}^{t}\ddot{\mathbf{d}} \qquad (2.4\text{-}9a) $$

Figure 2.9 Definition of lumped-mass representation [m] in Eq. (2.4-7a).

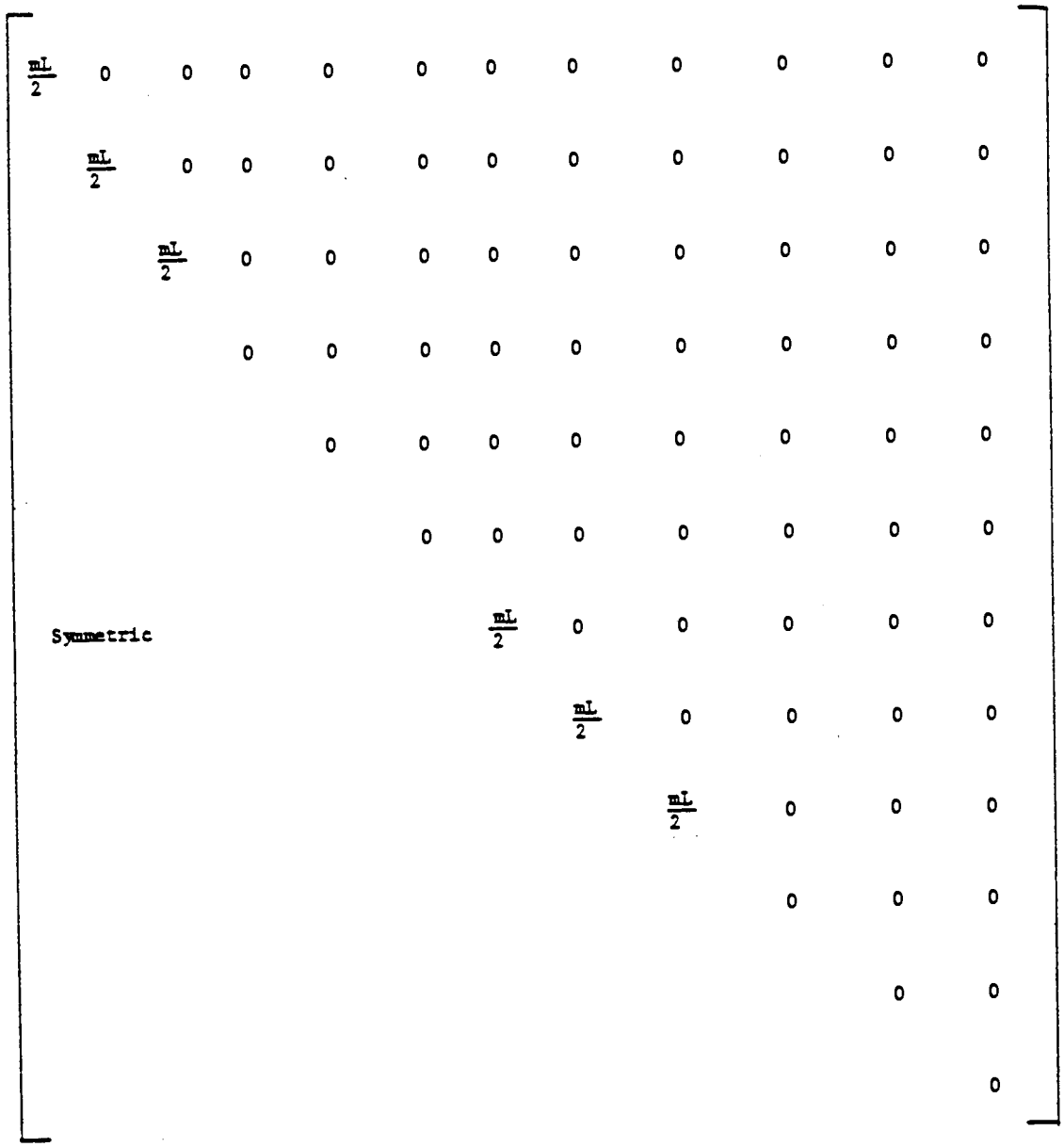

$$ {}^{t+\Delta t}\dot{\mathbf{d}}^{k} = {}^{t}\dot{\mathbf{d}} + \Delta t(1-\delta)\,{}^{t}\ddot{\mathbf{d}} + (\delta\Delta t)\,{}^{t+\Delta t}\ddot{\mathbf{d}}^{k} \qquad (2.4\text{-}9b) $$

in which

$$ {}^{t+\Delta t}\mathbf{d}^{k} = {}^{t+\Delta t}\mathbf{d}^{k-1} + {}^{t+\Delta t}\Delta\mathbf{d}^{k-1} \qquad (2.4\text{-}9c) $$

Coupling of the Newmark-beta integration method with the Newton-Raphson iteration technique provides a means of determining the kinematics and element stresses required to produce equilibrium at each discrete time, t+Δt. If the applied loads ${}^{t+\Delta t}\{\mathbf{r}\}$ are assumed to be known, expansion of the equilibrium function given by Eqs. (2.3-7) using Eqs. (2.4-9) gives

$$ {}^{t+\Delta t}\{\mathbf{r}\} - [\mathbf{k}]_{\mathbf{d}^{k-1}}\,{}^{t+\Delta t}\{\mathbf{d}^{k-1}\} - [\mathbf{m}]\,{}^{t+\Delta t}\{\ddot{\mathbf{d}}^{k-1}\} - [\mathbf{k}]_{\mathbf{d}^{k-1}}\{\Delta\mathbf{d}^{k-1}\} $$

$$ - \frac{1}{\alpha\Delta t^{2}}[\mathbf{m}]\,{}^{t+\Delta t}\{\Delta\mathbf{d}^{k-1}\} = \{0\} \qquad (2.4\text{-}10) $$

Solution of Eq. (2.4-10) for ${}^{t+\Delta t}\{\Delta\mathbf{d}^{k-1}\}$ provides an improved estimate for the structural configuration necessary to satisfy equilbrium. Iterative solutions for an equilibrium configuration terminates when specified convergence tolerances are met. Specification of proper tolerances is of great importance in the solution of nonlinear dynamics because of the path-dependent nature of the response. The convergence tolerance criteria recommended by Bathe (1982) are the following:

$$\frac{\| {}^{t+\Delta t}\mathbf{R} - {}^{t+\Delta t}\mathbf{F}^{k-1} \|}{\| \mathbf{R} - \mathbf{F} \|^{max}} \leq \text{RTOL} \qquad (2.4\text{-}11a)$$

and

$$\frac{\| {}^{t+\Delta t}_{\Delta}\mathbf{D}^{(k-1)T} \left({}^{t+\Delta t}\mathbf{R} - {}^{t+\Delta t}\mathbf{F}^{(k-1)} \right) \|}{\| {}^{t+\Delta t}_{\Delta}\mathbf{D}^{(1)T} \left({}^{t+\Delta t}\mathbf{R} - {}^{t+\Delta t}\mathbf{F}^{(1)} \right) \|} \leq \text{ETOL} \qquad (2.4\text{-}11b)$$

in which $\| \cdot \|$ denotes a vector norm; $\mathbf{R}$ = applied structural loads; $\mathbf{F}$ = structural resistance to applied loading; $\Delta\mathbf{D}$ = increment of structural displacements; RTOL = force tolerance; and ETOL = energy tolerance. Selecting iteration tolerances, ETOL and RTOL, that are excessively stringent results in unnecessary additional computational effort. Conversely, specifying tolerances that are not sufficiently tight can result in numerical instabilities or in an unwarranted energy loss from the system. Cook (1981) recommends a tolerance range between $10^{-2} < \text{TOL} < 10^{-6}$ for static nonlinear analysis. Because the dynamic response has a greater path dependency than the static response, it is appropriate to adopt tolerances which are in the more stringent portion of this interval [i.e., $10^{-5} < \text{TOL} < 10^{-6}$].

2.4.2) **Evaluation of Pipeline Response**

In the illustrative problem described in Section (2.4.1), a single finite element was used to model the nonlinear dynamic response of a small segment of the entire pipeline to a time-varying set of generalized forces. However, accurate simulation of the dynamic response of the entire continuous pipeline system using the finite element method requires that the dynamic response of many

elements be coupled. Coupling of the dynamic response of a individual elements with one another is achieved by requiring continuity between adjacent elements. This required continuity can be assured by coupling of the generalized coordinates between two adjacent finite elements because the position and shape of an element is defined by these generalized coordinates. Subsequently, generalized coordinates which are shared by two or more elements can be described by a mutual coordinate system. The components of the generalized coordinates in each of the adjacent elements can be evaluated by transforming the shared generalized coordinates into the **local** coordinate system of each element.

2.4.2a) **Problem Constraints**

Typically, a single coordinate system (global X,Y,Z) is utilized to describe all of the generalized coordinates in a finite element model. However, anticipating that the pipeline will slide only along a locally flat ocean bottom makes it advantageous to describe the generalized coordinates with respect to this ocean bottom. If it is further assumed that the ocean bottom is a slowly varying surface over the domain of the pipeline system, it then becomes possible to describe the shared generalized coordinates of any two adjacent elements in terms of the **nodal** coordinate systems at each node. Orienting the **nodal** coordinate systems at each node such that two of the coordinate axes are in the plane of the ocean bottom makes it possible to restrict the non-zero generalized coordinates so that all of the nodes remain in the plane of the ocean bottom. Imposition of this constraint reduces the number of gen-

eralized coordinates at each node from six to three and requires that the pipeline response at each node be limited to sliding in a locally flat facet of the ocean bottom. A solution for the generalized coordinates which produces an equilibrium of generalized forces within the entire pipeline system may be obtained by solving iteratively for the restricted generalized coordinates at each element node. A procedure for transforming element stiffnesses, forces, and generalized coordinates between the coordinate systems for assemblage in a system of simultaneous equations which models the response of the continuous pipeline is described in the following subsection.

2.4.2b) **Coordinate Systems and Transformations**

Three distinct sets of coordinate systems will be utilized to evaluate the dynamic response of the entire pipeline system. These sets are: 1) **global** coordinate system (X,Y,Z); 2) **local** or **element** coordinate systems (τ,η,β) associated with each element; and 3) **nodal** coordinate systems $(\hat{\tau},\hat{\eta},\hat{\beta})$ associated with each node. The **global** coordinate system (X,Y,Z) establishes the pipeline system relative to its environment. The **local** coordinate system (τ,η,β) of each element defines the orientation of the element and its associated generalized coordinates and forces. The **element** coordinate system, (τ,η,β) shown in Figure 4 is now chosen such that the β direction corresponds to the upward perpendicular to the ocean bottom at the mid point of the element. The **nodal** coordinate system $(\hat{\tau},\hat{\eta},\hat{\beta})$ at each node provides a means of constraining the motion of the pipeline to sliding only along the ocean bottom,

while effectively reducing the number of generalized coordinates for which a solution is required. The $\hat{\beta}$ axis at a given node is defined by the upward normal to the ocean bottom at that node. The $\hat{\tau}$ axis at a node is defined such that it bisects the τ axes of adjoining elements.

Transformation of the responses of an individual element to a mutual **global** coordinate system requires a relationship between the **global** forces ($\mathbf{F}_x$, $\mathbf{F}_y$, and $\mathbf{F}_z$) and the equivalent **local** forces ($\mathbf{F}_\tau$, $\mathbf{F}_\eta$, and $\mathbf{F}_\beta$) in the **local** coordinate system. By analytical geometry, it can be shown [McGuire and Gallagher (1979)] that

$$\begin{Bmatrix} \mathbf{F}_\tau \\ \mathbf{F}_\eta \\ \mathbf{F}_\beta \end{Bmatrix} = \begin{bmatrix} \boldsymbol{\ell}_1 & \mathbf{m}_1 & \mathbf{n}_1 \\ \boldsymbol{\ell}_2 & \mathbf{m}_2 & \mathbf{n}_2 \\ \boldsymbol{\ell}_3 & \mathbf{m}_3 & \mathbf{n}_3 \end{bmatrix} \begin{Bmatrix} \mathbf{F}_x \\ \mathbf{F}_y \\ \mathbf{F}_z \end{Bmatrix} \tag{2.4-12}$$

in which $\boldsymbol{\ell}_i$ = direction cosines between the **global** X axis and the **local** $\tau(i = 1)$, $\eta(i = 2)$, and $\beta(i = 3)$ axes; $\mathbf{m}_i$ = direction cosines between the **global** Y axis and the local $\tau(i = 1)$, $\eta(i = 2)$, and $\beta(i = 3)$ axes; and $\mathbf{n}_i$ = direction cosines between the **global** Z axis and the **local** $\tau(i = 1)$, $\eta(i = 2)$, and $\beta(i = 3)$ axes. Equation (2.4-12) is a matrix expression which can be used to transform any vector quantity (displacement, rotation, force, or moment) between the **global** coordinate system and the **local** coordinate system. The transformation maxtrix given by Eq. (2.4-12) may be used to obtain the relationship between **local** and **global** generalized coordinates according to

$$\underset{\{12 \times 1\}}{\{\mathbf{d}\}} = \underset{[12 \times 12]}{\begin{bmatrix} \mathbf{\Lambda} & 0 & 0 & 0 \\ 0 & \mathbf{\Lambda} & 0 & 0 \\ 0 & 0 & \mathbf{\Lambda} & 0 \\ 0 & 0 & 0 & \mathbf{\Lambda} \end{bmatrix}} \underset{\{12 \times 1\}}{\{\mathbf{D}\}} \tag{2.4-13a}$$

or

$$\{\mathbf{d}\} = [\mathbf{T}_1]\{\mathbf{D}\} \tag{2.4-13b}$$

in which

$$[\Lambda] = \begin{bmatrix} \ell_1 & m_1 & n_1 \\ \ell_2 & m_2 & n_2 \\ \ell_3 & m_3 & n_3 \end{bmatrix} \quad ; \quad [\mathbf{T}_1] = \begin{bmatrix} \mathbf{\Lambda} & 0 & 0 & 0 \\ 0 & \mathbf{\Lambda} & 0 & 0 \\ 0 & 0 & \mathbf{\Lambda} & 0 \\ 0 & 0 & 0 & \mathbf{\Lambda} \end{bmatrix} \quad ; \tag{2.4-13c}$$

$\{\mathbf{d}\}$ = the vector of local generalized coordinates for an element defined by Eq. (2.4-2c); and $\{\mathbf{D}\}$ = the global components of generalized coordinates which correspond to the elements of $\{\mathbf{d}\}$. The matrix $[\mathbf{T}_1]$ is the transformation matrix from the **global** coordinate system to the **local** element coordinate system. Because both coordinate systems are orthogonal [Cook (1981)] the transformation matrix $[\mathbf{T}_1]$ has the property that

$$[\mathbf{T}_1]^{-1} = [\mathbf{T}_1]^{\mathrm{T}} \ . \tag{2.4-14}$$

This property is useful in transforming the **local** equilibrium expression for an individual element into the **global** coordinate system where the equations would normally be combined and solved simultaneously. To demonstrate this transformation, the **local**

equilibrium equation for an individial element which has a linear dynamic response to a nonlinear applied load is given by

$$[\mathbf{m}]^{t+\Delta t}\{\ddot{\mathbf{d}}\} + {}^{t+\Delta t}[\mathbf{k}]^{t+\Delta t}\{\mathbf{d}\} = {}^{t+\Delta t}\{\mathbf{r}\} \qquad (2.3\text{-}6)$$

which is equivalent to

$$[\mathbf{m}][\mathbf{T}_1]^{t+\Delta t}\{\ddot{\mathbf{D}}\} + {}^{t+\Delta t}[\mathbf{k}][\mathbf{T}_1]^{t+\Delta t}\{\mathbf{D}\} = [\mathbf{T}_1]^{t+\Delta t}\{\mathbf{R}\} \qquad (2.4\text{-}15a)$$

in which $\{\mathbf{R}\}$ = the global components of the generalized load vector whose terms correspond to the terms of $\{\mathbf{r}\}$. Premultiplying Eq. (2.4-15a) by $[\mathbf{T}_1]^T$ yields

$$[\mathbf{T}_1]^T[\mathbf{m}][\mathbf{T}_1]^{t+\Delta t}\{\ddot{\mathbf{D}}\} + [\mathbf{T}_1]^{T(t+\Delta t)}[\mathbf{k}][\mathbf{T}_1]^{t+\Delta t}\{\mathbf{D}\} = {}^{t+\Delta t}\{\mathbf{R}\} \qquad (2.4\text{-}15b)$$

Equation (2.4-15b) defines the equilibrium of an element in terms of the generalized **global** coordinates. If the equilibrium expressions for each element are transformed to the **global** coordinate system, the global stiffnesses and mass representations of all elements can be combined with respect to their shared generalized coordinates. The total equilibrium expression for the pipe system may then be evaluated iteratively for the generalized **global** coordinates which produce equilibrium. Solving for the generalized

global coordinates in this iterative manner requires the evaluation of six degrees of freedom at each pipe node.

In order to reduce the computational effort required to solve for the dynamic response of the entire pipeline, as well as to constrain the motion of the pipeline to sliding only along the ocean bottom, the **global** equilibrium for each element given by Eq. (2.4-15b) can be transformed to the i and j **nodal** coordinate systems associated with an individual element. For the response of the element to be constrained exclusively to sliding, the only nonzero generalized coordinates in a **nodal** coordinate system are the translations in the $\hat{\tau} - \hat{\eta}$ plane and the rotations about the $\hat{\beta}$ axis. The general transformation between the **global** degrees of freedom $\{\mathbf{D}\}$ and the **nodal** degrees of freedom has the form

$$\underset{\{12 \times 1\}}{\begin{Bmatrix} \mathbf{u} \end{Bmatrix}} = \underset{[12 \times 12]}{\begin{bmatrix} \mathbf{\Lambda}_i & 0 & 0 & 0 \\ 0 & \mathbf{\Lambda}_i & 0 & 0 \\ 0 & 0 & \mathbf{\Lambda}_j & 0 \\ 0 & 0 & 0 & \mathbf{\Lambda}_j \end{bmatrix}} \underset{\{12 \times 1\}}{\begin{Bmatrix} \mathbf{D} \end{Bmatrix}} \qquad (2.4\text{-}16)$$

in which $[\mathbf{\Lambda}]$ = a 3 x 3 vector transformation matrix which contains the direction cosines between the **global** coordinate axes and the i or j (denoted by the subscript) **nodal** coordinate axes. For the special case when the components of $\{\mathbf{u}\}$ are constrained to remain in the $\hat{\eta} - \hat{\tau}$ plane for both the i and j nodes, the transformation relationship reduces to

$$\{\hat{u}\} = [T_2] \quad \{D\} \qquad (2.4\text{-}17a)$$

$\{6x1\}$ $[6x12]$ $\{12x1\}$

in which $\{\hat{u}\}$ = the non-zero components of the i and j generalized coordinates expressed in **nodal** coordinate systems;

$$\{\hat{u}\} = \begin{Bmatrix} u_1 \\ u_2 \\ u_6 \\ u_7 \\ u_8 \\ u_{12} \end{Bmatrix} ; \qquad (2.4\text{-}17b)$$

and in which $[T_2]$ is defined in Figure 2.10.

Using the transformation from the generalized **global** coordinates to the constrained **nodal** coordinates, Eq. (2.4-15b) is transformed from **global** to **nodal** coordinates in a manner similar to the transformation from Eq.(2.3-6) to Eq. (2.4-15b). Transforming Eq. (2.4-15b) to nodal coordinates yields

$$[\hat{m}]^{t+\Delta t}\{\ddot{\hat{u}}\} + {}^{t+\Delta t}[\hat{k}]^{t+\Delta t}\{\hat{u}\} = {}^{t+\Delta t}\{\hat{q}\} \qquad (2.4\text{-}18a)$$

$[6x6]$ $\{6x1\}$ $[6x6]$ $\{6x1\}$ $\{6x1\}$

in which $[\hat{m}]$ = the constrained mass representation for an element given by

$$[\hat{m}] = [T_2]\,[T_1]^T[m][T_1][T_2]^T ; \qquad (2.4\text{-}18b)$$

Figure 2.10 Definition of the transformation matrix from global to nodal coordinate system in which I and J denote the i and j nodes of a given element.

$$[T_2] = \begin{bmatrix} \ell_{1I} & m_{1I} & n_{1I} & 0 & 0 & 0 & 0 & 0 & 0 & 0 & 0 & 0 \\ \ell_{2I} & m_{2I} & n_{2I} & 0 & 0 & 0 & 0 & 0 & 0 & 0 & 0 & 0 \\ 0 & 0 & 0 & \ell_{3I} & m_{3I} & n_{3I} & 0 & 0 & 0 & 0 & 0 & 0 \\ 0 & 0 & 0 & 0 & 0 & 0 & \ell_{1J} & m_{1J} & n_{1J} & 0 & 0 & 0 \\ 0 & 0 & 0 & 0 & 0 & 0 & \ell_{2J} & m_{2J} & n_{2J} & 0 & 0 & 0 \\ 0 & 0 & 0 & 0 & 0 & 0 & 0 & 0 & 0 & \ell_{3J} & m_{3J} & n_{3J} \end{bmatrix}$$

$^{t+\Delta t}[\hat{k}]$ = the constrained stiffness of an element given by

$$^{t+\Delta t}[\hat{k}] = [T_2]\ [T_1]^T\ ^{(t+\Delta t)}[k][T_1][T_2]^T \ ; \qquad (2.4\text{-}18c)$$

and $^{t+\Delta t}\{\hat{q}\}$ = the constrained applied loads given by

$$\{\hat{q}\} = \begin{Bmatrix} q_1 \\ q_2 \\ q_6 \\ q_7 \\ q_8 \\ q_{12} \end{Bmatrix} \qquad (2.4\text{-}18d)$$

Transformation of the equilibrium relationship given by Eq. (2.3-6) to Eq. (2.4-18a) reduces the degrees of freedom associated with each element, and restricts the response of the elements to sliding only in the local facets defined by the **nodal** coordinate systems to which they adjoin. Because the mutual degrees of freedom between two adjacent elements are defined by a common **nodal** coordinate system, the resulting nodal equations at each node can be combined and solved iteratively for the equilibrium of the entire pipeline system. Combining the individual element equations to model the entire pipeline system yields

$$[\hat{M}]\ ^{t+\Delta t}\{\ddot{\hat{U}}\} + ^{t+\Delta t}[\hat{K}]\ ^{t+\Delta t}\{\hat{U}\} = ^{t+\Delta t}\{\hat{Q}\} \qquad (2.4\text{-}19)$$

in which

$$[\hat{M}] = \Sigma\ [\hat{m}]; \qquad ^{t+\Delta t}[\hat{K}] = \Sigma\ ^{t+\Delta t}[\hat{k}];$$

and in which $^{t+\Delta t}[\hat{U}]$ = the constrained nodal degrees of freedom of the pipeline system; and $^{t+\Delta t}\{\hat{Q}\}$ = the constrained generalized forces which are applied to the pipeline system.

Solving for the constrained nonlinear dynamic response of the entire pipeline system requires that Eq. (2.4-10) be transformed and combined in the same manner in which Eq. (2.3-6) was transformed and combined to yield Eq. (2.4-19). Because this transformation and subsequent combinations are analogous to those previously derived, the transformation of Eq. (2.4-10) will not be presented explicitly.

2.4.3 **Environmental Loadings**

Current pipeline design practices attempt to establish stability along the entire pipeline system. However, extreme wave episodes may result in wave-induced hydrodynamic pressures along the pipeline which are capable of initiating pipeline motion. During these extreme wave episodes, the dynamic pipeline response may be calculated using the finite element model described in Section (2.4.1c) as modified by the constraints of Section (2.4.2). Application of the finite element method requires that the continuous distribution of environmental force loadings along the pipeline be represented by discrete generalized forces.

The total environmental forces applied to the pipeline system are predicted by defining the generalized loading, $\{\mathbf{r}\}$, on each of the individual elements used to model the pipeline. The **local** forces on each of the elements are then transformed to the **nodal** coordinate systems and combined to yield the generalized **nodal**

forces, $\{\hat{Q}\}$. Because definition of the **local** forces applied to each element determines the generalized **nodal** forces necessary to evaluate pipeline response, evaluation of the applied pipeline forces is directed toward establishing the **local** element forces, $\{r\}$,for an individual element.

2.4.3a **Fluid Loading**

Considering the pipeline to be a small compliant body, it is accepted practice [cf. Lambrakos (1982), Karal and Halvorsen (1982)] to represent hydrodynamic loadings using a relative-motion Morison equation. The relative-motion Morison equation defines the components of the load per unit length of the pipeline in terms of a hydrodynamic lift, drag, and inertial force. Using the relative-motion Morison equation, the dynamic wave-induced pressure forces per unit length of pipeline are

$$F_\beta = .5C_L\rho_o D(v - \dot{u}_2)^2 \qquad \text{(lift)} \qquad (2.4\text{-}20a)$$

$$F_\eta = .5C_D\rho_o D(v - \dot{u}_2)|v - \dot{u}_2| + .25\pi\rho_o D^2 C_M[\dot{v} - (1 - \frac{1}{C_M})\ddot{u}_2]$$

$$\text{(drag and inertial)} \qquad (2.4\text{-}20b)$$

$$F_\tau = 0 \qquad (2.4\text{-}20c)$$

in which F_τ, F_η, and F_β = the distributed dynamic fluid loadings corresponding to the intrinsic τ,η, and β coordinate system shown in Fig. 2.1; v = fluid velocity in the intrinsic η direction; D =

pipeline diameter; C_L, C_D and C_M = lift, drag and inertial coefficients, respectively; ρ_o = fluid mass density; and u_2 = the intrinsic η component of pipeline displacement defined in Fig. 2.2. Equations (2.4-20) express the distributed wave-induced load components along the entire pipeline in an intrinsic coordinate system. The **local** coordinate systems for each individual element were established (Section 2.4-2b) to approximate the intrinsic coordinate system shown in Fig. 2.1. Therefore, Eqs. (2.4-20) define the wave-induced distribution on a given element in terms of the **local** coordinate system of the element. Having defined the distribution of the wave-induced dynamic fluid forces along a given element, it is necessary to represent this loading in terms of generalized **local** forces. Nonlinearities in the lift and drag forces on an element complicate the representation of the dynamic fluid forces [cf. Anagnostopoulos (1982) and Penzien and Teng (1978)]. In order to maintain a fully nonlinear representation for drag forces while preserving computational efficiency, a lumped-force approximation was adopted for the present simulation. A lumped-force formulation uncouples the interaction between applied forces at opposite ends of an element and simplifies the representation of the wave-induced hydrodynamic forces and of the linear-Taylor expansion of the hydrodynamic forces. Using a **lumped-force** formulation, the generalized wave-induced dynamic fluid forces at either end of an element are represented by the relative-motion Morison equation as a force per unit length (acting at the respective element end) distributed over one-half the element length.

Because lumped forces are uncoupled, the element load vector, $\{\mathbf{r}\}$, contains no moment components. Furthermore, if it is assumed that the **local** element β axis coincides closely with its associated **modal** $\hat{\beta}$ axis, then it is unnecessary to include lift forces in the element load vector because the constraints specified in Section (2.4.2) negate the influence of a lift force. To ensure that the element **local** coordinate systems and adjacent **nodal** coordinate systems vary slowly, it is necessary to refine the discretization of the pipeline system in areas where changes in the topography of the ocean bottom are more pronounced.

The linear-Taylor expansion of the generalized force vector $\{\mathbf{r}\}$ is given by

$$\{\mathbf{r}^k\} = \{\mathbf{r}^{k-1}\} + \left[\frac{\partial \mathbf{r}}{\partial \mathbf{d}}\right]_{\mathbf{d}^{k-1}} \{\Delta \mathbf{d}^{k-1}\} \ . \tag{2.4-21}$$

Neglecting the effects of lift and considering only the wave-induced dynamic fluid loadings, the components of Eq. (2.4-21) (for lumped forces) are given by

$$\mathbf{r}_i^{k-1} = 0 \qquad i \neq 2,8 \tag{2.4-22a}$$

$$\mathbf{r}_i^{k-1} = .25\, C_D \rho_o LD \left| v_i - \dot{\mathbf{d}}_i^{k-1} \right| (v_i - \dot{\mathbf{d}}_i^{k-1}) +$$

$$.125\pi \rho_o LD^2 C_M [\dot{v}_i - (1 - \frac{1}{C_M}) \ddot{\mathbf{d}}_i^{k-1}]$$

$$i = 2,8 \tag{2.4-22b}$$

and

$$\frac{\partial \mathbf{r}}{\partial \mathbf{d}}ij = 0 \qquad i \neq j \neq 2,8 \qquad (2.2\text{-}22c)$$

$$\frac{\partial \mathbf{r}}{\partial \mathbf{d}}ij = .5 \frac{\delta}{\alpha \Delta t} \rho_o L C_D D \left| v_i - \dot{\mathbf{d}}_i^{k-1} \right| + \frac{.125\pi}{\alpha \Delta t^2} \rho_o L D^2 (C_M - 1)$$

$$i = j = 2,8 \qquad (2.2\text{-}22d)$$

in which $\mathbf{r}_i$ = i^{th} component of the load vector $\{\mathbf{r}\}$; v_i = component of fluid velocity corresponding to generalized velocity $\mathbf{d}_i$; $\mathbf{d}_i$ = the i^{th} component of generalized coordinate vector $\{\mathbf{d}\}$; $\frac{\partial \mathbf{r}}{\partial \mathbf{d}}ij$ = the ij matrix component of $\left[\frac{\partial \mathbf{r}}{\partial \mathbf{d}}\right]_{\mathbf{d}^{k-1}}$ (i and j denoting position by row and column); δ and α = Newmark-beta integration parameters; and Δt = the time step for temporal integration.

Equations (2.4-22) define the nonlinear hydrodynamic load representation on an individual element. Hydrostatic pressure on the pipe cross-section produces an additional fluid load which modifies the pipeline response. Effects from hydrostatic pressure occur when a pressure differential between the internal operating pressure of the pipeline system and the surrounding fluid exists. This pressure differential creates a circumferential and a longitudinal stress in the pipeline. The resulting longitudinal stress, if compressive, will degrade the flexural stiffness of each element as reflected by the geometric stiffness of the element. Inclusion of the pressure differential in the solution algorithm is achieved by treating the longitudinal stress developed by this pressure differential as a pre-existing axial force within an element.

Treatment of the hydrostatic pressure effect within the solution algorithm assumes that the vertical displacment of each element is small and that changes in the pressure differential with time may be neglected. Under these conditions, the axial prestress in each element is calculated according to [Sandor (1978)]

$$\sigma_o = \frac{(PR + \rho_o g Z_{ave})D}{4WT} \qquad (2.4\text{-}23)$$

in which σ_o = initial axial stress; g = gravitational constant; Z_{ave} = the Z coordinate at the element mid point; PR = internal pipeline pressure; and WT = wall thickness of the load bearing pipeline cross-section. Since $Z_{ave} < 0.0$ in Eq. (2.4-23), deep-water pipeline systems operating at high internal pressures would normally be subjected to tensile initial stresses ($\sigma_0 > 0.0$) .

Evaluation of hydrodynamic forces using the Morison equation is dependent upon the proper selection of the coefficients C_D, C_M and C_L. In the present formulations these coefficients are assumed to be constants which may be selected independently for each element. Appropriate choice of these force coefficients is dependent upon the fluid flow regime and pipeline characteristics. Guidance in selecting the proper force coefficients has been given by Beckmann and Thibodeaux (1962), Brown (1967), Chakrabarti (1980), Grace, et al (1979), Sarpkaya (1975), Huang and Hudspeth (1982), Sarpkaya (1977), and Yamamoto, et al, (1973).

The fluid kinematics required during a simulated wave episode are obtained from linear wave theory. Linear wave theory results

in a boundary value problem for a scalar velocity potential which describes the irrotational flow of an incompressible, inviscid fluid.

The use of a scalar velocity potential to describe the flow field provides a linear relationship between the velocity potential and the fluid kinematics or the free surface [cf. Sarpkaya and Isaacson (1981) for further discussion of these relationships]. For a monochromatic, surface gravity wave given by

$$N_w(X,Y,t) = B \cos(\kappa X \cos\Theta + \kappa Y \sin\Theta - \omega t + \Phi) \qquad (2.4\text{-}24)$$

in which N_w = free surface profile; B = wave amplitude; κ = wave number (rad/length); ω = wave frequency (2π/period); Θ = wave angle relative to the **global** X axis; and Φ = phase shift, the fluid kinematics at any point in the flow field are given by

$$v_x(X,Y,Z,t) = B \frac{g\kappa}{\omega} \frac{\cosh(\kappa(Z+h))}{\cosh(\kappa h)} \cos\Theta \cos(\kappa X \cos\Theta + \kappa Y \sin\Theta - \omega t + \Phi) \qquad (2.4\text{-}25a)$$

$$v_y(X,Y,Z,t) = B \frac{g\kappa}{\omega} \frac{\cosh(\kappa(Z+h))}{\cosh(\kappa h)} \sin\Theta \cos(\kappa X \cos\Theta + \kappa Y \sin\Theta - \omega t + \Phi) \qquad (2.4\text{-}25b)$$

and

$$\dot{v}_x(X,Y,Z,t) = Bg\kappa \frac{\cosh(\kappa(Z+h))}{\cosh(\kappa h)} \cos\Theta \sin(\kappa X \cos\Theta +$$

$$\kappa Y \sin \Theta - \omega t + \Phi) \qquad (2.4\text{-}25c)$$

$$\dot{v}_y\,(X,Y,Z,t) = -Bg\kappa \frac{\cosh\,(\kappa(Z+h))}{\cosh\,(\kappa h)} \sin \Theta \sin\,(\kappa X \cos \Theta +$$

$$\kappa Y \sin \Theta - \omega t + \Phi) \qquad (2.4\text{-}25d)$$

in which v_x and v_y = X and Y **global** components of the fluid velocity; $\dot{v}_x$ and $\dot{v}_y$ = X and Y **global** components of the fluid acceleration; and h = local water depth at the midpoint of each element.

Equations (2.4-25) demonstrate the relationship between the water surface profile and the fluid kinematics for a monochromatic, surface gravity wave. The real ocean surface is found to be of a more chaotic form than that described by Eq. (2.4-24). However, the surface of a random sea may be represented as a linear sum of a sufficiently large number, N, of monochromatic waves. This type of random ocean surface is given as

$$N(X,Y,t) = \sum_{j=1}^{N} \sum_{n=1}^{N} B_{jn} \cos\,(\kappa_j X \cos n\Delta\Theta +$$

$$\kappa_j Y \sin n\Delta\Theta - j\Delta\omega t + \Phi_{jn}) \qquad (2.4\text{-}26)$$

in which B_{ij} = wave amplitude associated with the ij wave; $\Delta\omega$ = increment in wave frequency; $\Delta\Theta$ = increment in wave angle; κ_j = wave number associated with the jth wave frequency, and Φ_{jn} = a random phase angle associated with the jth wave component in nth

wave direction. Values for the wave amplitudes, B_{jn}, are specified for a given directional wave spectrum by

$$B_{jn} = 2.0 \sqrt{S\ (j\Delta\omega,\ n\Delta\Theta)\ \Delta\omega\Delta\Theta} \qquad (2.4\text{-}27)$$

in which $S(\omega,\Theta)$ = the directional wave spectrum [cf, Borgman (1969) for a discussion of possible theoretical spectral representations]. Once a general representation for the free surface has been obtained for a given random wave simulation, the same linear relationships demonstrated by Eq. (2.4-24) and Eqs. (2.4-25) are employed to compute the fluid kinematics during the random wave simulation. A more in-depth discussion of techniques for random wave simulations is presented by either Borgman (1982) or Sarpkaya and Isaacson (1981).

2.4.3b) **Sediment Loads**

Sediment resistance applied to a bottom supported pipeline system may aid in constraining pipeline motions. In the case of seafloor instabilities, sediment loads may be a principal cause of pipeline displacements and stresses. The discussion in this section, however, will be limited to developing a representation for those sediment loads which act to **resist** wave-or current-induced pipeline motions. These sediment forces may arise from either **cohesive** or **cohesionless** sediments.

Sediment resistance along a pipeline may be modeled using nonlinear springs located at the discrete pipe nodes [Audibert and Nyman (1977), Audibert, Lai, and Bea (1978) and Nyman (1982)]. The

springs are assumed to have a linear elastic-perfectly plastic stress-strain characteristic (Fig. 2.11) which may be determined independently for either **cohesive** or **cohesionless** sediments. This type of sediment resistance model can be easily applied to either **cohesive** or **cohesionless** sediments by defining an elastic-plastic spring which reflects the capacity and yield displacement for a given sediment. Once the spring characteristics have been assigned to pipeline nodes, the effect of resistance on the load vector ${}^{t+\Delta t}\{\mathbf{r}^{k-1}\}$, and on the tangent stiffness matrix ${}^{t+\Delta t}\left[\frac{\partial \mathbf{r}}{\partial \mathbf{d}}\right]_{\mathbf{d}^{k-1}}$ can be included in the application of the Newton-Raphson iterative technique to each element. The transformations developed in Section (2.4.2) are used to constrain the response of the elements to sliding along the ocean floor in the τ-η plane (cf. Fig. 2.1). Consequently, the nonlinear springs constrain only the τ and η translational motions of the i and j nodes for each element.

This simulation is directed toward evaluating the pipeline response only during peak wave episodes. The time interval between these episodes varies; but for the purposes of the proposed simulation, this time interval between episodes is considered to be of sufficient duration to allow the sediment resistive stresses to completely relax. Under these conditions, the hystersis shown in Fig. 2.11 is relaxed **between** episodes but not **during** an episode.

Modeling of the sediment resistance by discrete nonlinear springs provides a computationally efficient means of predicting sediment resistance along the pipeline. A significant feature of this model is its ability to do work through hysteresis [vide.,

Figure 2.11 Sediment resistance model.

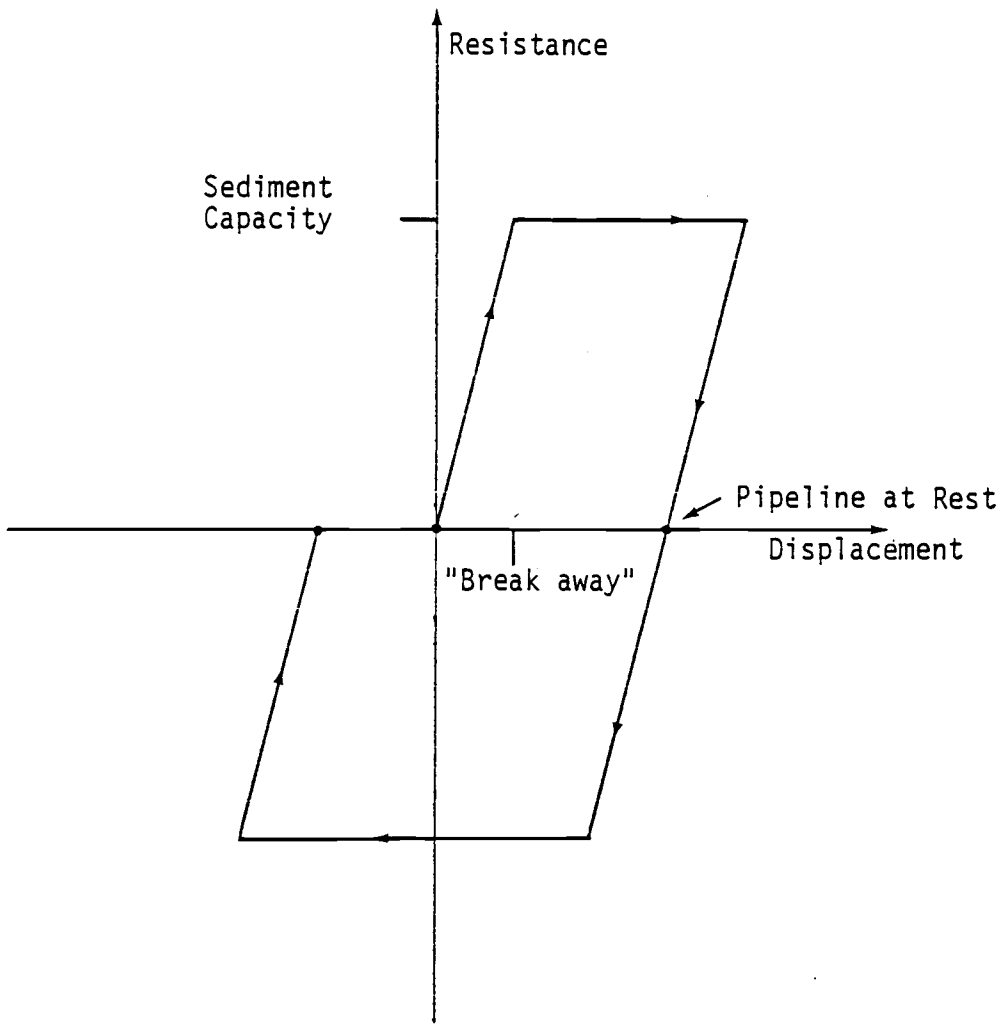

Fig. 2.11]. Other more complex sediment resistance models [e.g., Karal (1977), and Karal and Halvorsen (1982)] were reviewed. These more complex models address a possible **time-dependent** variation in the sediment resistance capacity and attempt to more precisely define the load-resistance curve. A concern for computional efficiency dictated that these more detailed approaches not be incorporated in the present algorithm.

Development of the nonlinear spring characteristics for representing sediment resistance is based upon the **static** capacity of the sediment to resist **lateral** or **axial** displacements of the pipe. Determination of the sediment capacity coupled with an estimate of the deformation necessary to develop this force defines the elastic-plastic characteristics for a given spring. Nonlinear spring models were developed for both **cohesionless** and **cohesive** sediments in both the **lateral** and **axial** modes.

The **lateral** and **axial** resistance of a **cohesionless** sediment to the corresponding displacement of a pipeline element has been shown to be a linear function of the effective weight of the pipeline segment [cf. Anand and Agarwal (1980) and Lyons (1973)]. Sediment resistance determined in this manner can be represented by a Coulomb friction model which has been well-documented in ocean engineering applications [cf. Audibert, Lai and Bea (1978); Corbishley (1982); Huang and Hudspeth (1982); Jones (1976); and Lambrakos (1982)]. The Coulomb friction model for **cohesionless** sediments is given by

$$SC_i = \mu_i (W_s - F_\beta) \qquad ; i = 1(\tau), 2(\eta) \qquad (2.4\text{-}28)$$

in which SC_i = the τ or η component of the sediment resistance capacity; μ_i = the τ or η Coulomb coefficient of friction; W_s = submerged pipe weight; F_β = fluid lift force; and 1 = τ and 2 = η modes. Selection of the Coulomb friction coefficient, μ_i, must be made from **in-situ** sediment data. Recommended values for the Coulomb coefficient of friction appear to be in the range between $0.5 \leq \mu_i \leq 1.5$.

Although the Coulomb friction model has been accepted for evaluating the resistance capacity for a **cohesionless** sediment, there are insufficient data presently available to determine the appropriate yield displacement for the nonlinear Coulomb friction spring. Fortunately, the precise specification of a yield point for the nonlinear spring model is not important for determining the gross dynamic response of a pipeline system that is evaluated only for peak environmental episodes. Consequently, order of magnitude estimates have been used to approximate the breakaway displacements and their corresponding yield stresses. Load deflection data from Lyons (1973) indicate that the yield displacement for the **lateral** deflection of a **cohesionless** sediment is approximately 2.0% of the pipe diameter. Load-deflection graphs from Anand and Agarwal (1980) indicate that the breakaway displacement of the **axial** deformation of a **cohesionless** sediment are approximately 0.2% of the pipe diameter. These values have been incorporated for the nonlinear spring characteristics for a **cohesionless** sediment in the FEM algorithm.

The Coulomb friction model does not appear to be justified for **cohesive** sediments [Karal (1977)]. Comprehensive FEM algorithms for **cohesive** sediment models have been developed which are capable of estimating soil forces very accurately. However, these FEM algorithms cannot be incorporated into a pipeline algorithm without a significant loss of computational efficiency. The nonlinear model that was adopted for determining the resistance capacity for a **cohesive** sediment is a rational balance between the Coulomb friction model and the more elaborate FEM models. The **cohesive** sediment resistance model incorporated in this FEM algorithm was developed by Swanson and Jones (1982). A similar formulation has also been given by Wantland, et.al., (1982). In this nonlinear **cohesive** sediment model, the settlement of the pipeline is first estimated and then passive sediment pressures are used to determine the resistance capacities of the **cohesive** sediment.

In accordance with the development given by Swanson and Jones (1982), the settlement of the pipeline section is determined by balancing the maximum stress under the pipeline, f_d, with the bearing capacity of the **cohesive** sediment, q_d. These stresses are represented by

$$f_d = N_\sigma \frac{W_s}{b} \tag{2.4-29a}$$

and

$$q_d = c\left(1 + \frac{.35s}{b}\right) N_c + \gamma_e s \tag{2.4-29b}$$

in which N_σ = stress coefficient (= 2.5); W_s = submerged pipe

weight; b = width of bearing below the pipe section; N_c = bearing capacity factor(= 5.14); c = average cohesion; s = depth of settlement; and γ_e = submerged unit weight of the sediment. Equating Eqs. (2.4-29a) and (2.4-29b) gives an expression which may be evaluated iteratively to determine the pipe settlement, s.

Having obtained the pipeline settlements, passive sediment pressures determine the **lateral** capacity while skin friction determines the **axial** capacity. **Cohesive** capacities established in this manner are given by [Swanson and Jones (1982)]

$$SC_1 = ca \qquad (2.4\text{-}30a)$$

$$SC_2 = cs\left(3 + \sqrt{\frac{D}{s} - 1}\right) + \frac{3}{2}\gamma_e s^2 \qquad \text{for } \frac{s}{D} < .5 \qquad (2.4\text{-}30b)$$

$$SC_2 = cs\left(3 + \frac{D}{2s}\right) + \frac{3}{2}\gamma_e s^2 \qquad \text{for } \frac{s}{D} > .5 \qquad (2.4\text{-}30c)$$

in which SC_1 = axial sediment capacity; SC_2 = **lateral** sediment capacity; a = contact area; and D = pipe diameter. Sample settlement calculations and corresponding sediment capacities are presented in Table 2.2 for several pipeline sizes and sediment weights. The sediment parameters selected for these calculations were: c = 40 psf, N_σ = 2.5 and N_c = 5.14.

The break away displacements for **cohesive** sediments are again estimated by assuming that the choice of the exact yield point for the nonlinear spring will not significantly affect the gross dynamic response of the pipeline during peak environmental force loading

episodes. Wantland, et al. (1979) have addressed the pipe settlement problem and the subsequent development of the load deflection characteristics for **cohesive** sediments. Their analysis suggests that some relationship exists between pipeline settlement and sediment yield displacement. Rather than attempting to determine this relationship directly from their data, the results from Nyman's investigations (1982) have been adopted. From an examination of Nyman's results, the **lateral** and **axial** breakaway displacements were estimated to be 2.0% of the calculated pipe settlements. It is recognized that the values suggested by Nyman (1982) are specifically identified for **cohesionless** soil and not for **cohesive** marine sediments. However, within the context of the entire pipeline simulation, these values seem to represent a reasonable engineering approximation.

The nonlinear sediment and fluid forces are combined into a single time-varying forcing function $\{\mathbf{r}\}$ which is applied to the individual pipeline elements. Sections (2.4.1) addressed the nonlinear dynamic response of individual elements and Section (2.4.2) described the coupling of these elements. This section has provided a description of the nonlinear sediment loadings that are applied to the pipeline. Application of the Newton-Raphson technique given by Eq. (2.3-8a) provides an estimate for establishing equilibrium at time $t+\Delta t$. The Newmark-beta integration scheme provides a method for coupling sequential time steps during an episode of peak environmental loading. In the next section, an

Table 2.2 Sample calculation for settlement and resistance capacity for pipeline sections on cohesive soils (N_σ = 2.5; N_c = 5.14; c = 40 psf).

Pipe Dia [D (ft)]	Submerged Weight (lb) W_s	Submerged Soil Density γ_e (pcf)	Settlement [s (ft)]	Soil Capacities Axial SC_1 (lb/ft)	Lateral SC_2 (lb/ft)
1.25	76.69	80	.15648	36.16	38.26
1.25	29.7	80	.02486	10.04	14.15
4.0625	663.24	80	2.0727	258.6	845.6
4.0625	255.23	80	.4384	108.78	126.08
1.25	76.69	30	.16806	37.54	38.49
1.25	29.7	30	.02515	14.23	10.07
4.0625	663.24	30	4.245	510.5	1401.4
4.0625	225.23	30	.5201	118.93	128.88

algorithm for simulating the pipeline response to such a peak forcing event is discussed.

2.4.4 Algorithm for Pipeline Simulation

Sections of Chapter 2 have focused on the development of a numerical procedure for predicting the nonlinear dynamic response of a deep ocean pipeline subjected to a random wave environment. This section is a brief summary of an algorithm which utilizes the numerical techniques presented in the previous sections to evaluate the pipeline responses.

For simplicity, a single grid system is used to define the bathymetry, the engineering properties of the sediment, and the fluid kinematics to which the pipeline is exposed. Figure 2.12 demonstrates the sequence in which the FORTRAN programs AGSSIM, AGWSIM and AGAPIP are linked to compute the sediment properties and the fluid kinematics within the grid; and the pipeline response during peak wave episodes.

Separation of the solution algorithm into three main modules provides greater flexibility for simulating a variety of wave and sediment conditions with a minimum of computer core. Directional random seas simulated by AGWSIM provide the linear wave theory fluid kinematics. AGAPIP determines the stochastic values for the sediment properties and fluid kinematics at the pipeline nodes from the values at the grid nodes by means of a Best Linear Unbiased Estimator (BLUE) which interpolates stochastically within the grid network. Values for the sediment parameters are determined at the initial pipeline nodes prior to the initiation of a wave episode

Figure 2.12 General solution algorithm for simulation of pipeline response in a random wave environment.

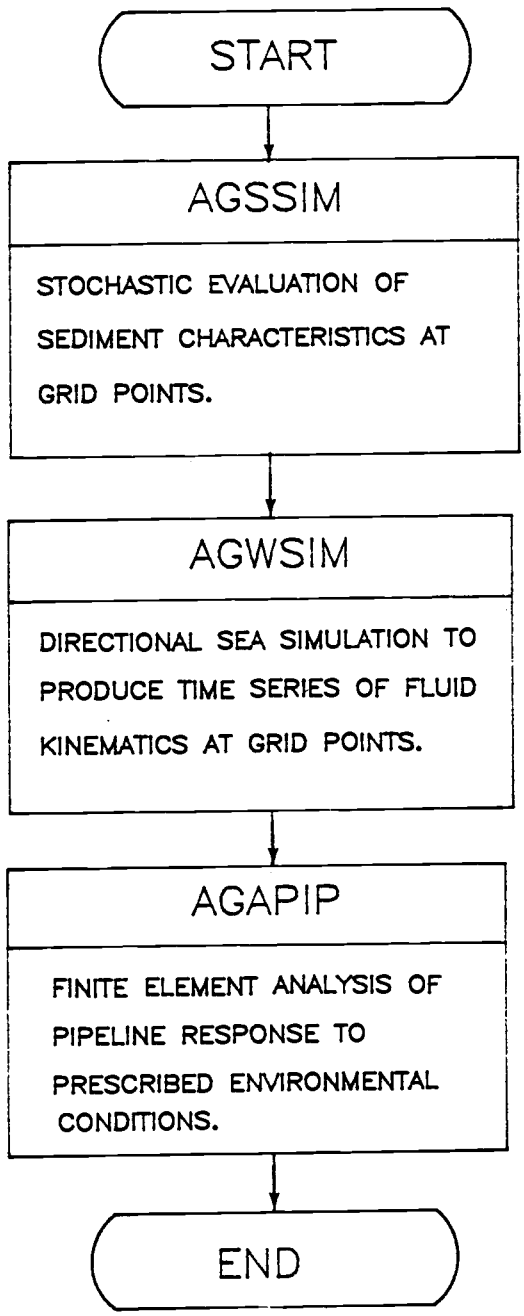

and remain constant during the episode. Fluid kinematics during an episode are updated along the instantaneous pipeline location at a time step which is consistent with the wave simulation time increment used by the FFT algorithms in AGWSIM. Fluid kinematics are treated as constant values during the intermediate solution steps for the pipeline response if they are simulated at discrete time steps which are greater.

Development of the statistical principles necessary to formulate the computer algorithms AGSSIM and AGWSIM is not within the scope of the present discussion pertaining to the evaluation of pipeline response for a prescribed set of environmental conditions. A detailed discussion of these statistical simulation methods have been given by Borgman (1982). With regard to the numerical evaluation of the pipeline response, it is only necessary that the definition of the environmental loads provided by AGSSIM and AGWSIM be in a format which is compatible with the finite element algorithm, AGAPIP. To avoid prohibitive computational expenditures when evaluating pipeline responses, it is advantageous to filter the wave simulation data from AGWSIM and to analyze the pipeline response for a specified sequence of peak wave events only.

A general flow diagram for AGAPIP is illustrated in Fig. 2.13. A detailed description of the program variables and the input/output parameters is given in Appendix A. Figure 2.13 demonstrates that SUBROUTINE DYPIPE performs the analysis of the pipeline response during a peak wave event. The fundamental equation

Figure 2.13 General flow diagram of main PROGRAM AGAPIP.

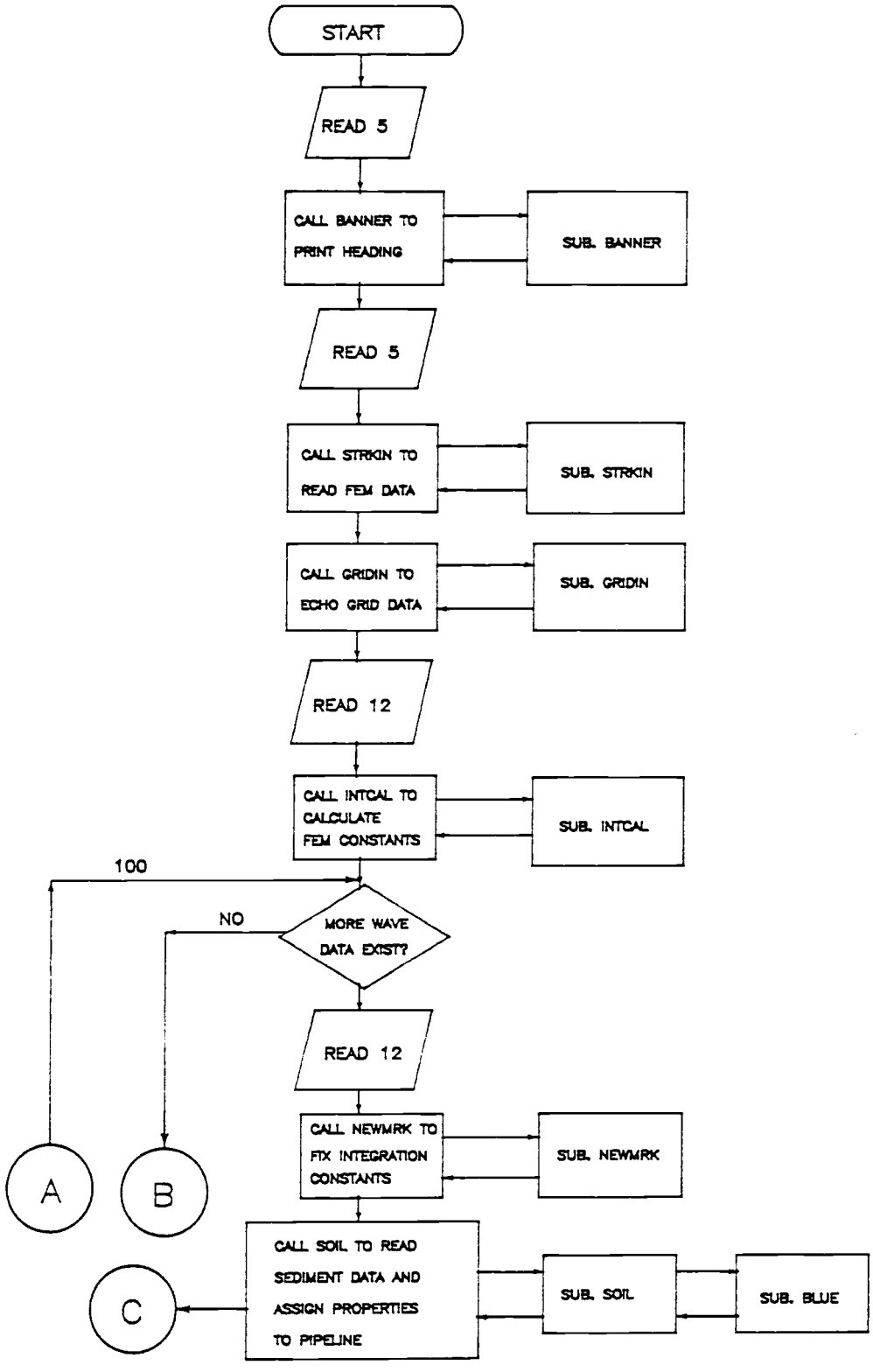

Figure 2.13 (Continued).

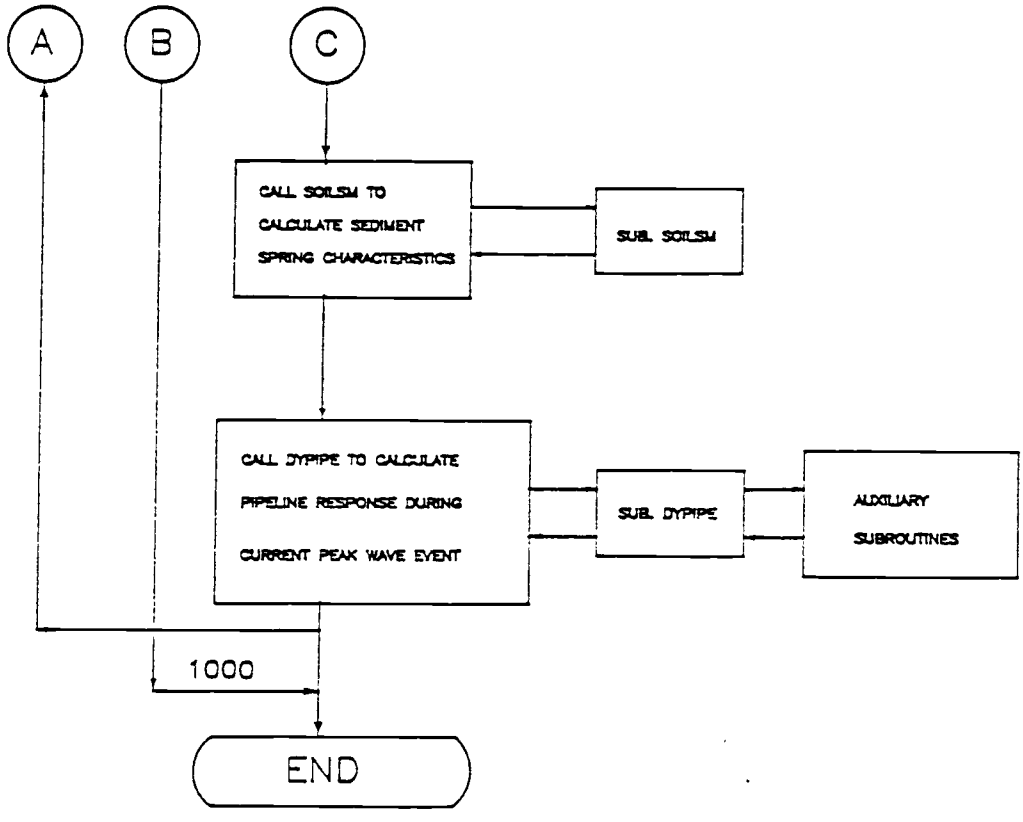

solved in this routine is a linear Tayor series expansion of Eq. (2.4-19). The expansion of this equation has the form

$$ {}^{t+\Delta t}\{\hat{Q}\}^{k-1} - {}^{t+\Delta t}[\hat{K}]_{\hat{\overline{U}}^{k-1}}\,{}^{t+\Delta t}\{\hat{\overline{U}}\}^{k-1} - [\hat{M}]\,{}^{t+\Delta t}\{\hat{\ddot{U}}\}^{k-1} = $$

$$ {}^{t+\Delta t}\left(\frac{1}{\alpha\Delta t^2}[\hat{M}] + [\hat{K}]_{\hat{\overline{U}}^{k-1}} - [\frac{\partial\hat{Q}}{\partial\hat{U}}]\right)^{k-1}\{\Delta\hat{U}\}^{k-1} \qquad (2.4\text{-}31a) $$

or more compactly

$$ {}^{t+\Delta t}\{\mathbf{IMBAL}\}^{k-1} = {}^{t+\Delta t}[T]_{\hat{\overline{U}}^{k-1}}\,{}^{t+\Delta t}\{\Delta\hat{U}\}^{k-1} \qquad (2.4\text{-}31b) $$

in which ${}^{t+\Delta t}\{\mathbf{IMBAL}\}^{k-1}$ = the left hand side of Eq. (2.4-31a) and represents an imbalance of forces; and ${}^{t+\Delta t}[\mathbf{T}]_{\hat{\overline{U}}^{k-1}}$ = **the tangent stiffness** represented by the right hand side of Eq. (2.4-31a). The tangent stiffness matrix, $[\mathbf{T}]$, is formulated within AGAPIP by a procedure which combines the tangent stiffness equations for individual elements into the tangent stiffness matrix for the entire pipeline. An illustration of the matrix $[\mathbf{T}]$ is given in Fig. 2.14. The submatrices, $[\mathbf{t}_i]$, represent the contribution of the element to the tangent stiffness of the entire pipeline. The overlapping of the element tangent stiffness matrices and the sparsity of entire pipeline matrix, $[\mathbf{T}]$, occurs for sequentially numbered pipline nodes. Sequential numbering of the nodes along the pipeline requires the **nodal** generalized coordinates at the end of an element and the **nodal** generalized coordinates at the beginning of the next element along pipeline to be the same. The symbolic over-

Figure 2.14 Tangent stiffness representation of a pipeline [T], in which [t_i] are the submatrix contribution from the ith individual element.

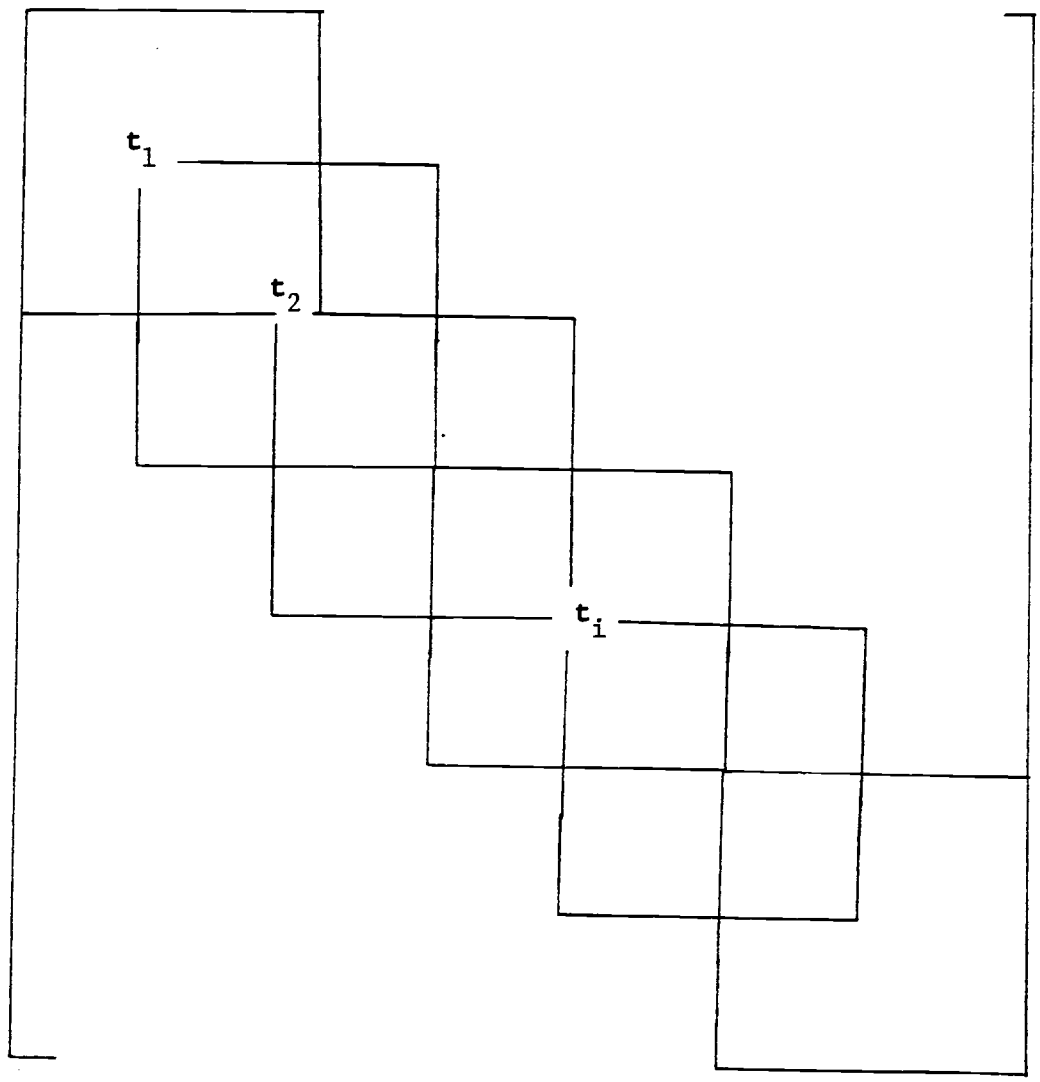

lapping of submatricies in Figure 2.14 represents the matrix addition of those terms in the overlapped areas which results from the required continuity between adjacent elements.

Figure 2.15 depicts an interior element submatrix, $[\mathbf{t}_i]$, for the specialized condition when **global**, **local**, and both **nodal** coordinates system for the element are parallel. Specification of such a constraint permits the illustration of an element tangent stiffness matrix without the complications of transformations between coordinate systems. The nonzero components of the submatrix $[\mathbf{t}_i]$ are listed in Table 2.3. The tangent stiffness contributitions from the elements at the two terminal ends of the pipeline are similar to that of a general element shown in Fig. 2.15 except that the rows and columns of the submatrix are deleted. These deleted rows and columns correspond to the **prescribed** boundary conditions of the generalized coordinates.

To illustrate the solution algorithm employed for predicting the dynamic pipeline response, a general flow diagram of the SUBROUTINE DYPIPE is shown in Figure 2.16. The major variables in SUBROUTINE DYPIPE are defined in Appendix A. Figure 2.16 shows that Eq. (2.4-31b) is evaluated iteratively throughout an episode by a nested loop which formulates the contribution from an element; assembles the tangent stiffness array for the entire pipeline; and computes an incremental correction to the position of the pipeline for the given imbalance of forces.

The core of the finite element solution technique that has been formulated in Chapter 2 is represented in Fig. 2.15. A number

Figure 2.15 Tangent stiffness matrix, $[t_i]$, for an interior pipe element when the coordinate transformation matrices $[T_1]$,and $[T_2]$ correspond to the identity matrix.

$$\begin{bmatrix} t_{11} & 0 & 0 & t_{14} & 0 & 0 \\ & t_{22} & t_{23} & 0 & t_{25} & t_{26} \\ & & t_{33} & 0 & t_{35} & t_{36} \\ & & & t_{44} & 0 & 0 \\ & \text{Symmetric} & & & t_{55} & t_{56} \\ & & & & & t_{66} \end{bmatrix}$$

Table 2.3. Contributory components of the element tangent stiffness submatrix [t] as given in Figure 2.15. Subscript i or j indicating i or j nodal quantity and S_A and S_L refer to the axial and lateral sediment spring stiffness respectively.

$$t_{11} = S_{Ai} + \frac{mL}{2\alpha\Delta t^2} + \frac{EA}{L} + \frac{p}{L}$$

$$t_{14} = t_{41} = \frac{-EA}{L} - \frac{p}{L}$$

$$t_{22} = S_{Li} + \frac{mL}{2\alpha\Delta t^2} + \frac{12EI}{L^3} + \frac{6p}{L} + \frac{\delta\rho_o L}{2\alpha\Delta t} C_D D\left|v_i - \dot{d}_2^{k-1}\right| + \frac{\pi\rho_o LD^2}{8\alpha\Delta t^2}(C_M - 1.0)$$

$$t_{23} = t_{32} = \frac{6EI}{L^2} + \frac{p}{10}$$

$$t_{25} = t_{52} = -\frac{12EI}{L^3} - \frac{6p}{5L}$$

$$t_{26} = t_{62} = \frac{6EI}{L^2} + \frac{p}{10}$$

$$t_{33} = \frac{4EI}{L} + \frac{2pL}{15}$$

$$t_{35} = t_{53} = -\frac{6EI}{L^2} - \frac{p}{10}$$

$$t_{36} = t_{63} = \frac{2EI}{L} - \frac{pL}{30}$$

$$t_{44} = S_{Aj} + \frac{mL}{2\alpha\Delta t^2} + \frac{EA}{L} + \frac{p}{L}$$

$$t_{55} = S_{Lj} + \frac{mL}{2\alpha\Delta t^2} + \frac{12EI}{L^3} + \frac{6p}{L} + \frac{\delta\rho_o L}{2\alpha\Delta t} C_D D\left|v_j - \dot{d}_8^{k-1}\right| + \frac{\pi\rho_o LD^2}{8\alpha\Delta t^2}(C_M - 1.0)$$

$$t_{56} = t_{65} = -\frac{6EI}{L^2} - \frac{p}{10}$$

$$t_{66} = \frac{4EI}{L} + \frac{2pL}{15}$$

Figure 2.16 General flow diagram of algorithm employed by SUBROUTINE DYPIPE.

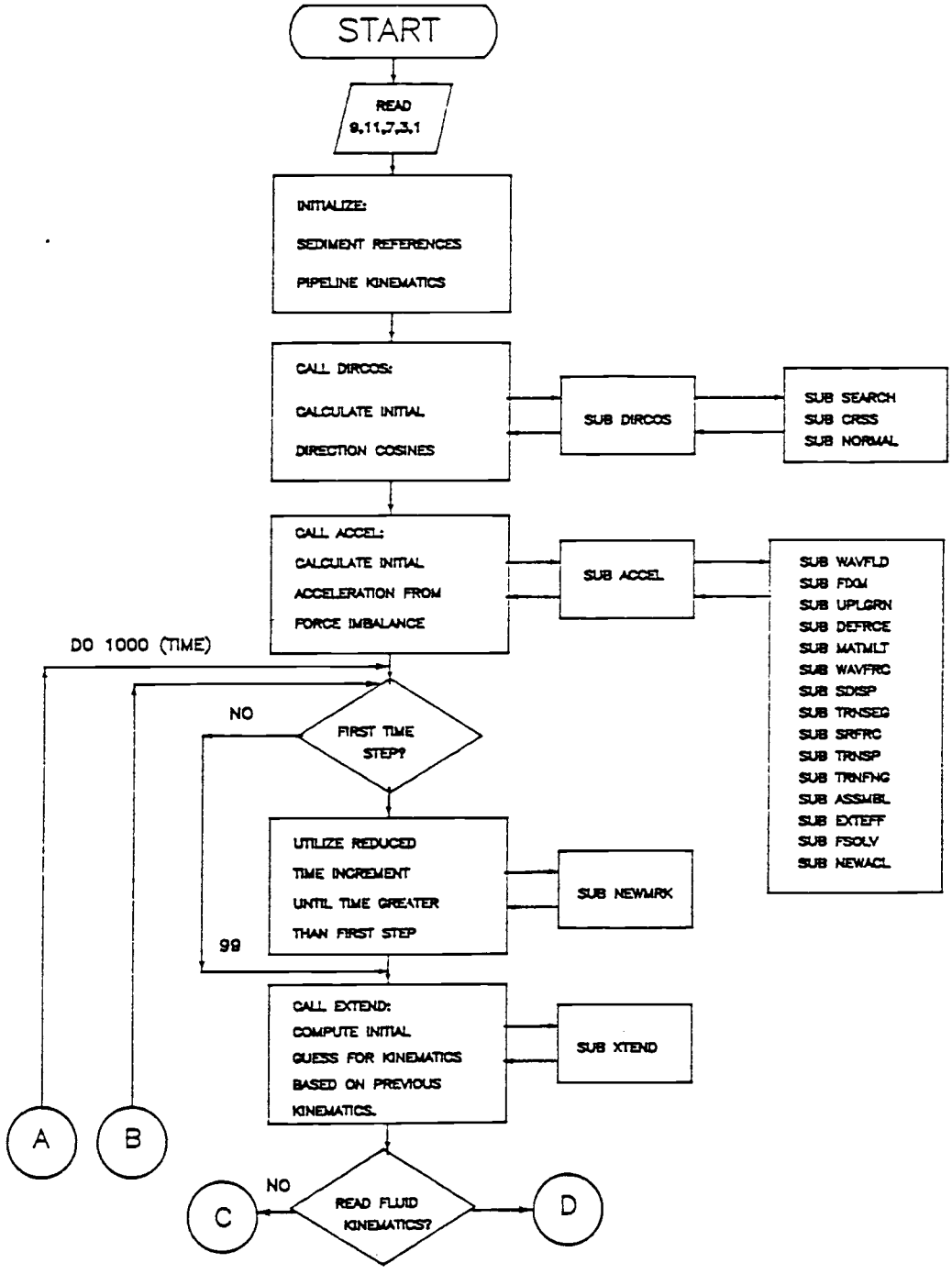

Figure 2.16 (Continued).

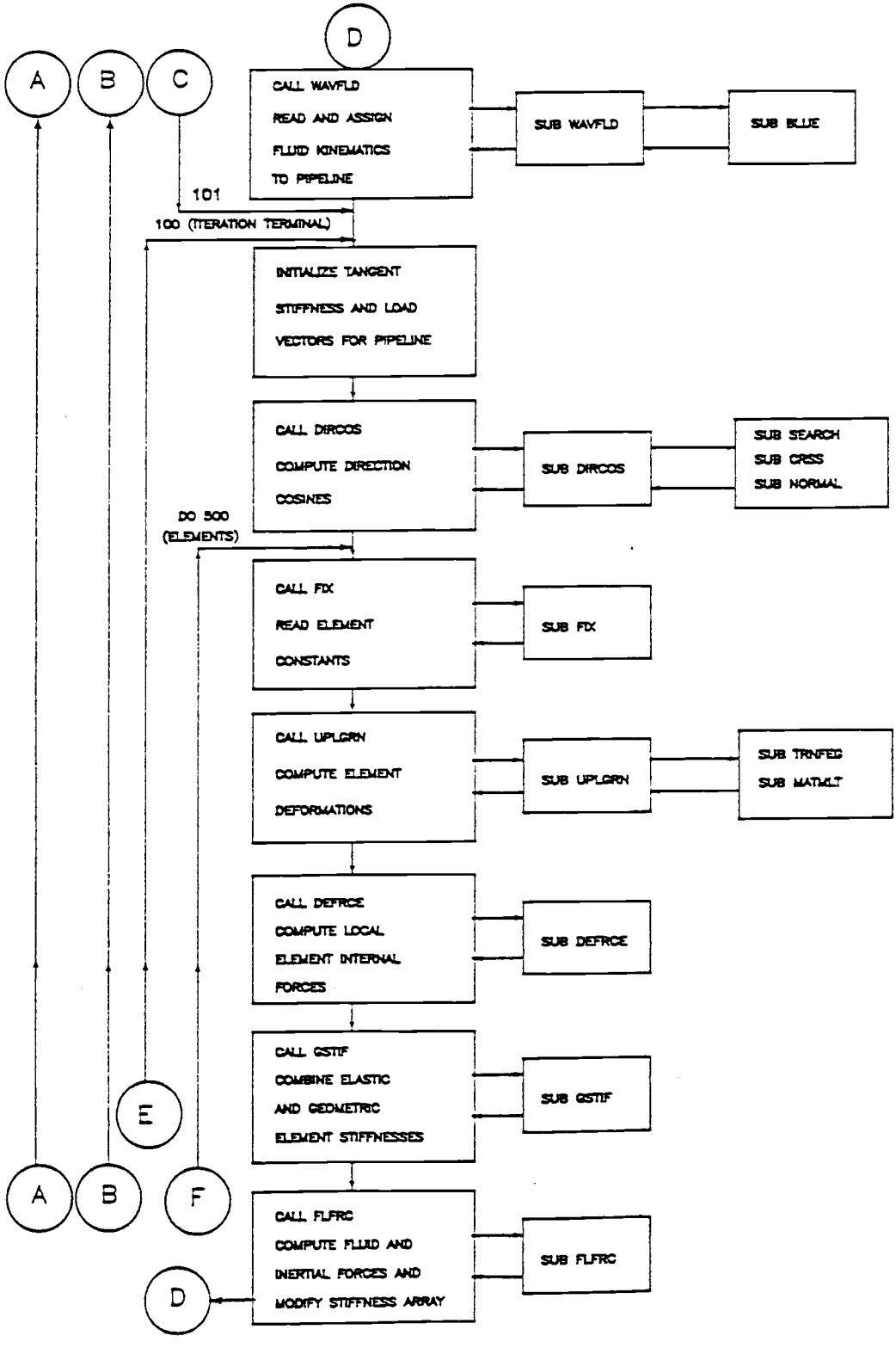

Figure 2.16 (Continued).

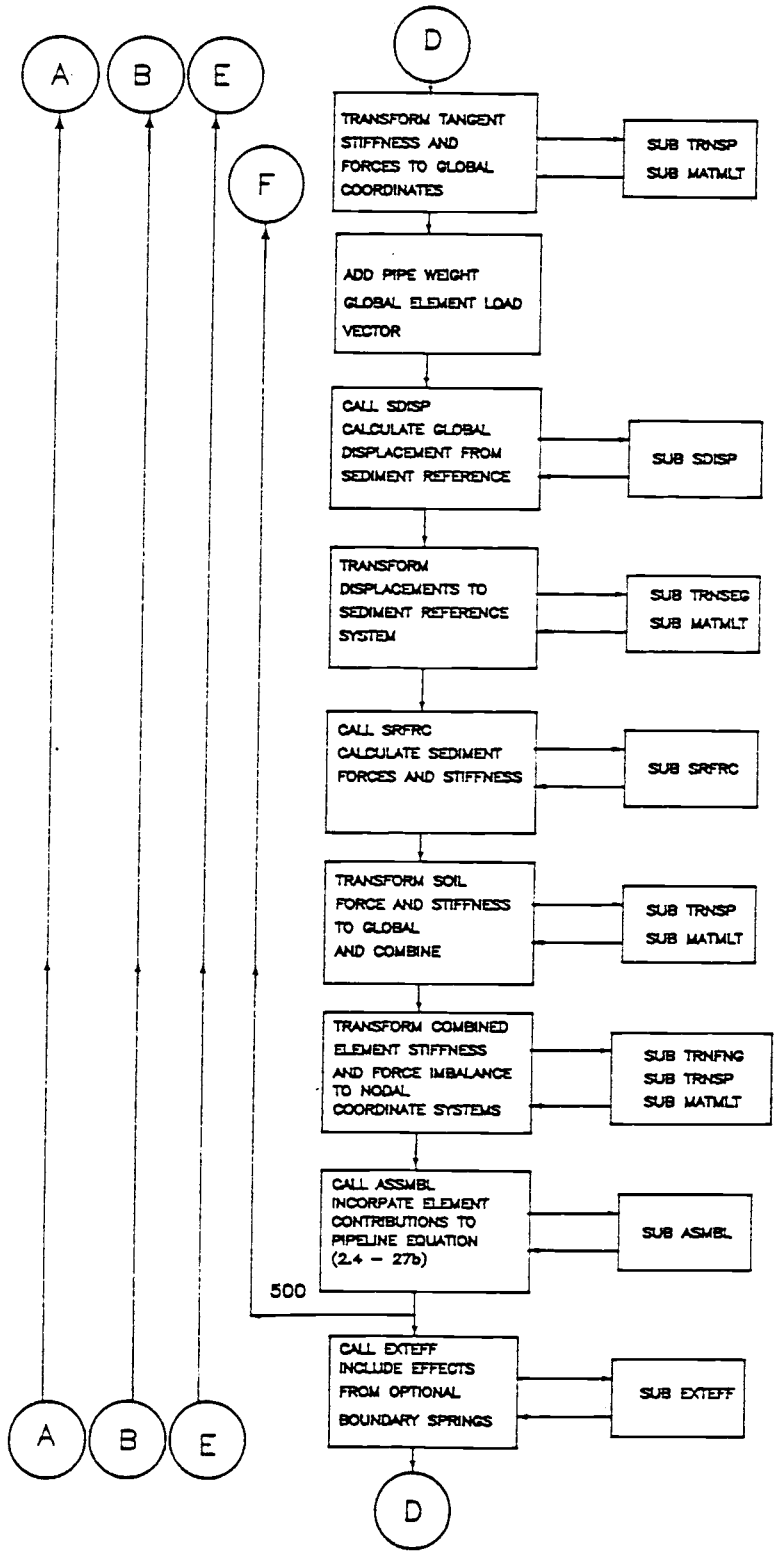

Figure 2.16 (Continued).

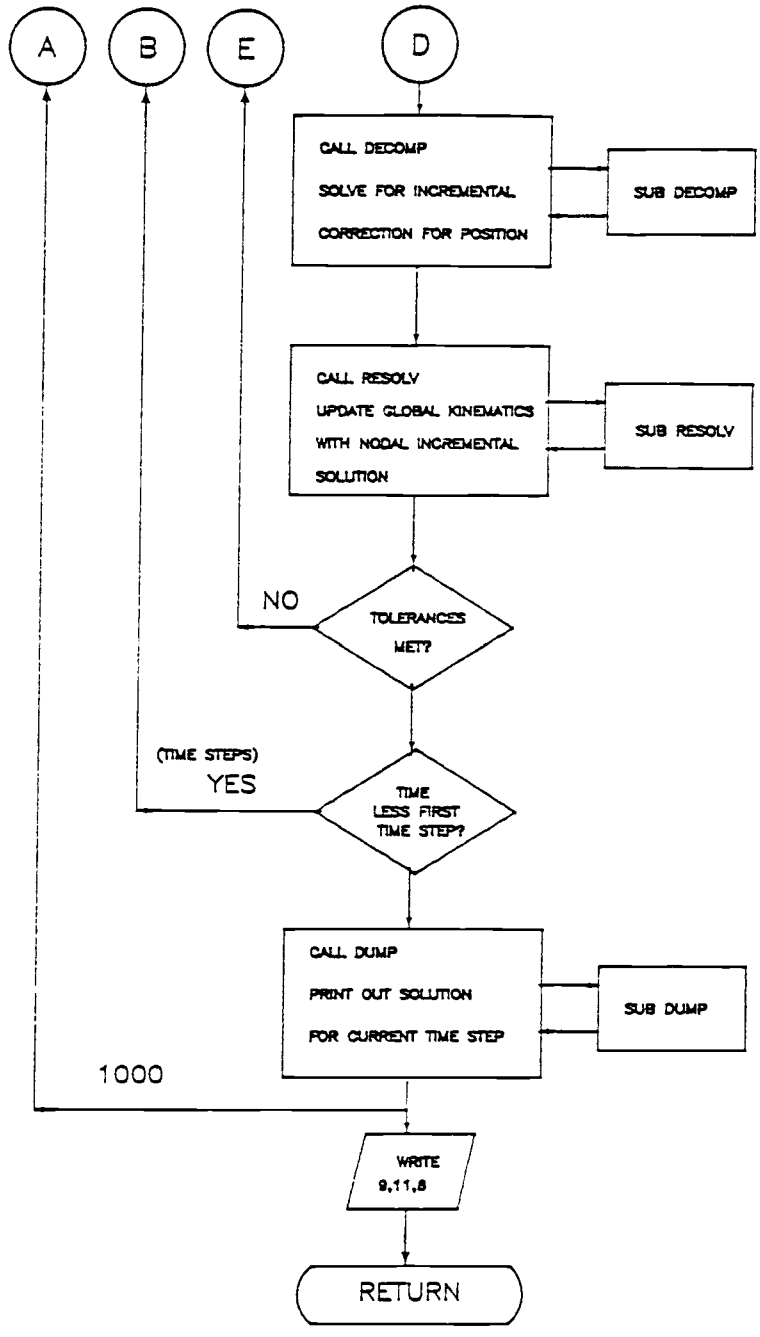

of example simulations were analyzed to evaluate the performance of the solution algorithm. The results of these test problems together with the results of more realistic ocean engineering simulations are presented in Chapter 3.

3.0 Sample Problems

3.1 Basis for Problem Selection

A number of test problems have been analyzed to demonstrate the accuracy and efficiency of the solution algorithm developed in Chapter 2. Because this algorithm was developed specifically to model the fluid-structure-sediment interaction problem for an offshore pipeline, comparisons of results from all features of the FEM algorithm with analytical solutions, or with experimental data for a prototype problem, was not possible.

In this chapter a number of test problems of increasing complexity and applicability are examined to provide qualitative and quantitative verification of the algorithm. Section (3.2) describes several example problems which were designed to test individual modules of the solution algorithm. In Section (3.3), the predicted pipeline response to a monochromatic wave loading is presented. The predicted pipeline response to a sequence of short random wave episodes is presented in Section (3.4). Solutions for the example problems presented in Sections (3.2) and (3.3) required minor modifications to the solution algorithm shown Fig. 2.13, and where practical, these changes are discussed in detail. The physical characteristics of the two types of pipe elements analyzed in the example problems of Chapter 3 are summarized in Table 3.1.

3.2 Comparison with Analytical Solutions

3.2.1 Impact Response of a Cantilever Beam

The dynamic response of a cantilever beam subjected to an impact load at full span was investigated in this problem. The

Table 3.1 Pipe section specifications for Chapter 3. (cf. Fig. 2.2 for typical cross-section of pipeline).

Section Properties	Pipe Element Type 1	Pipe Element Type 2
Youngs Modulus (psf)	4.32×10^9	4.32×10^9
Poisson's ratio	0.3	0.3
Steel pipe diameter (ft.)	1.06667	1.66667
Steel wall thickness (ft.)	0.0416667	0.0416667
Mass density of steel section (slug/ft^3)	13.97516	13.97516
Outer sleeve diameter (ft.)	1.25	2.0
Mass density of outer sleeve (slug/ft^3)	4.34783	4.75778
Ratio of pipeline density/fluid density	1.35	1.20
Area of steel (sq. in.)	19.32	30.63
Moment of inertia (in.^{4})	365.38	1455.91
Mass per unit length (slug/ft)	3.32541	7.53983

problem was selected specifically to provide a numerical comparison with a known analytical solution. In particular, this problem provides a comparison of the maximum dynamic deflection and the fundamental period of vibration of a cantilever beam computed from a closed form linear solution with the values obtained from the FEM algorithm. This example also demonstrates the numerical stability of the solution algorithm and the suitability of the numerical procedures for transient analysis.

For a given load, the maximum expected deflection for the cantilever beam can be computed as the product of the dynamic amplification factor (ratio of the amplitudes of dynamic and static response) and the static deflection produced by the load. For an undamped linear structural system, the dynamic amplification factor for an impact load is 2.0 [Clough and Penzien (1975), p. 92]. The static tip deflection of a cantilever for a vertical point load at full span [vide Fig. 2.1] is given by Sandor (1978), [p. 411] as

$$\Delta_s = \frac{P\ell^3}{3EI} \tag{3.1}$$

in which Δ_s = static deflection; P = applied load; ℓ = length of span; E = Youngs Modulus and I = moment of inertia. The expected displacement amplitude, Δ_D, for the dynamic response is, therefore;

$$\Delta_D = \frac{2P\ell^3}{3EI} \quad . \tag{3.2}$$

The predicted first mode response frequency, f_1, for a linear cantilever beam is given by Blevins (1979), [p. 108] as

$$f_1 = \frac{(1.87510407)^2}{2\pi \ell^2} \left(\frac{EI}{m}\right)^{1/2} \tag{3.3}$$

in which f_1 = first mode frequency (hertz); and m = mass per unit length. The corresponding fundamental period for the cantilever may be computed by inverting Eq. 3.3.

The cantilever beam model chosen for this example was 100 ft. long and was discretized into four equal length elements which were oriented to respond in the global X-Y plane [vide Fig. 2.1]. The physical properties of the elements are described in Table 3.1 under pipe element type 1. The impact load on the pipeline was simulated in the computer model by selecting Morison coefficients of

$$C_D = C_L = 0.0 \tag{3.4a}$$

and

$$C_M = 1.0 \tag{3.4b}$$

and by specifying the fluid velocity and acceleration at all of the pipeline nodes (except for the node at the cantilever tip) as zero ($v = \dot{v} = 0.0$) . The fluid velocity at the tip node was also specified as zero ($v = 0.0$); however, the fluid acceleration at this node was given a constant magnitude of 20 ft/s^2. The direction of this acceleration was maintained in the horizontal plane and was perpendicular to the original cantilever axis. Description of the fluid kinematics for this example required modification of the PROGRAM AGAPIP to allow the specification of global fluid kine-

matics at any pipe node. Sediment loadings and other environmental considerations were negated by specifying the gravitational constant as zero (g = 0.0) and by selecting a **cohesionless** sediment with friction coefficients equal to zero ($\mu_1 = \mu_2 = 0.0$) .

Initially, the response associated with the finite element model corresponded to the cantilever beam impact problem; however, as the finite element model of the cantilever deflects, the inertial fluid loading at the tip of the cantilever is computed and applied **normal** to the **deflected** shape of the element at the free end of the cantilever. Consequently, unlike the analytic problem, both the magnitude and direction of the applied load changed slightly as the beam deflected. Another difference between the finite element model and the analytic problem arose as a result of the large deflection formulation used for the finite element computations.

Figure 2.8 illustrates the effects of the nonlinearities on the linear solution. The relationship between the cantilever tip deflection and the applied static load, where the static load is given in terms of $P\ell^2/EI$, is demonstrated in Fig. 2.8. The impact load was modeled by the inertial component of the fluid load from Eq. (2.4-22b) with a magnitude of P = 613.6 lb. The computed value of $P\ell^2/EI$ for this load is 0.081, which is on the linear portion of the load curve (approximately, $0.0 \leq P\ell^2/EI \leq 1.0$) . However, because of the previously described difference between the finite element model and the analytical model, a slight descrepancy between the closed form solution and the FEM solution was antici-

Figure 3.1 Computed cantilever tip deflections for an applied impact loading.

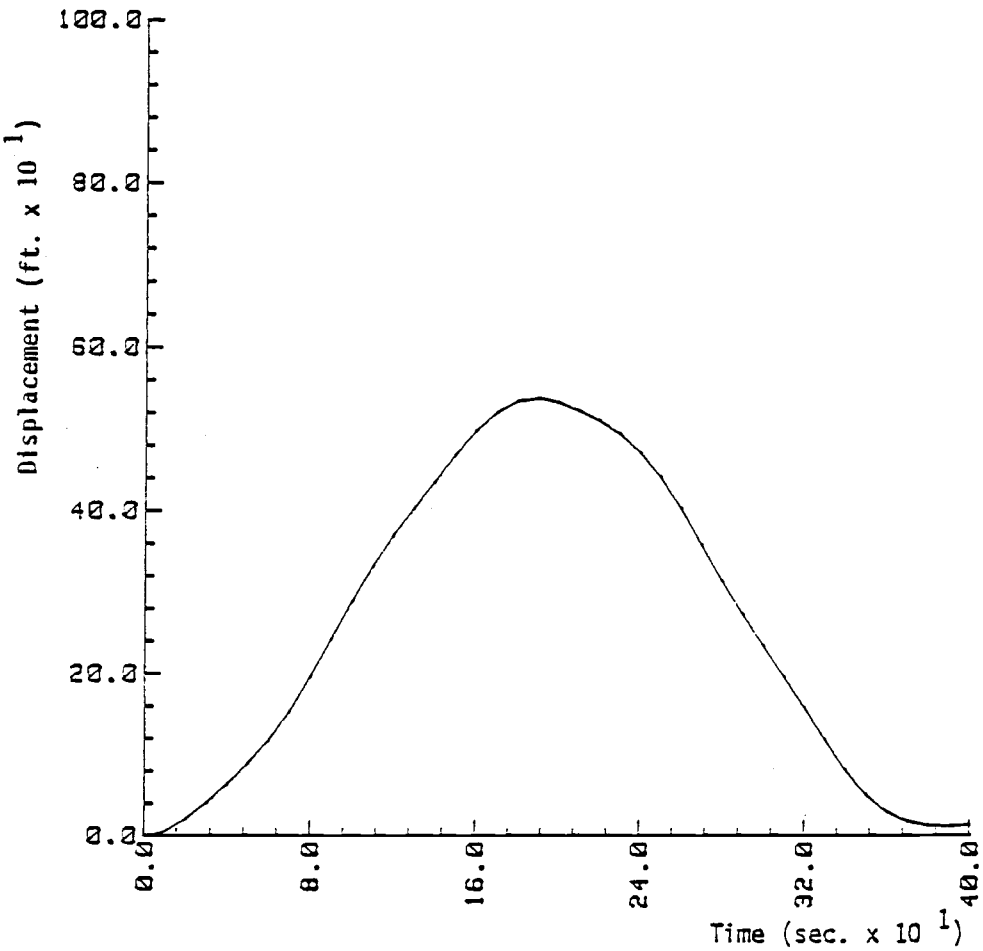

pated. These differences are negligible, however, and do not prohibit a comparison between the analytic and the FEM solution.

In Fig. 3.1 the computed transverse tip deflection as a function of time is depicted. The finite element analysis which rendered these results utilized a 0.1 second time step for temporal integration. Figure 3.1 illustrates some of the previously anticipated descrepancies between the analytic and finite element models; however, the plot of the tip deflection demonstrates primarily the expected first mode response. The maximum computed deflection obtained from the FEM solution was 5.389 ft., which compares favorably with the predicted linear analytical solution of 5.374 ft. The slightly greater computed maximum deflection is attributed to contributions from excitation of higher modes of response by the inertial fluid loading (which rotates in order to remain normal to the element at the free end of the cantilever). The effects of the higher response modes may be observed in Fig. 3.1 where the higher frequency vibrations are superimposed on the fundamental sinusoidal response. The FEM results also indicated that the cantilever does not oscillate between its original position and the maximum displacement amplitude. This behavior is attributed to the fact that the applied inertial fluid load is computed as the component of fluid acceleration normal to the element at the free end of the cantilever.

Comparison of results for the fundamental vibration periods for the FEM and the analytical solutions can only be made to within the accuracy of the time step chosen for the numerical solution.

The closed form prediction for the fundamental vibration period is 3.77 seconds. The finite element model exhibited a vibration period of 3.8 seconds.

In summary, by slightly modifying the FEM solution algorithms, it was possible to obtain close agreement of results with a closed form analytical solution for a dynamically loaded cantilever beam. General agreement between the finite element values with theoretical large deflection predictions has already been demonstrated in Chapter 2 (vide Fig. 2.8); therefore, the present example focused on evaluating the dynamic analysis capabilities of the FEM algorithm. The computations for this example were not carried beyond the first oscillatory cycle (Fig. 3.1) because the analytical and finite element solutions had begun to diverge at this point as a result of modeling constraints, and further computations would have provided no additional verifiable information.

3.2.2 Impact Response of a Cantilever Beam on an Inclined Plane

The dynamic response of a cantilever beam subjected to an impact load at full span was examined in this example. The problem was identical to that discussed in Section (3.2.1), except that the response of the cantilever was constrained to remain in a plane which had been positively rotated about the longitudinal axis of the cantilever to a 25.0% slope. This problem was selected specifically to provide a verifiable test for the transformations between the **local**, **global**, and **nodal** coordinate systems.

Except for the rotation of the grid system, the problem definition and program modifications necessary to formulate this

problem were as described in Section (3.2.1). However, the fluid acceleration assigned to the tip of the cantilever in each problem was computed as the component of acceleration parallel to the plane in which the tip node was free to respond. The cantilever response described in Section (3.2.1) was constrained to remain in the X-Y plane and the fluid acceleration at the cantilever tip was specified in the **global** Y direction. The component of the **global** Y fluid acceleration parallel to the inclined slope for this problem was 19.4 ft/s^2. The corresponding ratio of impact loadings for this example and the example of Section (3.2.1) is 0.97. In the nearly linear response range of this problem, the expected results are 97.0% of the computed results for the problem described in Section (3.2.1).

Figure 3.2 depicts the **global** Y and Z components of tip deflection for the response of the cantilever on an inclined slope. Evaluation of the numerical results for this problem indicated that the magnitude of the vector combination of these displacement components were 97.0% of the cantilever deflections computed in Section (3.2.1). Examination of the **local** force information provided as part of the solution data showed the **local** forces in this example to be 97.0% of those computed in Section (3.2.1). Furthermore, the out of plane forces for both solutions remained negligible. The vibration period for the response of the inclined cantilever was 3.8 seconds which matched that of the horizontal cantilever to within the accuracy to which the solution results for either problem could be interpreted.

Figure 3.2 Computed components of tip deflection for a cantilever responding on an inclined slope to an impact loading.

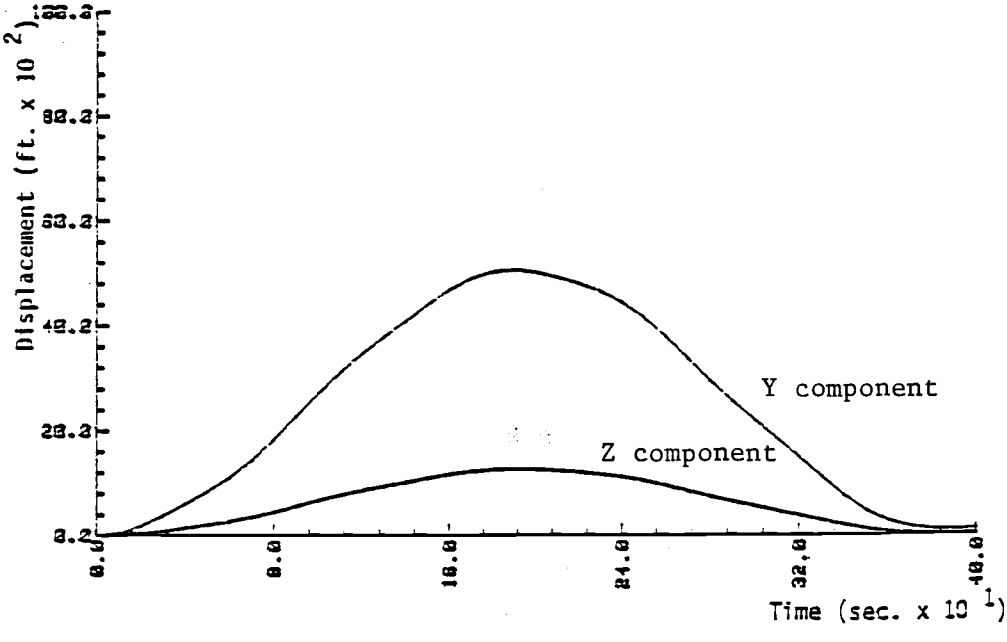

This example problem provided a control check on the coordinate system transformations utilized by the solution algorithm. The predicted deflection amplitude of 5.228 ft. and the computed deflection amplitude of 5.229 ft. compare very well for this example.

3.2.3 Reponse of a Pipeline to a Steady Current Load.

The response of a section of pipeline subjected to a steady transverse current of 5.0 ft/sec. was modeled in this example. This problem was selected specifically to demonstrate the ability of the solution algorithm to accurately predict steady state behavior. Because the fluid loading for this example was applied as an impact loading, this example also provides an indication of the amount of viscous damping introduced by fluid drag.

The finite element model for this simulation consisted of six equal length elements spanning a total length of 240.0 ft. The **prescribed** boundary conditions at both ends of the span were fixed (i.e., no displacement and no rotation) and the specified pipeline characteristics are described in Table 3.1 as pipe element type 1. Current loads were simulated with a steady fluid velocity of 5.0 ft/sec. acting transverse to the original pipeline configuration. Morison coefficients were specified as $C_D = C_M = 1.0$ and $C_L = 0.0$. Environmental factors other than hydrodynamic loading were negated by specifying the gravitational constant as zero ($g = 0.0$) and by specifying a **cohesionless** sediment with friction coefficients of zero ($\mu_1 = \mu_2 = 0.0$) . A temporal integration step of 0.1 second was used in the simulation.

The expected pipeline response for this simulation was a rapidly decaying vibration which approached a steady state pipeline deflection equivalent to the deflection of the same pipeline that was statically loaded with a uniform Morison drag force. Figure 3.3 depicts the computed midpoint deflection of the pipeline as a function of time for this simulation. Interpretation of the simulation results and comparison of the results from linear structural theory indicates that the pipeline response is nonlinear. A closed form solution for the large deflection static response of a uniformly loaded fixed-fixed beam is not available. However, a numerical solution for this problem was obtained using the FEM computer program LDEFL [Zimmerman (1982)] which produced Fig. 2.8. Results from the nonlinear static analysis predicted a midpoint deflection of 1.651 ft. Figure 3.3 demonstrates that the dynamic response of the pipeline subjected to the current load has reached steady state after approximately 3.0 seconds. The computed midpoint deflection after 3.0 seconds was 1.642 ft.

Simulation of other steady current problems indicated similar steady state behavior. The amount of damping present in the other simulations varied with the specified magnitude of the current. These additional simulations were performed for durations up to 20.0 seconds without exhibiting any tendency to diverge from the predicted steady state behavior.

Figure 3.3 Midpoint deflection of a fixed-fixed beam subject to a steady 5.0 ft/sec. current.

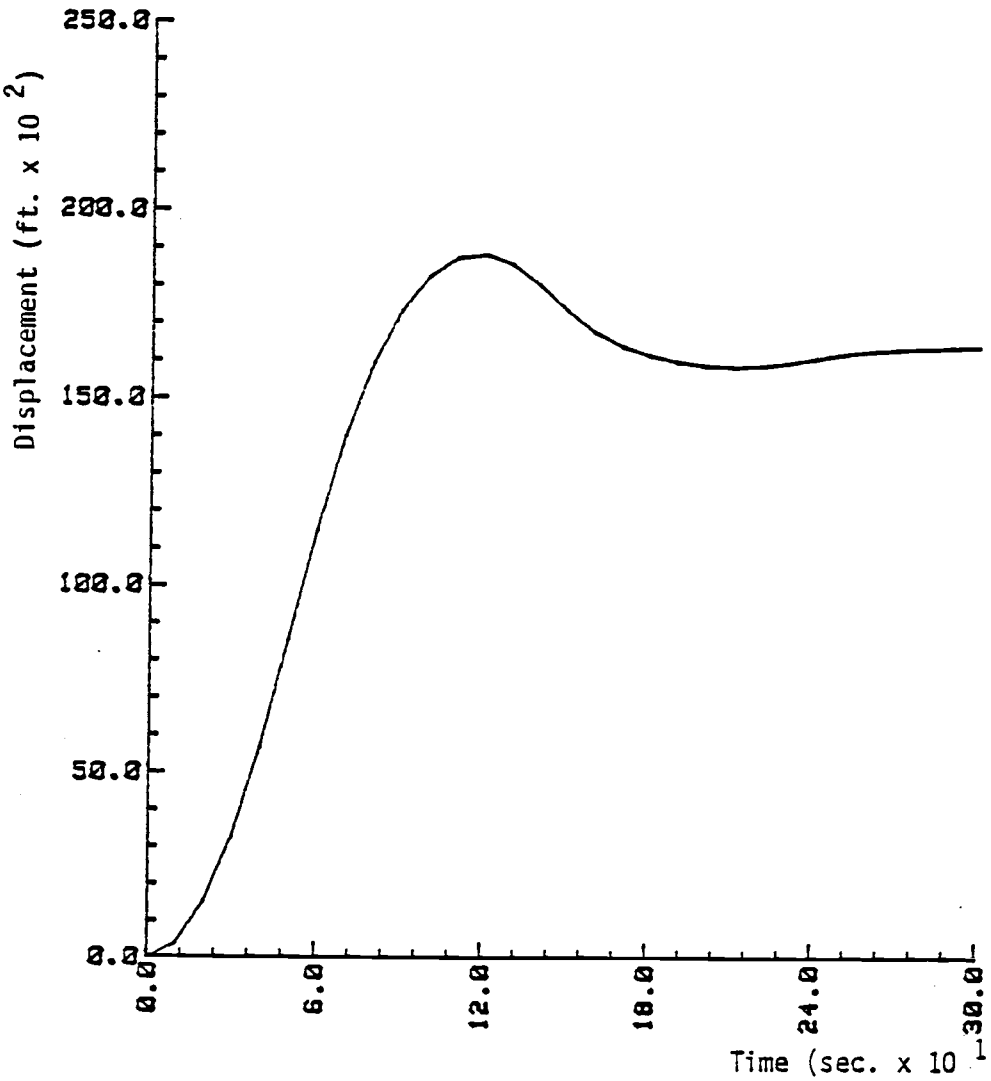

3.2.4 Pipeline Response on an Elastic Foundation

The effects of the nonlinear springs that modeled the sediment forces on the dynamic response of the pipeline was examined. This problem was selected in order to provide comparisons of the maximum dynamic deflection and the fundamental period of vibration of a simply supported beam on an elastic foundation.

A 300 ft. section of a simply supported pipeline (i.e., unrestrained rotation at the pipe terminals) was subjected to an impact loading from a 1.0 ft/sec. steady current. The finite element representation of this system was discretized into six equal length elements which were oriented to respond in the global X-Y plane. The physical properties specified for the elements are described in Table 3.1 as pipe element type 2. Sediment spring characteristics were computed in accordance with Section (2.4.3b) for the **cohesive** sediment having a cohesion (c) value of 40.0 psf and an effective weight (γ_e) of 21.0 pcf. The impact loading on the pipeline was simulated with a steady current of 1.0 ft/sec. oriented transverse to longitudinal axis of the pipeline. Morison coefficients were chosen as $C_D = C_M = 1.0$ and $C_L = 0.0$. Fluid kinematics and pipeline response were both computed with a 0.01 second time step.

The expected response for this simulation was a damped linear oscilation with a dynamic amplification factor of approximately 2.0 and a fundamental period of vibration slightly greater than the undamped fundamental period of an equivalent simply supported beam on an elastic foundation. The fundamental frequency for an

undamped simply supported beam on a spring foundation is given as [Blevins (1979), p. 107]

$$f_1 = \frac{\pi}{2\ell^2}\left(1 + E_f \frac{\ell^4}{EI\,\pi^4}\right)^{1/2} \left(\frac{EI}{m}\right)^{1/2} \tag{3.5}$$

in which f_1 = first mode frequency (hertz); ℓ = length of span; m = mass per unit length; E = Youngs modulus; I = moment of inertia; and E_f = foundation modulus (load per unit length per unit deflection). Equation (3.5) for this simulation gives f_1 = 8.687 hz., or equivalently, a first mode period of .115 second. The numerical solution for this problem is expected to have a period slightly longer than that predicted by Blevins due to the damping introduced by the fluid.

Figure 3.4 illustrates the pipeline deflection at midspan as a function of time. Interpretation of these results reveals that the computed vibration period was 0.118 seconds [cf. 0.115 seconds from Eq. (3.5)].

Further review of these simulation results demonstrated that the pipeline response was linear and was dominated entirely by the sediment resistance. The static midpoint deflection of the pipeline to a Morison drag load of 2.0 lb/ft that is resisted only by the sediment springs yielded a predicted midpoint deflection of 8.9 x 10^{-5} ft. Using this value and the FEM computed maximum of 1.761 x 10^{-4} ft., the computed dynamic amplification for this simulation was 1.98 which compares favorably with the analytic prediction of 2.0 (Clough and Penzien (1975), [p. 92]).

Figure 3.4 Illustration of sediment spring response for a simply supported pipeline subjected to an impact loading from a 1.0 ft/sec. current.

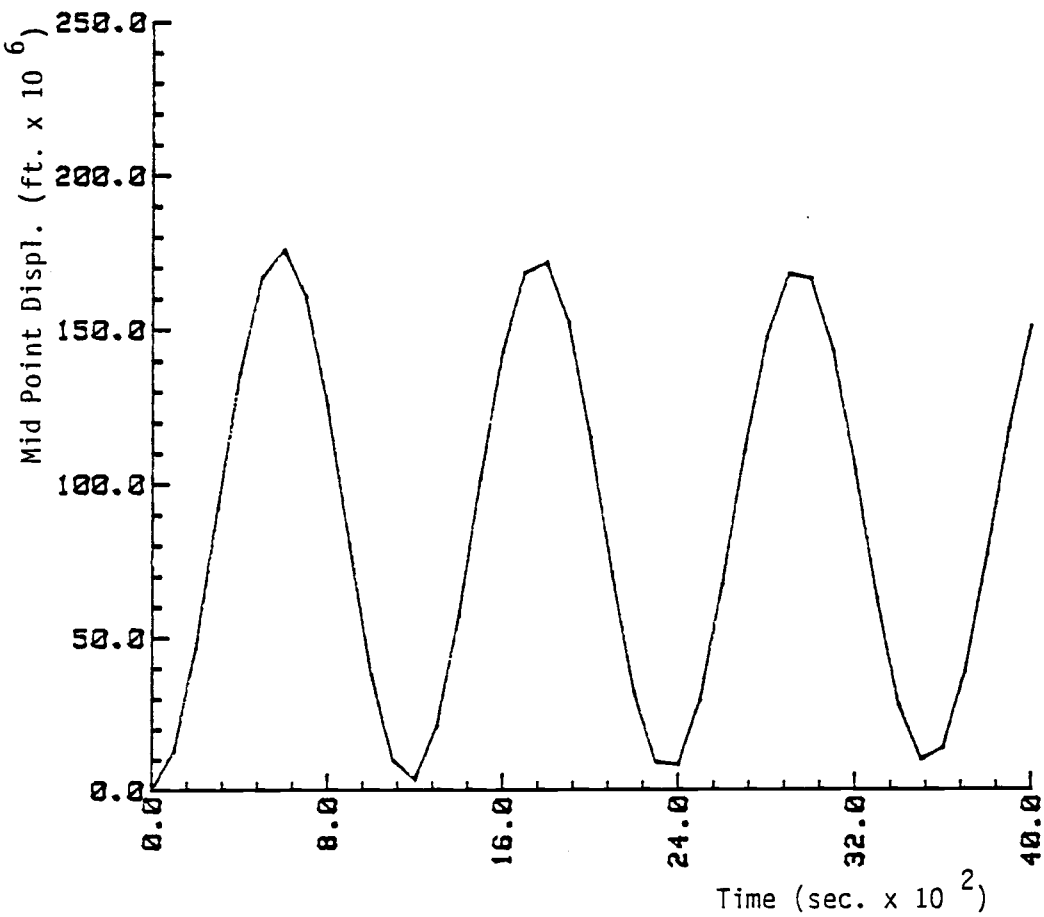

In reviewing the results from this example, it is noted that although the analytical and FEM response of the pipeline compared well, the computed response of the pipeline for this problem was a small amplitude, high frequency vibration. Because the assumptions made in formulating the FEM solution algorithm were oriented toward evaluating the gross dynamic behavior of the pipeline, it is not expected that the computed results for this problem would emulate the actual pipeline response for this type of loading.

3.3 Pipeline Response to Monochromatic Wave Loadings

The pipeline response to monochromatic waves was also examined. The simulations from monochromatic waves demonstrates the fluid-structure-sediment aspects of the algorithm that were difficult to illustrate with results obtained from stochastic wave loadings. Furthermore, simulation results for monochromatic wave loadings provide a source for qualitative comparison with the numerical solutions of other investigators [e.g., Karal and Halvorsen (1982)].

Three representative example problems were examined for monochromatic wave loadings. Input parameters for the three example problems are given in Table 3.2 and the pipeline properties for these examples are described in Table 3.1 as pipe element type 2. The grid system for each problem was a horizontal plane, and sediment characteristics throughout the grid were uniform. The FEM algorithm for these example problems were modified to compute the fluid kinematics at pipeline nodes without using interpolation (SUBROUTINE BLUE). Fluid kinematics were calculated from a linear

Table 3.2 Pipeline, sediment and wave data for monochromatic wave simulations.

Internal pressure (PR)	1440.0 psi.
Pipeline length between terminal constraints (ℓ)	2500.0 ft.
Drag, lift, and inertial coefficients (C_D, C_L, C_M)	$C_D = 1.0$ $C_M = 2.0$ $C_L = 1.0$
Fluid mass density (ρ_o)	2.0 (slugs/cf.)
Sediment cohesion (c)	40 psf.
Sediment effective weight (γ_e)	21 pcf.
Monochromatic wave specifications:	
Water depth (h)	200.0 ft.
Wave height (H)	30.0 ft.
Wave period ($2\pi/\omega$)	12.0 sec.
Phase shift (Φ)	90°
Wave angle from X axis (Θ)	90°, 60°, 30°

monochromatic wave traveling at an angle Θ to the **global** X axis, with a free surface profile given by

$$N_w = (X,Y,t) = \frac{H}{2} \cos (\kappa X \cos \Theta + \kappa Y \sin \Theta - \omega t + \Phi) \qquad (3.6)$$

in which N_w = water surface profile; H = wave height; κ = wave number (rads/length); ω = wave frequency (rads/time); and Φ = phase shift. The fluid kinematics and the structural response were calculated using a 0.2 second time step.

The finite element model of the pipeline system in each example problem consisted of 50 elements. The **prescribed** boundary conditions at the pipe terminals were specified as fixed (i.e., no displacement and no rotation). The longitudinal axis of the pipeline in the preloading stage was selected to coincide with the **global** X axis; therefore, the wave angle Θ corresponds to the angle of wave attack relative to the original configuration of the pipeline.

The calculated deflections at the pipeline midpoint (x = 1250 ft.) and the horizontal water particle velocity are given as a function of time in Fig. 3.5 for a normally incident wave (Θ = 90°). The flat portions of the displacement plot illustrated in Fig. 3.5b reflect the hystereses effect from the sediment forces. The phase relationship exhibited in Fig. 3.5 between the fluid velocity and the pipeline response indicates that inertial fluid loading is an important component of the applied environmental loading. In addition, Fig. 3.5 demonstrates the importance of the

Figure 3.5 Effect of (a) water particle velocity on (b) pipeline response at X=1250.0 ft. for a normally incident monochromatic wave, $\theta=90^{o}$.

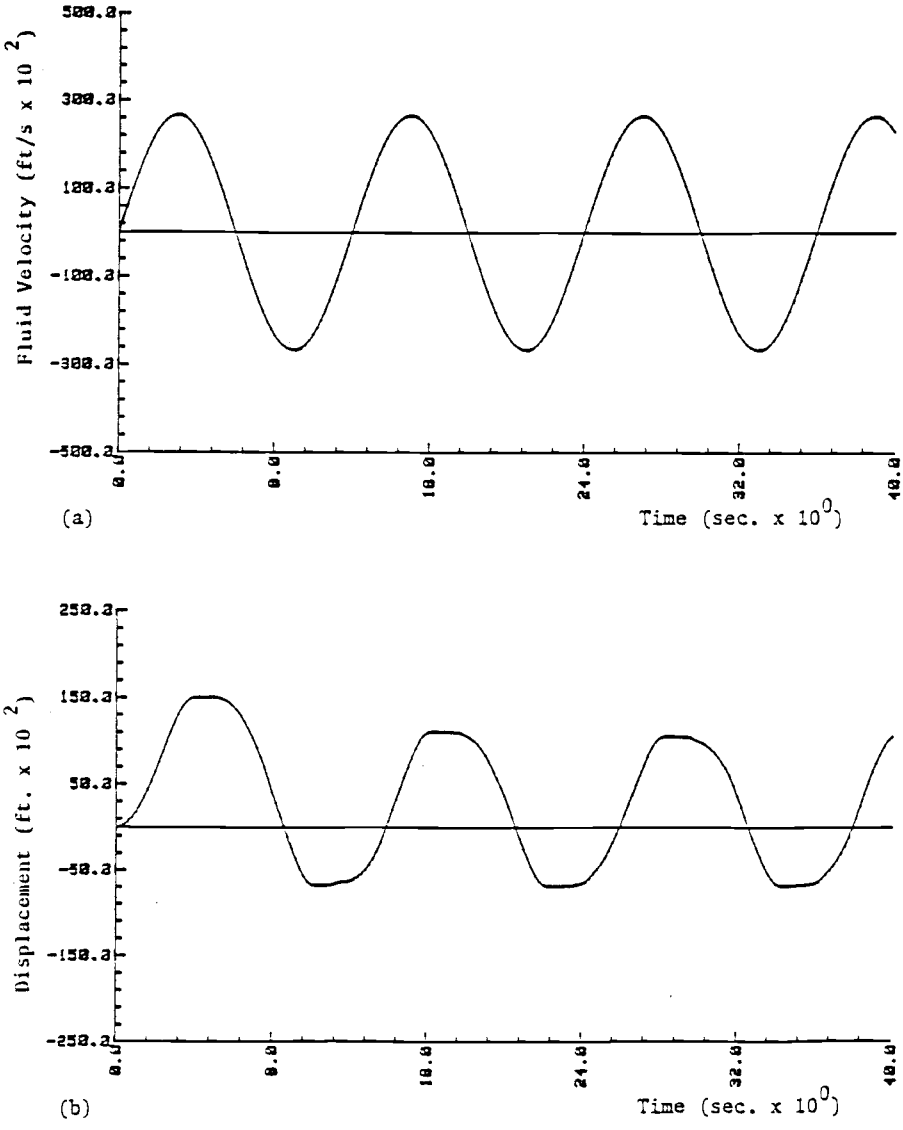

initial transient motion and sediment hysteresis in determining the net lateral displacement of the pipeline.

The maximum deflections, the longitudinal stresses and their location along the pipeline are given in Table 3.3 for both normally incident and obliquely incident (Θ = 60°, 30°) waves. The results tabulated in Table 3.3 reveal that the directionality of a wave field greatly affects both the magnitude and location of the maximum pipeline response. Furthermore, the computed results show that even for a normally incident wave, the maximum pipeline deflections do not necessarily occur at the midpoint of the pipeline or during the first wave in a group of waves. The normally incident wave results (Θ = 90°) are symmetric.

A literature search was unable to locate an example solution which was analogous to the examples described in this section. However, the work of Karal and Halvorsen (1982) provides a source of qualitative comparison for a normally incident monochromatic wave. Karal and Halvorsen (1982) employed a finite difference technique with a nonlinear fluid drag force and a nonlinear hysteresis function for the sediment forces to evaluate the response of a 1000.0 meter long pipeline subjected to a harmonically varying fluid load. A comparison of the time-displacement plot illustrated in Fig. 3.5b with that presented by Karal and Halvorsen (1982) reveals that both responses have the same general form. A comparison of the phase relationship between the fluid velocity and the midpoint displacement with that illustrated by Karal and Halvorsen (1982), shows an apparent discrepancy. Figure 3, (p. 310) pre-

Table 3.3 Computed results for a monochromatic wave.

Wave Angle	Max values for 0 < x < 2500 ft.				Max values for midpoint x = 1250 ft.	
	Lateral displ.		Longitudinal stress[1]			
θ	$\lvert u_2 \text{ max} \rvert$	x (u_2 max)	σ_{max}	x (σ_{max})	$\lvert u_2 \text{ max} \rvert$	σ_{max}
degrees	ft	ft	ksi	ft	ft	ksi
90[2]	1.77 (t = 39.8 sec)	570.0 & 1930.0	19.6 (t = 39.8 sec)	0.0 & 2500.0	1.51 (t = 4.0 sec)	14.1 (t = 27.2 sec)
60	.74 (t = 33.6 sec)	2220.0	18.6 (t = 37.0 sec)	2500.0	.36 (t = 14.0 sec)	14.5 (t = 33.2 sec)
30	0.006 (t = 8.2 sec)	853.3	13.7 (t = 7.2 sec)	853.3	-	-

1. Initial stress = 13.5 ksi
2. Results are symmetric about midpoint

sented by Karal and Halvorsen (1982) depicts significant pipeline motion only in phase with peak fluid velocity. Furthermore, the net lateral displacement predicted by the finite difference algorithm was proportionally greater than that obtained from the FEM solution. Both of these discrepancies indicate that the Karal-Halvorsen algorithm predicts greater sediment resistive forces than the FEM formulation; however, insufficient data are available to directly compare these sediment force values.

Further comparison of the results published by Karal and Halvorsen (1982) with the results computed by the FEM algorithm reveals that both solution procedures predict that the location of the maximum pipeline deflection for a normally incident wave is a function of the wave length (or wave period for linear waves). The Karal and Halvorsen results indicate this directly in tabular form (Table 1, p 310). The FEM results reflect this effect in the numerical results obtained for a pipeline subjected to a steady current [Section 3.2.3)] and to a normally incident wave. The results from the steady current (infinite period) simulation indicated a maximum deflection at mid span, where as the results for a normally incident wave (12.0 sec. period) reported in Table 3.3 indicate a maximum deflection that is symmetric about, but not at, the pipeline midpoint.

3.4 **Pipeline Response to Random Wave Loadings**

Dynamic pipeline response for a sequence of three episodic loadings from a directional sea simulation was analyzed. The wave-induced fluid kinematics for this simulation were obtained from the

program AGWSIM using a FFT time step of 1.0 second and a water depth of 165.0 ft. To reduce computational expenses, the 17 minutes of data provided by AGWSIM was filtered to obtain episodes of peak forces. The specific loading episodes which were analyzed used the wave data from 0 to 39 seconds, from 269 to 309 seconds and from 539 to 580 seconds. The selection of these data intervals was chosen to represent a sequence of peak wave occurrances during the design life of the pipeline. However, because the selection of these data intervals was somewhat arbitrary, it is probable that a worst case scenario may not be represented by the intervals selected.

The pipeline and sediment characteristics for this simulation are described in Table 3.4. The physical characteristics of the pipe cross section are given in Table 3.1 as pipe element type 2. The finite element model for this simulation consisted of 50 elements with fixed **prescribed** boundary conditions (i.e., no displacement and no rotation at the pipe terminals). A temporal integration step of 0.2 second was utilized in the Newmark-beta integration.

In Fig. 3.6, the computed pipeline configurations after each of the three wave episodes is illustrated. This figure reveals the chaotic nature of the forces produced by waves from a random directional sea.

The calculated maximum deflections and longitudinal stresses and their respective locations along the pipeline are presented in Table 3.5 for each of the subsequent wave episodes. These results

Table 3.4 Pipeline, sediment and wave data for random sea simulation

Internal pressure (PR)	1440.0 psi
Pipeline length between terminal constraints (ℓ)	2500.0 ft.
Morison coefficients (C_D, C_L, C_M)	C_D = 1.0 C_M = 2.0 C_L = 1.0
Sediment cohesion (c)	40 psf.
Sediment effective weight (γ_e)	21 pcf.
Grid spacing	65.6 ft.
Water depth (h)	164.0 ft.

Figure 3.6 Pipeline configuration after each of three sequential wave episodes from a directional sea simulation.

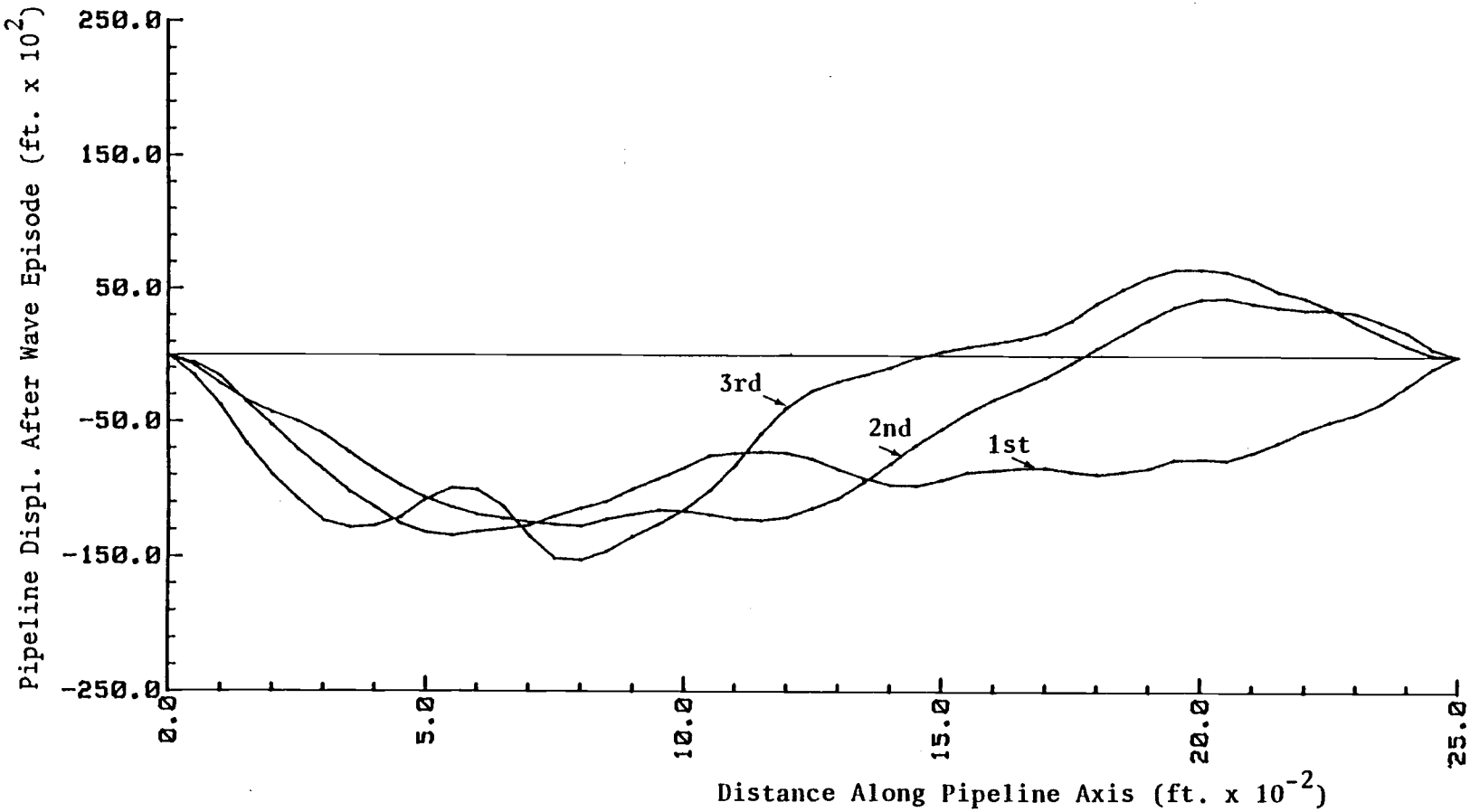

Table 3.5 Computed results for random wave episodes

Wave Episode	Max values for $0 \leq x \leq 2500$ ft			
	Lateral displ.		Longitudinal stress[3]	
	u_2 max	$x(u_2 \text{ max})$	σ_{max}	$x(\sigma_{max})$
	ft.	ft.	ksi.	ft.
1 ($0 \leq t \leq 39$ sec)	2.76 (t = 20.0 sec)	750.0	37.5 (t = 35.0 sec)	0.0
2 ($269 \leq t \leq 309$ sec)	2.00 (t = 301.0 sec)	300.0	27.8 (t = 301.8 sec)	0.0
3 ($539 \leq t \leq 580$ sec)	2.12 (t = 559.8 sec)	300.0	28.1 (t = 560.8)	0.0

3. Initial stress = 13.67 ksi

indicate maximum displacements and stresses considerably greater than those obtained from the monochromatic wave simulations previously described. This increased response magnitude for the directional sea simulation is indicative of the large energy content of the waves during the peak wave events selected for the simulation.

Review of the results described in Table 3.5 indicates that all of the maximum stress occurrances for this simulation were located at the pipeline terminals. The computed maximum longitudinal stress of 37.5 ksi indicates that stress levels during these wave simulations approached yield values for some steels, and therefore additional weight coating for this pipe section may have been required. Further investigation of the FEM results from the random wave simulation indicated that maximum mean deflection for the pipeline during any wave episode was -0.0624 ft. at x = 1300.0 ft. and occurred during the third wave episode. The maximum mean deflection for the pipeline during the entire simulation was -0.0412 ft. at x = 1350.0 ft.

A review of available literature was unable to locate an analogous solution for a directional sea simulation; however, the work of Lambrakos (1982) was similar in scope. The pipeline displacements predicted by Lambrakos (1982) were distinctly greater than those described in Table 3.5 or in Fig. 3.6. This difference arises because of differences between the nonlinear structural formulation presently employed and the linear structural formulation employed by Lambrakos (1982). The linear formulation for

structural response is expected to over estimate the displacements of a stiffening struture such as the pipeline systems analyzed by the FEM algorithm.

4.0 Summary and Recommendations

4.1 Summary and Conclusions

The nonlinear, dynamic response of bottom-laid deep ocean pipelines to stochastic directional wave loadings has been investigated. The study utilized the finite element method (FEM) to obtain a nonlinear time domain solution for the predicted response of a pipeline system. The differential momentum equations for the pipeline motions were transformed via variational principles to equivalent integral energy relationships. These integral energy equations were discretized using the finite element concepts. Solving numerically the integral energy equations by the FEM in contrast to solving the differential momentum equations by finite difference methods eliminated the possibility of numerical instabilities and improved the reliability of the computed results. The discrete structural model for the pipeline system was developed from an application of well-known energy methods which were then modified to accurately predict large-deflection responses by using a convected coordinate system. The environmental pipeline loadings due to nonlinear sediment resistances and to nonlinear wave- and current-induced forces were simulated by state-of-the-art models. To develop the FEM algorithm, it was assumed that: 1) only the gross dynamic response of the pipeline during peak wave episodes having a long return period was of interest; and 2) pipeline strains will remain small even though large pipeline displacements may occur.

The FORTRAN algorithm AGAPIP was developed and verified numerically using several example problems of various types in order to test both transient and steady state responses. The numerical verification problems reported in Sections (3.2) demonstrated excellent correlation with predicted analytical solutions. Numerical results for the dynamic response of prototype pipeline systems to both monochromatic and random, directional waves indicated that both the stress levels and displacements predicted for these simulations remained within present design specifications. Comparison between the dynamic responses to both monochromatic and random wave simulations presented in Sections (3.3) and (3.4) with the dynamic responses reported by other investigators indicated significantly smaller displacements were predicted by the FEM algorithm. However, these smaller displacements were an anticipated consequence of the differences between the **linear** formulation used by the other investigators compared to the **nonlinear** FEM algorithm. The numerical comparisons suggest that the dynamic response of a long bottom-laid pipeline to stochastic directional seas is not accurately modeled by linear structural theory. It should also be noted, however, that the CPU times for the nonlinear FEM algorithm are not insignificant and can approach a ratio of CPU/real time of 105:1 for stochastic, directional seas. In addition, the FEM algorithm is not economical to use for simulations that result in nearly **static** pipeline responses; i.e., very small displcements due to very low hydrodynamic wave- and current-induced forces. The FEM algorithm has been optimized for

the strongly nonlinear dynamic response of a pipeline to large wave- and current-induced hydrodynamic loadings.

4.2 Recommendation for Future Research

These results provide a frame work for more complex and comprehensive efforts to evaluate the dynamic response of marine pipelines. The flexibility of the FEM algorithm to model a variety of prototype pipeline systems provides a practical tool for an in-depth parametric evaluation of the effects on the dynamic performance of bottom-supported pipelines, of a directional sea state, of the bottom contours, and of selected pipeline parameters. Initial efforts should be directed toward minimizing computational costs and toward making the algorithm more **user friendly.**

Additional effort should also be directed toward sensitivity analyses that would include such factors as the selection of appropriate convergence tolerances and time steps; the discretization of FEM element sizes; the interpolation used to obtain the environmental parameters within a grid; and the evaluation of the effects of the differences between the time step used in the FFT simulation for the fluid kinematics and the numerical integration time step. Perhaps most importantly, a modification of the Swanson-Jones sediment model to eliminate the sharp discontinuity that presently exists in their elastic-plastic modal deserves high priority.

Finally, physical data for both the overall dynamic pipeline response and for the dynamic sediment and fluid load representations are needed in order to complete the verification of the FEM algorithm.

BIBLIOGRAPHY

American Petroleum Institute, (1979), API Recommended Practice for Planning and Constructing Fixes Offshore Platforms. p. 35-36.

Anagnostopoulos, S.W., (1982), "Dynamic Response of Offshore Platforms to Extreme Waves Including Fluid-Structure Interaction," Engineering Structures, Vol. 4, July, pp 179-185.

Anand, S. and Agarwal, S.L., (1980), "Field and Laboratory Studies for Evaluating Submarine Pipeline Frictional Resistance," Twelfth Offshore Technology Conference, Houston, TX, OTC 3781, Vol. II, pp 371-382.

Audibert, J., Lai, N. and Bea, R., (1978), "Design of Pipelines - Sea Bottom Loads and Restraints," Pipelines in Adverse Environments, Volume 1, Proceedings of the ASCE Pipeline Division Specialty Conference, New Orleans, Louisiana, January 15-17, pp 184-203.

Audibert, J. and Nyman, K., (1977), "Soil Restraint Against Horizontal Motion of Pipes," Journal of the Geotechnical Engineering Division, ASCE, Vol. 103, No. GT10, Oct., pp 1119-1142.

Bathe, K., (1982), "Solution of Equilibrium Equations in Static Analysis," and "Solution of Equilibrium Equations in Dynamic Analysis," Finite Element Procedures in Engineering Analysis, Prentice-Hall Inc., Englewood Cliff, NJ, pp 96-186, pp 300-341, and pp 441-553.

Beckmann, H., and Thibodeaux, M.H., (1962), "Wave Force Coefficients for Offshore Pipelines," Journal of the Waterways and Harbors Division, ASCE, Vol. 88, No. WW2, May, pp 125-138.

Belytschko, T. and Hsieh, B.J., (1973), "Non-linear Transient Finite Element Analysis with Convected Co-ordinates," International Journal for Numeric Methods in Engineering, Vol. 7, pp 255-271.

Blevins, R.D., (1979), "Straight Beams," Formulas for Natural Frequency and Mode Shape, Van Nostrand Reinhold Co., New York, NY, pp 107-108.

Borgman, L.E., (1969), "Ocean Wave Simulation for Engineering Design," Journal of the Waterways and Harbors Division, ASCE, Vol. 95, No. WW4, Nov., pp. 557-583.

Borgman, L.E., (1972), "Statistical Models for Ocean Wave Forces," Advances in Hydrosciences, V.T. Chow, editor, Academic Press, New York, NY, pp. 139-181.

Borgman, L.E., (1982), "Techniques for Computer Simulation of Ocean Waves," Topics in Ocean Physics, Soc, Italiana di Fisica, Bologna, Italy, pp. 387-417.

Bowles, J.E., (1977), Foundation Analysis and Design, McGraw-Hill, Inc., New York, NY, pp. 113-122.

Brown, R.J., (1967), "Hydrodynamic Forces on A Submarine Pipeline," Journal of the Pipeline Division, Proceedings of the American Society of Civil Engineers, Vol. 93, No. PL1, March, p. 9-19.

Chajes, A., (1974), "Torsional Buckling," Principles of Structural Stability Theory, Prentice-Hall Inc., Englewood Cliffs, NJ, pp 76-99, pp 133-142, and pp 195-233.

Chakrabarti, K., (1980), "Impact of Analytical Model and Field Studies on the Design of Offshore Structures," International Symposium on Ocean Engineering Ship Handling, Swedish Maritime Research Center, SSPA, Gothenburg.

Clough, R.W. and Penzien, J., (1975), "Overview of Structural Dynamics," and "Partial Differential Equations of Motion," Dynamics of Structures, McGraw-Hill, Inc., New York, NY, pp 9-11, pp 118-175, pp 260-270, and pp 293-307.

Cook, R.D., (1981), "Introduction to Nonlinear Problems," Concepts and Applications of Finite Element Analysis, John Wiley and Sons, Inc., pp 35-45, pp 61-102, pp 148-162, pp 304-308, pp 320-323, pp 333-341 and pp 351-363.

Corbishley, T., (1982), "How to Stabilize Subsea Pipelines," Pipe Line Industry, March, pp 63-70.

Davis, D.A., and Ciani, J.B., (1976) "Wave Forces on Submerged Pipeline - A Review with Design Aids," Technical Report, No. R 844, Civil Engineering Laboratory, Naval Construction Battalion Center, Port Hueneme, California, July, p. 55.

Demars, K.R., Nacci, V.A., and Wang, W.D., (1977), "Pipeline Failure: A Need for Improved Analysis and Site Surveys," Offshore Technology Conference, Houston, TX, OCT 2966, Vol. IV pp 63-70.

Efthymiou, M. and Narayanan, R., 1980, "Wave Forces on Unburied Pipelines," Journal of Hydraulic Research, 18 No. 3, pp 197-211.

Ells, J.W., (1975), "Scours and Spanning Threaten Sea Lines," Oil and Gas Journal, Vol. 73, No. 27, July 7, pp 67-71.

Eshbach, O.W., (1974), Handbook of Engineering Fundamentals, Third ed., John Wiley & Sons, New York, p. 480.

Fredsoe, J., (1979), "Natural Backfilling of Pipeline Trenches," Journal of Petroleum Technology, Oct, pp 1223-1230.

Garrison, C.J., (1972), "Added Mass of a Circular Cylinder in Contact with a Rigid Boundary," Journal of Hydronautics, Vol. 6, No. 1, Jan., pp 59-60.

Goodman, T.R., (1973), "Comment on 'Aided Mass of a Circular Cylinder in Contact with a Rigid Boundary," Journal of Hydronautics, Vol. 7, No. 2, April, p. 96.

Grace, R.A., (1978), Marine Outfall Systems, Planning, Design and Construction, Prentice-Hall, Inc., New Jersey, pp 386-400.

Grace, R.A., Castiel, J., Shak, A.T., and Zee, G., (1979) , "Hawaii Ocean Test Pipe Project: Force Coefficients," Proceeding of the Specialty Conference, Civil Engineering in the Oceans, Vol. 1, pp 99-110.

Gravesen, H. and Nielson, R., (1981), "Some Environmental Design Aspects of Marine Pipelines for Danish North Sea Service," Offshore Oil and Gas Pipeline Technology, 1981, European Seminar, London, February.

Hildebrand, F.B., (1965), "Calculus of Variations and Applications," Methods of Applied Mathematics, Prentice Hall Inc., Englewood Cliffs, NH, pp 119-144.

Herbich, J.B., (1981), "Forces on Offshore Pipelines," Offshore Pipeline Design Elements, Marcel Dekker, Inc., New York, NY, pp 141-179.

Horikawa, K., (1978), Coastal Engineering, An Introduction to Ocean Engineering, John Wiley & Sons, New York, pp 9-18, 105-108.

Huang, M.C. and Hudspeth, R.T., (1982), "Stability of Pipelines Under Shoaling Finite Amplitude Waves," Journal of the Waterway, Port, Coastal and Ocean Division, ASCE, Vol. 108, No. WW2, May, pp 125-145.

Hudspeth, R.T., (1971), "Determination of the Limiting Depth for the Stabilization of Submarine Pipeline," Proceedings Eighth U.S. Navy Symposium on Military Oceanography, Vol. 1, Naval Postgraduate School, Monterey, CA, pp 78-88.

Hudspeth, R.T., and Slotta, L.S., (1978), "Linear and Non-linear Wave Action Estimates," Journal of the Engineering Mechanics Division, ASCE, Vol. 104, No. EM2, April, pp 319-334.

Ippen, A.T., Editor, (1966), Estuary and Coastal Hyrodynamics, Engineering Society Monographs, McGraw-Hill, New York, pp 1-27, 162-166, and 257-263.

Jones, W.T., (1976), "On-Bottom Pipeline Stability in Steady Water Currents," Eight Annual Offshore Technology Conference, Houston, TX, OTC 2598, Vol. II, pp 763-787.

Karal, K., (1977), "Lateral Stability of Submarine Pipelines," Ninth Annual Offshore Technology Conference, Houston, TX, OTC 2967, Vol. IV, pp 71-78.

Karal, K., (1983), "Time Effects on Lateral Resistance to Pipeline Supported by Cohesive Soils," Proc. International Offshore Mechanics/Arctic Engineering Symposium, Energy-Sources Technology Conference and Exhibition, Houston, ASME.

Karal, K. and Halvorsen, S.A., (1982), "Dynamics of the Water-Pipeline-Soil Interaction," Trans. ASME, J. Energy Resources Technology, Vol. 104, December, pp 307-312.

Lambrakos, K.F., (1982), "Marine Pipeline Dynamic Response to Waves from Directional Wave Spectra," Ocean Engineering, Vol. 9, No. 4, pp 385-405.

Lyons, C.G., (1973), "Soil Resistance to Lateral Sliding of Marine Pipelines," Fifth Annual Offshore Technology Conference, Houston, TX, OTC 1876, Vol. II, pp 479-484.

Machemel, J.L., (1978), "Pipelines in the Coastal Ocean," Pipelines in Adverse Environments, Vol. 1, Proceedings of the ASCE Pipeline Division Specialty Conference, New Orleans, Louisiana, January 15-17, pp 205-221.

McGuire, W. and Gallagher, R.H., (1979), "Stiffness Analysis of Frames," Matrix Structural Analysis, John Wiley & Sons, New York, NY., pp 69-146.

Meek, J.L., (1971), "The Displacement Method of Analysis," and "Nonlinear Aspects of Structural Behavior," Matrix Structural Analysis, McGraw-Hill, New York, NY., pp 372-375 and pp 543-588.

Mei, C.C., (1978), "Numerical Methods in Water-Wave Diffraction and Radiation," Annual Review of Fluid Mechanics, Vol. 10, pp 393-416.

Nyman, K.J., (1982), "Soil Response Against the Horizontal-Vertical Motion of Pipes," ASCE Preprint 82-534, New Orleans, LA, October 25-29.

Ogilvie, T.F., (1963), "First and Second-Order Forces on a Cylinder Submerged Under a Free Surface," Journal of Fluid Mechanics, Vol. 16, Part 3, July, pp 451-472.

Penzien, J. and Tseng S., (1978), Numerical Methods in Offshore Engineering, John Wiley & Sons, New York, NY., pp 229-234.

Potynody, J.G., (1961), "Skin Friction Between Various Soils and Construction Materials," Geotechnique, Vol. 11, pp 339-353.

Sandor, B., (1978), Strength of Materials, Prentice Hall, Inc., New York, NY., pp 128-133.

Sarpkaya, T., (1975), "Forces on Cylinders and Spheres in a Sinusoidally Oscillating Fluid," Transactions of ASME, Journal of Applied Mechanics, Paper presented at Applied Mechanics Western Conference, University of Hawaii, Honolulu, March, pp 32-37.

Sarpkaya, T., (1977), "In-line and Transverse Forces on Cylinders in Oscillatory Flow at High Reynolds Numbers," Journal of Ship Research, Vol. 21, No. 4, Dec., pp 200-216.

Sarpkaya, T. and Isaacson, M., (1981), "Wave Theories," and "Random Waves and Wave Forces," Mechanics of Wave Forces on Offshore Structures, Van Nostrand Reinhold Co., New York, NY., pp 150-167 and pp 504-520.

Schiller, F.C., (1971), "Wave Forces on Submerged Horizontal Cylinder," Master's Thesis, Naval Postgraduate School, Monterey, CA, June.

Small, S.W., Tamburello, R.D., and Piaseckyj, P.J., (1972), "Submarine Pipeline Support by Marine Sediments," Journal of Petroleum Technology, Vol. 24, No. 3, March, pp 317-322.

Swanson, R.C. and Jones, W.T., (1982), "Mudslide Effects on Offshore Pipelines," Transportation Engineering Journal of ASCE, Vol. 108, No. TE6, November, pp 585-600.

Taylor, J.L.T., (1930), "Some Hydrodynamic Inertia Coefficients," Philosphical Magazine, Ser. 7, Vol. 9, pp 161-183.

Timoshenko, S.P. and Gere, J., (1972), Mechanics of Material, Van Nostrand Reinhold Co., New York, NY., pp 208-212,

Townsend, D.R., and Farley, D.W., (1973), "Design Criteria for Submarine Pipeline Crossings," Journal of the Hydraulics Division, ASCE, Vol. 99, No. HY10, Oct., pp 1659-1678.

Valent, P.J., (1979), "Coefficients of Friction Between Calcareous Sands and Some Building Materials, and Their Significance," Technical Note, No. N-1542, Civil Engineering Laboratory, Naval Construction Battalion Center, Port Hueneme, California, January, 25 p.

Wantland, G.M., O'Neill, M.W., Reese, L.C., and Kalajian, E.J., (1979), "Lateral Stability of Pipelines in Clay," Eleventh Annual Offshore Technology Conference, Houston, TX, OTC 3477, Vol. II, pp 1025-1034.

Wantland, G.M., O'Neill, M.W., Kalajian, E.H., and Reese, L.C., (1982), "Pipeline Lateral Stability in Soft Clay," Journal of Petroleum Technology, January, pp 217-220.

Wehausen, J.W., and Laitone, E.V., (1960), Surface Waves, Encyclopedia of Physics, Springer-Verlag, Vol. 9, pp 469-501.

Wright, J.C., (1976), "Wave Forces on a Horizontal Circular Cylinder Near a Plane Boundary," Master's Thesis, Oregon State University, Corvallis, OR, June, 180 p.

Yamamoto, T., Nath, J., and Slotta, L., (1973), "Yet Another Report on Cylinder Drag or Wave Forces on Horizontal Submerged Cylinders," Engineering Experiment Station Bulletin, No. 47, Oregon State University, Corvallis, OR, April, 139 p.

Zimmerman, M.E., (1982), BASIC Computer Program "LDEFL", Large Deflection Static Analysis Algorithm, Oregon State University, Corvallis, OR.

Appendix

Appendix A

Description of Computer Algorithm AGAPIP

AGAPIP is a finite element analysis program designed as one module in a suite of a three program package which has been developed to predict the nonlinear dynamic response of a bottom-layed deep ocean pipeline to wave- and current-induced hydrodynamic pressures. General flow diagrams that illustrate how the three modulus (viz. AGSSIM, AGWSIM, and AGAPIP) are linked and that document the computational flow within AGAPIP have been presented in Section (2.4). Example problems have been used to numerically verify either AGAPIP or slightly modified versions of AGAPIP. Numerical comparisons from these examples were reported in Chapter 3.

Appendix A represents a users manual for the program AGAPIP. The documentation in this section consists of the following: 1) a brief users guide which includes detailed information on user-supplied data along with a sample data deck and the corresponding program output; 2) Table A.2 which supplies a variable list for AGAPIP and its major subroutines; 3) an alphabetical listing and brief description of all subroutines; and 4) Table A.3 which supplies Input/Output specification for each TAPE UNIT used by AGAPIP.

This appendix is not intended to be a substitute for a thorough understanding of the numerical methods utilized in the solution algorithm. Because much of the user-supplied input data for AGAPIP is discretionary (e.g. time step size or the FEM element

discretization), it is recommended that program users be familiar with the solution techniques described in Chapter 2. It is strongly suggested that the users carefully review their numerical results and perform some logic checks to ensure that their numerical values are consistent with sound engineering practice. Furthermore, because the CPU times for AGAPIP are significant, it is recommended that a careful review of all user-supplied data be made prior to executing the program in order to avoid unnecessary CPU expenditures.

AGAPIP USER'S GUIDE

A list of the user-supplied data necessary to analyze a pipeline response to stochastic, directional seas is given in Table A.1. Further information is available in Table A.3 which describes the Input/Output specifications required by AGAPIP for each TAPE UNIT utilized during program execution. AGAPIP has been designed to function as only one module in a suite of three modules and successful execution depends upon the supportive input data on TAPE 1, TAPE 2, and TAPE 12 which have been produced by the other program modules. Without these supportive data, successful execution of AGAPIP will not be possible.

The list of user-supplied data in Table A.1 is organized by typical 80 column card images. However, all user-supplied data for AGAPIP are format list directed. The COMMENTS for each 80 column card image in Table A.1 describe user options, default parameters, and special considerations or recommendations.

The physical description of the finite element model used for a simulation must be established with the coordinate systems defined by Fig. 2.1. All user-supplied input data, as well as the inputs from the other 2 program modules, MUST be given in consistent units (i.e., English or metric).

A sample data deck is illustrated in Fig. A.1. This deck provides the control data for a 30 sec. simulation of a random wave event. All data for the simulation are in English Units (viz. feet and pounds). Figure A.2 demonstrates the use of the generating options for nodal locations and the assignment of element parameters.

Table A.1. USER INPUTS

Card No.	Variable List	Comments
1	ETIM, ROEØ, GRAV, PRSS, STEP	Ending time for structural simulation; Fluid mass density; Gravitational constant (>0.0); Internal pipeline pressure; Time step for numerical integration.
2	VK, STRT, ALPHA, DELL	Fluid kinematic viscosity; Number of time substeps for the initial time step of each episode (>1); Newmark integration parameter α; Newmark integration parameter δ. Normally, α = .25; δ = .5. (default: ALPHA = .25, DELL = .5, if ALPHA = 0.0).
3	PINTVL	Number of discrete time steps between printed output (>1)
4	NNODES, NEPR, NMPR, RTOL, ETOL	Total number of pipeline nodes; Number of element property cards; Number of material property cards; Convergence tolerance for force imbalance; Convergence tolerance for energy imbalance. (default: ETOL = RTOL = .00001; if ETOL = RTOL = 0.0)
Repeat Card 5 NNODES Times or Until M = NNODES		
5	M, XR, (1,M), XR (2,M), XR (3,M)	Node number; X location; Y location; Z location (<0.0). First node input should be 1. Node numbers must increase each card. Node numbers which are skipped will be back generated with equal spacing. Original pipeline direction should have node numbers increasing in the positive X direction (see Figure 2.1 and Section 2.4.1b).

Table A.1. USER INPUTS (Continued)

Card No.	Variable List	Comments
Repeat Card 7 NEPR Times		
7 or (5 + NNODES)	EPR(J), EPR(J+1), EPR(J+2), EPR(J+3), EPR(J+4), EPR(J+5)	Steel pipe diameter; Steel wall thickness; Outer sleeve diameter; Drag coefficient; Lift coefficient; Inertial coefficient. Input of negative drag coefficient causes program to compute the drag coefficient as a function of Reynolds number. (default $C_D = C_L = 1.0$, $C_M = 2.0$; if $C_D = C_L = C_M = 0.0$) [J = 1 to G*NEPR]
Repeat Card 8 NMPR Times (REAL)		
8 or (5 + NNODES + NEPR)	MPR (J), MPR (J+1), MPR (J+2),	Young's modulus for steel section; Poisson's ratio for steel section; Mass density for steel section; Mass density MPR(J+3)for outer sleeve. [J = 1 to 4*NMPR]
Repeat Card 9 NNODES-1 Times or Until I = NNODES - 1		
9 or (9 + NNODES + NEPR + NMPR)	I, ICODE (1,I), ICODE (2,I)	Element number; Element property card number; Material property card number. Element numbers must increase with each input. Element numbers which are skipped will be assigned the element and material card numbers of the most recent (highest) element number.
10	(BRC(I), I=1,6)	Boundary restraint codes (BRC) for node 1 and node NNODES. I = 1 = axial diaplacement for node 1; I = 2 = lateral displacement for node 1; I = 3 = rotation for node 1; I = 4 = axial displacement for node NNODES; I = 5 = lateral displacement for node NNODES; I = 6 = rotation for node NNODES. Prescribed boundary restraint codes signify either a fixed or active degree of freedom at the pipeline terminals (of Chapter 2). FREE = 1.0; FIXED = 0.0. If either BRC (1) = 0.0 or BRC (4) = 0.0, the initial axial stress will be set to 0.0.

Table A.1. USER INPUTS (Continued)

Card No.	Variable List	Comments
11	(BSC(I), I=1,4)	Axial spring constant for node 1; lateral spring constant for node 1; rotational spring for node 1; pretension force in pipeline. Pretension load is treated as a constant initial stress throughout the entire pipeline.
12	(BSC(I), I=5,7)	Axial spring constant for node NNODES; lateral spring constant for node NNODES; rotational spring constant for NNODES.

Figure A.1 Sample data input for AGAPIP.

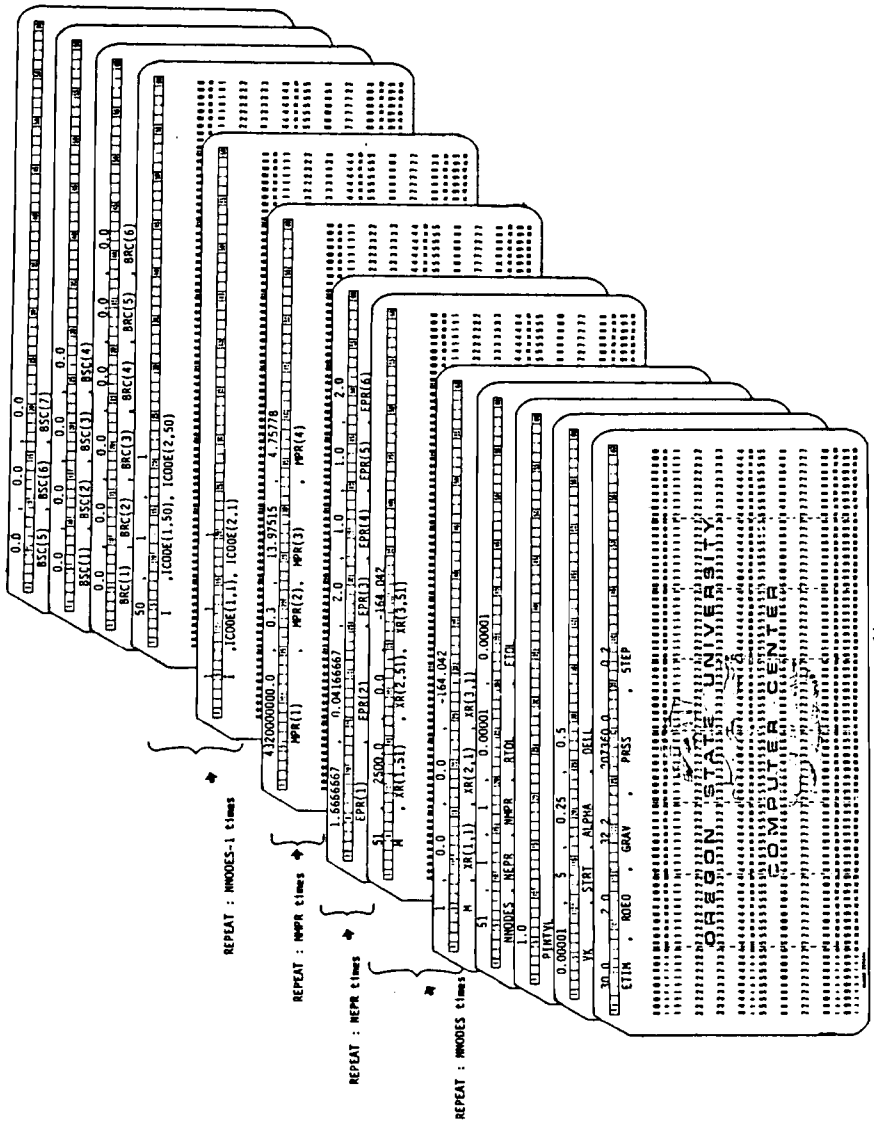

Figure A.2 Sample output for sample input deck in Fig. A.1.

```
          AA      GGGGG      AA      PPPPPP  IIIIII PPPPPP  EEEEEEEE
         AAAA    GGGGGG     AAAA     PP   PP   II   PP   PP EE
        AA  AA  GG         AA  AA    PP   PP   II   PP   PP EE
       AAAAAAAA GG   GGG  AAAAAAAA   PPPPPP    II   PPPPPP  EEEEEE
      AA    AA  GG   GG  AA    AA    PP        II   PP      EE
     AA      AA  GGG GGG AA      AA   PP        II   PP      EE
    AA        AA  GGGGGG AA      AA   PP      IIIIII PP      EEEEEEEE


    ANALYSIS PACKAGE FOR NONLINEAR RESPONSE OF BOTTOM-LAID DEEP-OCEAN
    PIPELINE SYSTEMS SUBJECT TO HYDROELASTIC LOADS FROM A RANDOM WAVE
    ENVIRONMENT.


 SIMULATION CONTROL INFORMATION:

  DATE: 83/07/18.

  SIMULATION DURATION  =    30.0000
   TIME STEP SELECTED  =      .2000
  INTEGRATION CONSTANTS:
              ALPHA    =      .2500
               DELL    =      .5000
   INTERNAL PRESSURE   =   207360.0
  GRAVITATIONAL CONSTANT=   32.2000
   PEAK WAVE FREQUENCY  =      .1000
  FLUID MASS DENSITY    =     2.0000
   FLUID KINEMATIC VISCOSITY=  .100000E-04
  NUMBER OF SUB STEPS FOR INITIAL TIME STEP=     5.0000


   PRINT CONTROL INFORMATION:

 PRINT INTERVAL= 1.00


   STRUCTURAL CONTROL INFORMATION:
  NUMBER OF NODES=   51
   NUMBER OF ELEMENT PROPERTY SECTIONS=     1
  NUMBER OF MATERIAL PROPERTY SECTIONS=     1
   FORCE TOLERANCE FOR CONVERGENCE= .1000E-04
  ENERGY TOLERANCE FOR CONVERGENCE= .1000E-04
```

Figure A.2 Sample output data for sample input deck (continued).

GENERATED NODAL DATA FOR PIPELINE

NODE NUMBER	NODAL POINT COORDINATES		
	X	Y	Z
1	0.000	0.000	-164.042
2	50.000	0.000	-164.042
3	100.000	0.000	-164.042
4	150.000	0.000	-164.042
5	200.000	0.000	-164.042
6	250.000	0.000	-164.042
7	300.000	0.000	-164.042
8	350.000	0.000	-164.042
9	400.000	0.000	-164.042
10	450.000	0.000	-164.042
11	500.000	0.000	-164.042
12	550.000	0.000	-164.042
13	600.000	0.000	-164.042
14	650.000	0.000	-164.042
15	700.000	0.000	-164.042
16	750.000	0.000	-164.042
17	800.000	0.000	-154.042
18	850.000	0.000	-164.042
19	900.000	0.000	-164.042
20	950.000	0.000	-164.042
21	1000.000	0.000	-164.042
22	1050.000	0.000	-164.042
23	1100.000	0.000	-164.042
24	1150.000	0.000	-164.042
25	1200.000	0.000	-164.042
26	1250.000	0.000	-164.042
27	1300.000	0.000	-164.042
28	1350.000	0.000	-164.042
29	1400.000	0.000	-164.042
30	1450.000	0.000	-164.042
31	1500.000	0.000	-164.042
32	1550.000	0.000	-164.042
33	1600.000	0.000	-164.042
34	1650.000	0.000	-164.042
35	1700.000	0.000	-164.042
36	1750.000	0.000	-164.042
37	1800.000	0.000	-164.042
38	1850.000	0.000	-164.042
39	1900.000	0.000	-164.042
40	1950.000	0.000	-164.042
41	2000.000	0.000	-164.042
42	2050.000	0.000	-164.042
43	2100.000	0.000	-164.042
44	2150.000	0.000	-164.042
45	2200.000	0.000	-164.042
46	2250.000	0.000	-164.042
47	2300.000	0.000	-164.042
48	2350.000	0.000	-164.042
49	2400.000	0.000	-164.042
50	2450.000	0.000	-164.042
51	2500.000	0.000	-164.042

Figure A.2 Sample Output data for sample input deck (continued).

3/D PIPE ELEMENTS

ELEMENT PROPERTIES

SECTION NUMBER	OUTER STRUCTURAL DIAMETER	STRUCTURAL WALL THICKNESS	TOTAL PIPE SECTION DIAMETER	DRAG COEFFICIENT	LIFT COEFFICIENT	INERTIAL COEFFICIENT
1	1.66667	.04167	2.00000	1.0000	1.0000	2.0000

MATERIAL PROPERTIES:

SECTION NUMBER	ELASTIC MODULUS	POISSONS RATIO	STRUCTURAL MASS DENSITY	OUTER SLEVE MASS DENSITY
1	.4320E+10	.3000	13.97516	4.75778

Figure A.2 Sample output data for sample input deck (continued).

GENERATED ALLOCATION OF MEMBER PROPERTIES:

ELEMENT NUMBER	GEOMETRIC SECTION	MATERIAL SECTION
1	1	1
2	1	1
3	1	1
4	1	1
5	1	1
6	1	1
7	1	1
8	1	1
9	1	1
10	1	1
11	1	1
12	1	1
13	1	1
14	1	1
15	1	1
16	1	1
17	1	1
18	1	1
19	1	1
20	1	1
21	1	1
22	1	1
23	1	1
24	1	1
25	1	1
26	1	1
27	1	1
28	1	1
29	1	1
30	1	1
31	1	1
32	1	1
33	1	1
34	1	1
35	1	1
36	1	1
37	1	1
38	1	1
39	1	1
40	1	1
41	1	1
42	1	1
43	1	1
44	1	1
45	1	1
46	1	1
47	1	1
48	1	1
49	1	1
50	1	1

Figure A.2 Sample output for sample input deck (continued)

PIPE TERMINAL SPECIFICATIONS

END CONSTRAINTS (0=FIXED,1=FREE)

	TANGENTIAL DISPLACEMENT	NORMAL DISPLACEMENT	BINORMAL ROTATION
BEGINNING:	0.	0.	0.
END:	0.	0.	0.

TERMINAL STIFFNESSES AND PRETENSION:

	TANGENTIAL STIFFNESS	NORMAL STIFFNESS	BINORMAL STIFFNESS	PRETENSION
BEGINNING:	0.	0.	0.	0.
END:	0.	0.	0.	

Figure A.2 Sample output for sample input deck (continued).

GRID CONTROL INFORMATION:
PLAN LOCATION OF GRID ORIGIN:

X LOCATION= -32.8
Y LOCATION= -131.
SPACING OF GRID POINTS = 65.6

GRID DATA

GRID NUMBER	X LOCATION	Y LOCATION	Z LOCATION	COHESION	BOUYANT WEIGHT OR AXIAL FACTOR	STRESS FACTOR OR LATERAL FACTOR	BEARING CAPACITY FACTOR
1, 1	-32.81	-131.2	-164.0	40.00	21.00	2.500	5.140
2, 1	32.81	-131.2	-164.0	40.00	21.00	2.500	5.140
3, 1	98.43	-131.2	-164.0	40.00	21.00	2.500	5.140
4, 1	164.0	-131.2	-164.0	40.00	21.00	2.500	5.140
5, 1	229.7	-131.2	-164.0	40.00	21.00	2.500	5.140
6, 1	295.3	-131.2	-164.0	40.00	21.00	2.500	5.140
7, 1	360.9	-131.2	-164.0	40.00	21.00	2.500	5.140
8, 1	426.5	-131.2	-164.0	40.00	21.00	2.500	5.140
9, 1	492.1	-131.2	-164.0	40.00	21.00	2.500	5.140
10, 1	557.7	-131.2	-164.0	40.00	21.00	2.500	5.140

(OUTPUT EDITED)

54, 5	3445.	131.3	-164.0	40.00	21.00	2.500	5.140
55, 5	3510.	131.3	-164.0	40.00	21.00	2.500	5.140
56, 5	3576.	131.3	-164.0	40.00	21.00	2.500	5.140
57, 5	3642.	131.3	-164.0	40.00	21.00	2.500	5.140
58, 5	3707.	131.3	-164.0	40.00	21.00	2.500	5.140
59, 5	3773.	131.3	-164.0	40.00	21.00	2.500	5.140
60, 5	3839.	131.3	-164.0	40.00	21.00	2.500	5.140
61, 5	3904.	131.3	-164.0	40.00	21.00	2.500	5.140
62, 5	3970.	131.3	-164.0	40.00	21.00	2.500	5.140
63, 5	4035.	131.3	-164.0	40.00	21.00	2.500	5.140
64, 5	4101.	131.3	-164.0	40.00	21.00	2.500	5.140

Figure A.2 Sample output for sample input deck (continued).

SOLUTION OUTPUT: (OUTPUT FOR FIRST TWO TIME INCREMENTS ONLY)
TIME= .200
ITERATION EFFORT= 3

DISPLACEMENTS

NODE NUMBER	X	Y	Z	XX	YY	ZZ
1	0.	0.	0.	0.	0.	0.
2	-.8882E-12	-.3557E-05	0.	0.	0.	.4004E-07
3	-.3553E-12	-.2565E-05	0.	0.	0.	.2085E-07
4	-.1421E-11	-.2608E-05	0.	0.	0.	.8233E-08
5	.1421E-11	-.2732E-05	0.	0.	0.	.2832E-08
6	-.1421E-11	-.2742E-05	0.	0.	0.	-.6852E-09
7	.2842E-11	-.2733E-05	0.	0.	0.	.3221E-09
8	.4263E-11	-.2728E-05	0.	0.	0.	.5394E-10
9	0.	-.2723E-05	0.	0.	0.	.1215E-09
10	-.2842E-11	-.2717E-05	0.	0.	0.	.1052E-09
11	-.2842E-11	-.2712E-05	0.	0.	0.	.1090E-09
12	0.	-.2707E-05	0.	0.	0.	.1082E-09
13	.2842E-11	-.2701E-05	0.	0.	0.	.1084E-09
14	-.2842E-11	-.2696E-05	0.	0.	0.	.1084E-09
15	0.	-.2690E-05	0.	0.	0.	.1084E-09
16	-.5684E-11	-.2685E-05	0.	0.	0.	.1084E-09
17	0.	-.2680E-05	0.	0.	0.	.1084E-09
18	-.1137E-10	-.2674E-05	0.	0.	0.	.1084E-09
19	-.5684E-11	-.2669E-05	0.	0.	0.	.1085E-09
20	-.5684E-11	-.2663E-05	0.	0.	0.	.1085E-09
21	-.5684E-11	-.2658E-05	0.	0.	0.	.1085E-09
22	-.1137E-10	-.2652E-05	0.	0.	0.	.1085E-09
23	0.	-.2647E-05	0.	0.	0.	.1085E-09
24	0.	-.2642E-05	0.	0.	0.	.1085E-09
25	0.	-.2636E-05	0.	0.	0.	.1085E-09
26	.5684E-11	-.2631E-05	0.	0.	0.	.1089E-09
27	.5684E-11	-.2625E-05	0.	0.	0.	.1071E-09
28	0.	-.2620E-05	0.	0.	0.	-.1144E-09
29	.5684E-11	-.2614E-05	0.	0.	0.	.8693E-10
30	0.	-.2609E-05	0.	0.	0.	.1837E-09
31	.5684E-11	-.2602E-05	0.	0.	0.	-.1248E-09
32	.5684E-11	-.2605E-05	0.	0.	0.	.7886E-09
33	0.	-.2573E-05	0.	0.	0.	-.1257E-08
34	-.4547E-10	-.2701E-05	0.	0.	0.	-.1236E-08
35	-.2274E-10	-.2667E-05	0.	0.	0.	.7416E-09
36	-.2274E-10	-.2669E-05	0.	0.	0.	-.9745E-10
37	0.	-.2660E-05	0.	0.	0.	.2134E-09
38	0.	-.2654E-05	0.	0.	0.	.1159E-09
39	0.	-.2647E-05	0.	0.	0.	.1436E-09
40	-.1137E-10	-.2640E-05	0.	0.	0.	.1364E-09
41	-.1137E-10	-.2633E-05	0.	0.	0.	.1375E-09
42	-.1137E-10	-.2626E-05	0.	0.	0.	.1406E-09
43	-.1137E-10	-.2619E-05	0.	0.	0.	.1256E-09
44	-.1137E-10	-.2612E-05	0.	0.	0.	.1882E-09
45	-.1137E-10	-.2605E-05	0.	0.	0.	-.6032E-10
46	-.2274E-10	-.2601E-05	0.	0.	0.	.6738E-09
47	-.3411E-10	-.2580E-05	0.	0.	0.	-.2386E-08
48	-.2274E-10	-.2639E-05	0.	0.	0.	.7869E-08
49	-.4547E-10	-.2346E-05	0.	0.	0.	-.1910E-07
50	-.7956E-10	-.3338E-05	0.	0.	0.	.3741E-07
51	0.	0.	0.	0.	0.	0.

Figure A.2 Sample output for sample input deck (continued).

ELEMENT FORCES

ELEMENT NUMBER	AXIAL FORCE	TORSION I	TORSION J	MOMENT I NORMAL	MOMENT J NORMAL	MOMENT I BINORMAL	MOMENT J BINORMAL
1	.419E+06	0.	0.	0.	0.	.228E+01	.165E+01
2	.419E+06	0.	0.	0.	0.	-.165E+01	-.703E+00
3	.419E+06	0.	0.	0.	0.	.703E+00	.249E+00
4	.419E+06	0.	0.	0.	0.	-.249E+00	-.763E-01
5	.419E+06	0.	0.	0.	0.	.762E-01	.213E-01
6	.419E+06	0.	0.	0.	0.	-.213E-01	-.558E-02
7	.419E+06	0.	0.	0.	0.	.557E-02	.138E-02
8	.419E+06	0.	0.	0.	0.	-.140E-02	-.339E-03
9	.419E+06	0.	0.	0.	0.	.323E-03	.686E-04
10	.419E+06	0.	0.	0.	0.	-.845E-04	-.250E-04
11	.419E+06	0.	0.	0.	0.	.904E-05	-.411E-05
12	.419E+06	0.	0.	0.	0.	-.118E-04	-.861E-05
13	.419E+06	0.	0.	0.	0.	-.725E-05	-.764E-05
14	.419E+06	0.	0.	0.	0.	-.818E-05	-.782E-05
15	.419E+06	0.	0.	0.	0.	-.797E-05	-.777E-05
16	.419E+06	0.	0.	0.	0.	-.799E-05	-.776E-05
17	.419E+06	0.	0.	0.	0.	-.797E-05	-.774E-05
18	.419E+06	0.	0.	0.	0.	-.795E-05	-.772E-05
19	.419E+06	0.	0.	0.	0.	-.794E-05	-.770E-05
20	.419E+06	0.	0.	0.	0.	-.792E-05	-.769E-05
21	.419E+06	0.	0.	0.	0.	-.790E-05	-.765E-05
22	.419E+06	0.	0.	0.	0.	-.791E-05	-.775E-05
23	.419E+06	0.	0.	0.	0.	-.777E-05	-.718E-05
24	.419E+06	0.	0.	0.	0.	-.831E-05	-.967E-05
25	.419E+06	0.	0.	0.	0.	-.578E-05	.131E-05
26	.419E+06	0.	0.	0.	0.	-.167E-04	-.454E-04
27	.419E+06	0.	0.	0.	0.	.297E-04	.143E-03
28	.419E+06	0.	0.	0.	0.	-.159E-03	-.588E-03
29	.419E+06	0.	0.	0.	0.	.573E-03	.206E-02
30	.419E+06	0.	0.	0.	0.	-.210E-02	-.692E-02
31	.419E+06	0.	0.	0.	0.	.690E-02	.199E-01
32	.419E+06	0.	0.	0.	0.	-.199E-01	-.507E-01
33	.419E+06	0.	0.	0.	0.	.506E-01	.510E-01
34	.419E+06	0.	0.	0.	0.	-.510E-01	-.201E-01
35	.419E+06	0.	0.	0.	0.	.201E-01	.696E-02
36	.419E+06	0.	0.	0.	0.	-.697E-02	-.212E-02
37	.419E+06	0.	0.	0.	0.	.210E-02	.578E-03
38	.419E+06	0.	0.	0.	0.	-.593E-03	-.161E-03
39	.419E+06	0.	0.	0.	0.	.146E-03	.336E-04
40	.419E+06	0.	0.	0.	0.	-.489E-04	-.324E-04
41	.419E+06	0.	0.	0.	0.	.173E-04	.651E-04
42	.419E+06	0.	0.	0.	0.	-.804E-04	-.314E-03
43	.419E+06	0.	0.	0.	0.	.300E-03	.128E-02
44	.419E+06	0.	0.	0.	0.	-.129E-02	-.517E-02
45	.419E+06	0.	0.	0.	0.	.516E-02	.197E-01
46	.419E+06	0.	0.	0.	0.	-.198E-01	-.707E-01
47	.419E+06	0.	0.	0.	0.	.707E-01	.231E+00
48	.419E+06	0.	0.	0.	0.	-.231E+00	-.652E+00
49	.419E+06	0.	0.	0.	0.	.652E+00	.153E+01
50	.419E+06	0.	0.	0.	0.	-.153E+01	-.212E+01

Figure A.2 Sample output for sample input deck (continued).

SOLUTION OUTPUT:
TIME= .400
ITERATION EFFORT= 7

DISPLACEMENTS

NODE NUMBER	X	Y	Z	XX	YY	ZZ
1	0.	0.	0.	0.	0.	0.
2	-.1421E-10	-.4285E-04	0.	0.	0.	-.6637E-06
3	-.1243E-10	-.4477E-04	0.	0.	0.	.1265E-06
4	-.1137E-10	-.4410E-04	0.	0.	0.	-.1874E-07
5	-.8527E-11	-.4414E-04	0.	0.	0.	.4622E-08
6	-.1279E-10	-.4403E-04	0.	0.	0.	.1494E-08
7	-.5684E-11	-.4395E-04	0.	0.	0.	.1734E-08
8	-.2842E-11	-.4386E-04	0.	0.	0.	.1776E-08
9	-.8527E-11	-.4377E-04	0.	0.	0.	.1748E-08
10	-.1137E-10	-.4368E-04	0.	0.	0.	.1758E-08
11	-.8527E-11	-.4359E-04	0.	0.	0.	.1755E-08
12	-.5684E-11	-.4351E-04	0.	0.	0.	.1756E-08
13	.2842E-11	-.4342E-04	0.	0.	0.	.1756E-08
14	-.2842E-11	-.4333E-04	0.	0.	0.	.1756E-08
15	.2842E-11	-.4324E-04	0.	0.	0.	.1757E-08
16	-.5684E-11	-.4315E-04	0.	0.	0.	.1757E-08
17	0.	-.4307E-04	0.	0.	0.	.1757E-08
18	-.5684E-11	-.4298E-04	0.	0.	0.	.1757E-08
19	-.1137E-10	-.4289E-04	0.	0.	0.	.1757E-08
20	0.	-.4280E-04	0.	0.	0.	.1757E-08
21	-.5684E-11	-.4271E-04	0.	0.	0.	.1758E-08
22	-.5684E-11	-.4263E-04	0.	0.	0.	.1758E-08
23	.5684E-11	-.4254E-04	0.	0.	0.	.1758E-08
24	.5684E-11	-.4245E-04	0.	0.	0.	.1758E-08
25	.5684E-11	-.4236E-04	0.	0.	0.	.1758E-08
26	0.	-.4227E-04	0.	0.	0.	.1756E-08
27	.1137E-10	-.4219E-04	0.	0.	0.	.1759E-08
28	0.	-.4210E-04	0.	0.	0.	.1756E-08
29	.1137E-10	-.4201E-04	0.	0.	0.	.1753E-08
30	.1137E-10	-.4192E-04	0.	0.	0.	.1833E-08
31	.1137E-10	-.4184E-04	0.	0.	0.	.1222E-08
32	.1705E-10	-.4173E-04	0.	0.	0.	.5052E-08
33	.5684E-11	-.4170E-04	0.	0.	0.	-.1568E-07
34	.5684E-10	-.4299E-04	0.	0.	0.	.1541E-07
35	-.3411E-10	-.4293E-04	0.	0.	0.	.5540E-08
36	-.3411E-10	-.4281E-04	0.	0.	0.	.1668E-08
37	0.	-.4270E-04	0.	0.	0.	.2286E-08
38	.1137E-10	-.4259E-04	0.	0.	0.	.2204E-08
39	.1137E-10	-.4248E-04	0.	0.	0.	.2210E-08
40	.1137E-10	-.4239E-04	0.	0.	0.	.2211E-08
41	-.1137E-10	-.4226E-04	0.	0.	0.	.2211E-08
42	-.2274E-10	-.4215E-04	0.	0.	0.	.2209E-08
43	-.1137E-10	-.4203E-04	0.	0.	0.	.2218E-08
44	-.1137E-10	-.4192E-04	0.	0.	0.	.2192E-08
45	-.2274E-10	-.4181E-04	0.	0.	0.	.2231E-08
46	-.2274E-10	-.4170E-04	0.	0.	0.	.2453E-08
47	-.3411E-10	-.4162E-04	0.	0.	0.	-.4460E-09
48	-.3411E-10	-.4138E-04	0.	0.	0.	.2120E-07
49	-.6821E-10	-.4132E-04	0.	0.	0.	-.1133E-06
50	-.1023E-09	-.3984E-04	0.	0.	0.	.8186E-06

Figure A.2 Sample output for sample input deck (continued).

ELEMENT FORCES

ELEMENT NUMBER	AXIAL FORCE	TORSION I	TORSION J	MOMENT I NORMAL	MOMENT J NORMAL	MOMENT I BINORMAL	MOMENT J BINORMAL
1	.419E+06	0.	0.	0.	0.	.254E+02	.150E+02
2	.419E+06	0.	0.	0.	0.	-.150E+02	-.268E+01
3	.419E+06	0.	0.	0.	0.	.269E+01	.418E+00
4	.419E+06	0.	0.	0.	0.	-.415E+00	-.499E-01
5	.419E+06	0.	0.	0.	0.	.527E-01	.381E-02
6	.419E+06	0.	0.	0.	0.	-.103E-02	.272E-02
7	.419E+06	0.	0.	0.	0.	.674E-04	.732E-03
8	.419E+06	0.	0.	0.	0.	.206E-02	.162E-02
9	.419E+06	0.	0.	0.	0.	.116E-02	.134E-02
10	.419E+06	0.	0.	0.	0.	.146E-02	.142E-02
11	.419E+06	0.	0.	0.	0.	.138E-02	.140E-02
12	.419E+06	0.	0.	0.	0.	.140E-02	.140E-02
13	.419E+06	0.	0.	0.	0.	.140E-02	.140E-02
14	.419E+06	0.	0.	0.	0.	.140E-02	.140E-02
15	.419E+06	0.	0.	0.	0.	.140E-02	.141E-02
16	.419E+06	0.	0.	0.	0.	.140E-02	.141E-02
17	.419E+06	0.	0.	0.	0.	.141E-02	.141E-02
18	.419E+06	0.	0.	0.	0.	.141E-02	.141E-02
19	.419E+06	0.	0.	0.	0.	.141E-02	.141E-02
20	.419E+06	0.	0.	0.	0.	.141E-02	.141E-02
21	.419E+06	0.	0.	0.	0.	.141E-02	.141E-02
22	.419E+06	0.	0.	0.	0.	.141E-02	.141E-02
23	.419E+06	0.	0.	0.	0.	.141E-02	.141E-02
24	.419E+06	0.	0.	0.	0.	.141E-02	.142E-02
25	.419E+06	0.	0.	0.	0.	.141E-02	.141E-02
26	.419E+06	0.	0.	0.	0.	.142E-02	.144E-02
27	.419E+06	0.	0.	0.	0.	.140E-02	.138E-02
28	.419E+06	0.	0.	0.	0.	.146E-02	.137E-02
29	.419E+06	0.	0.	0.	0.	.147E-02	.273E-02
30	.419E+06	0.	0.	0.	0.	.110E-03	-.943E-02
31	.419E+06	0.	0.	0.	0.	.123E-01	.721E-01
32	.419E+06	0.	0.	0.	0.	-.693E-01	-.393E+00
33	.419E+06	0.	0.	0.	0.	.396E+00	.400E+00
34	.419E+06	0.	0.	0.	0.	-.397E+00	-.701E-01
35	.419E+06	0.	0.	0.	0.	.729E-01	.124E-01
36	.419E+06	0.	0.	0.	0.	-.958E-02	.825E-04
37	.419E+06	0.	0.	0.	0.	.274E-02	.146E-02
38	.419E+06	0.	0.	0.	0.	.136E-02	.145E-02
39	.419E+06	0.	0.	0.	0.	.137E-02	.139E-02
40	.419E+06	0.	0.	0.	0.	.144E-02	.144E-02
41	.419E+06	0.	0.	0.	0.	.140E-02	.136E-02
42	.419E+06	0.	0.	0.	0.	.148E-02	.162E-02
43	.419E+06	0.	0.	0.	0.	.122E-02	.804E-03
44	.419E+06	0.	0.	0.	0.	.204E-02	.265E-02
45	.419E+06	0.	0.	0.	0.	.193E-03	.366E-02
46	.419E+06	0.	0.	0.	0.	-.842E-03	-.461E-01
47	.419E+06	0.	0.	0.	0.	.490E-01	.387E+00
48	.419E+06	0.	0.	0.	0.	-.384E+00	-.249E+01
49	.419E+06	0.	0.	0.	0.	.249E+01	.139E+02
50	.419E+06	0.	0.	0.	0.	-.139E+02	-.236E+02

SUBROUTINE DESCRIPTIONS

A brief description of the SUBROUTINES in the FORTRAN PROGRAM AGAPIP are given below. For reference purposes, the SUBROUTINES are listed in alphabetical order. Control to these SUBROUTINES is directed by the main PROGRAM AGAPIP as indicated in Fig. 2.13.

ACCEL. Directs the solution for the initial acceleration which the pipeline experiences as a result of a force imbalance at the beginning of an episode. The logic for this routine is similar to that of the SUBROUTINE DYPIPE; however, this subroutine computes accelerations rather than displacements. (called by: DYPIPE)

ASSMBL. Assembles the **nodal** stiffness contributions from individual elements into a banded upper diagonal tangent stiffness matrix for the pipeline. It includes the **prescribed** or **material** boundary conditions. (called by: ACCEL, DYPIPE)

BANNER. Echos a heading and simulation control information. (called by: AGAPIP)

BLUE. Provides a Best Linear Unbiased Estimate at the pipeline nodes of the grid point values for the fluid kinematics and soil properties. (called by SOIL, WAVFLD)

CDCALC. Computes a drag coefficient for an element which is a function of the average Reynolds during a given time step. This routine is only called if user-supplied drag coefficient is negative. (called by: WAVFRC, FLFRC)

CRSS. Computes the cross product of two vectors. (called by: DIRCOS)

DECOMP. Decomposes the pipeline tangent stiffness matrix and computes the pipeline incremental **nodal** displacements for the current load imbalance. This routine was taken from p. 42, R. Cook (1981). (called by: DYPIPE)

DEFRCE. Multiples **local** element deformations and nonzero components of current element stiffness to obtain **local** element forces. (called by: ACCEL, DYPIPE)

DIRCOS. Computes **local** element and **nodal** direction cosines. The **local** τ direction is directed between the i and j element nodes. The **nodal** τ is approximately the average of the adjacent **local** τ directions. The **nodal** $\hat{\beta}$ is obtained by crossing the **nodal** $\hat{\tau}$ unit vector and a vector in the plane of the ocean bottom. The **local** β unit is approximately the average of the adjacent **nodal** $\hat{\beta}$ vectors. Normal unit vectors are defined by the cross product of binormal and tangential vectors β and τ, or $\hat{\beta}$ and $\hat{\tau}$. (called by: DYPIPE)

DUMP. Outputs simulation solutions. (called by: DYPIPE)

DYPIPE. Directs evaluation of pipeline response during individual peak wave episodes. The Flow diagram for this routine appears in Figure 2.16. (called by: AGAPIP)

EXTEFF. Modifies the pipeline tangent stiffness matrix and load vector to account for optional boundary springs. (called by: ACCEL, DYPIPE)

FIX. Reads element constants and the element elastic stiffness matrix. (called by: DYPIPE)

FIXM. Reads element constants and the element elastic stiffness matrix and then substitutes the element mass and added mass matrix (lumped mass) in place of the elastic stiffness matrix. (called by: ACCEL)

FLFRC. Computes nonlinear fluid drag force; fluid inertial force; and structural (element) inertial force. It also modifies the element tangent stiffness matricies to include the effect of these loadings. All of the loads in this subroutine use a lumped force formulation. (called by: DYPIPE)

FSOLV. Decomposes the pipeline mass matrix and computes initial **nodal** accelerations from the initial force imbalance. Rotational accelerations are assumed to be zero. (called by: ACCEL)

GRIDIN. READs grid data provided by AGSSIM (see Figure 2.13) and echos this data. (called by: AGAPIP)

GSTIF. Adds geometric stiffness terms to the **local** element elastic stiffness matrix. (called by: DYPIPE)

INTCAL. Computes element constants and the **local** elastic stiffness matrix for each element and stores this information on TAPE 10. (called by: AGAPIP)

MATMLT. Multiples two ([6x6] or less) matricies and returns the results in a third matrix.

NEWACL. Transforms solution the vector of **modal** accelerations to **global** accelerations. (called by: ACCEL)

NEWMRK. Computes Newmark-beta integration constants for temporal integration. (called by: AGAPIP, DYPIPE)

NORMAL. Reduces a vector to a unit vector. (called by: DIRCOS)

OUT. Provides crude numerical data prior to aborting a simulation because of excessive iterative effort. (called by: DYPIPE)

RESOLV. Transforms the incremental solution vector of **modal** displacements to **global** displacements. It also updates the current total displacements and kinematics to reflect the computed incremental displacements. (called by: DYPIPE)

SDISP. Computes the **global** displacement and velocity (relative to the reference position at the beginning of an episode) of each end of an element. It is part of the sequence of subroutines which establish sediment resistive forces. (called by: ACCEL, DYPIPE)

SEARCH. Provides a reference grid point near a pipeline node to aide in establishing the **nodal** and **local** direction cosines. (called by: DIRCOS)

SIZER. Expands BLANK COMMON to the maximum core allocation required for FORTRAN IV execution of AGAPIP. FORTRAN V versions of AGAPIP must specify BLANK COMMON allocation immediately, therefore, when executing in FORTRAN V, core selection in SIZER should match the previous allocation required. (called by: AGAPIP)

SOIL. READs grid data provided by AGSSIM (see Figure 2.12) and assigns sediment properties to pipeline nodes. (called by: AGAPIP)

SOILSM. Computes sediment spring characteristics from sediment properties at pipeline nodes. Sediment spring characteristics are computed independently for cohesive and cohesionless sediment characteristics. (called by: AGAPIP)

SRFRC. Computes sediment resistive forces on an element in the original reference coordinate system established at the beginning of an episode (ie. the load vs. displacement function is relative to the reference position at the beginning of an episode). Sediment spring stiffness is modified, if necessary, to accelerate convergence. (called by: ACCEL, DYPIPE)

STRKIN. Reads and generates data necessary to describe the finite element model of the pipeline. (called by: AGAPIP)

TRNFEG. Constructs a [6x6] transformation matrix for **global** to **local** transformations. (called by: UPLGRN)

TRNFNG. Constructs a [3x6] transformation matrix for **global** to **nodal** transformations. (called by: ACCEL, DYPIPE)

TRNSEG. Constructs a [6x6] transformation matrix for **global** to the sediment reference **local** transformations. (called by ACCEL, DYPIPE)

TRNSP. Transposes a ([6x6] or less) matrix. (called by: ACCEL, DYPIPE)

UPLGRN. Computes **local** element deformations using an updated Lagrangian formulation. (called by: ACCEL, DYPIPE)

WAVFLD. READs fluid kinematics at grid points provided by AGWSIM (see Figure 2.13) and assigns fluid kinematics to pipeline node points. (called by: ACCEL, DYPIPE)

WAVFRC. Computes lumped fluid drag loads and lumped loads which result from the "**absolute**" component of the initial fluid force at the start of a wave episode. (called by: ACCEL)

XTEND. Provides an initial estimate for the position of the pipeline at the beginning of a time step which is based upon the kinematics at the previous time step. (called by: DYPIPE)

Table A.2. Partial Variable List for Main Portions of AGAPIP

Program/ Subroutine	Variables
AGAPIP	AØ, A1, A2, A3, A4, A5, A6, A7 = Newmark integration constants.
	ALPHA, DELL = Newmark parameters (α and δ).
	DT = FFT simulation time step.
	EP = Episode counter.
	ETIM = Simulation duration for structural response.
	ETMAX = Energy imbalance for first iteration of each time step.
	ETOL = Energy tolerance criteria for conver gence.
	GRAV = Gravitational constant (assumed to act in negative global Z direction).
	GS,GX,GY = Grid spacing; X location; and Y location of grid origin.
	ITER = Interation counter.
	NDOF = Number of degrees of freedom = number of equations.
	NEPR = Number of element property cards.
	NEVENT = Number of wave episodes.
	NMPR = Number of material property cards.
	NNODES = Number of pipeline nodes.-

Table A.2 (continued)

PINTVL = Number of simulation solution steps between printed output.

PKHZ = Peak wave frequency (hertz)

PRSS = Interal pipeline pressure (gauge)

RM = Nondimensionalizing mass scale.

AGAPIP (cont.) ROEØ = Fluid mass density.

RTMAX = Force imbalance at first iteration of a time step.

RTOL = Force imbalance criteria for convergence.

SL = Nondimensionalizing length scale.

STRT = Number of time substeps during first time step of an episode.

TØ, T1 = Beginning and ending time for an episode.

TIMB, TIMF = CPU (second) counters.

TYME = Current simulation time.

VK = Kinematic fluid viscosity.

SUBROUTINE BANNER refer to variable list for AGAPIP

SUBROUTINE STRKIN refer also to variable list for AGAPIP

XR (I,J) = Reference pipeline location

I: 1 = X location; 2 = Y location;

3 = Z location

4 = X rotation; 5 = Y rotation;

6 = Z rotation

Table A.2 (continued)

J: 1-NNODES = node number

BRC(I) = Boundary restraint codes (0 = Fixed; 1 = Free)

I: 1 = axial code for node 1

2 = lateral code for node 1

3 = rotational code for node 1

4 = axial code for node NNODES

5 = lateral code for node NNODES

6 = rotational code for node NNODES.

STRKIN (cont.) BSC(I) = Boundary spring constants and pretension.

I: 1 = axial spring constant at node 1

2 = lateral spring constant at node 1

3 = rotational spring constant at node 1

4 = pretension force

5 = axial spring constant at node NNODES

6 = lateral spring constant at node NNODES

7 = rotational spring constant at node NNODES

EPR(I) = Vector storage of element property card data.

MPR(I) = Vector storage of material property card data.

Table A.2 (continued)

ICODE(I,J) = Codes for assignment of element and material property cards to individual elements

I: 1 = element property card number

2 = material property card number

J: J = 1-(NNODES-1) = node number

WG(I,J,K) = Pipeline displacements and kinematics

I: 1 = X; 2 = Y; 3 = Z; 4 = X rotation; 5 = Y rotation; 6 = Z rotation

J: 1 - NNODES = node number

K: 1 = displacement

2 = velocity

3 = acceleration

SUBROUTINE GRIDIN

(refer also to variable list for AGAPIP)

NX, NY = number of grid points parallel to X and Y axes. (64 and 5)

SOILS (I,J,K) = sediment properties at grid points.

I: 1-64 = X grid number

J: 1-5 = Y grid number

K: 1 = cohesion of sediment (c) or $\emptyset$.

2 = effective sediment unit weight (γ_e) or axial friction coefficient (μ_1).

Table A.2 (continued)

3 = sediment stress factor (N_σ) or lateral friction coefficient (μ_2) .

4 = bearing capacity factor (N_c) or Ø.

ZG (I,J) = Z location of grid points.

I: 1-64 = X grid number.

J: 1-5 = Y grid number.

VPS (4,8) = statisical covariance estimation for the sediment properties for BLUE.

SUBROUTINE (refer also to variable list for AGAPIP and SUBROUTINE STRKIN)

INTCAL

E = Youngs modulus.

F = . Moment of inertia.

S = Element length.

D1 = cross-sectional diameter of load bearing pipe section.

D2 = diameter of outer sleeve.

EM = pipeline mass per unit length.

AS = cross-sectional area of load bearing pipe section.

P = initial axial load in element.

XØ, YØ, ZØ = X,Y,Z components of the element length in the original element position.

Table A.2 (continued)

CD, CL, CM = drag, lift, and inertial coefficients.

SKII (6,6), SKIJ (6,6), SKJJ (6,6) = upper left, upper right, and lower right submatrices which form the representation of the **local** elastic element stiffness matrix.

SUBROUTINE SOIL (refer also to the variable lists for AGAPIP, and SUBROUTINES GRIDIN and STRKIN).

SOILN (K,J) = sediment properties at pipeline nodes

K: 1 = cohesion (c) or $\emptyset$.

2 = effective sediment unit weight (γ_e) or axial friction coefficient (μ_1)

3 = sediment stress factor (N_σ) or lateral friction coefficient (μ_2).

4 = bearing capacity factor (N_c) or $\emptyset$.

J: 1-NNODES = pipeline node number

X(I,J) = current pipeline nodal location (description same as XR(I,J).

SUBROUTINE SOILSM (refer also to the variable lists for AGAPIP, and SUBROUTINES SOIL and INTCAL).

SOYL (I,J) = sediment spring characteristics at pipeline nodes

Table A.2 (continued)

I: 1 = Ø.Ø (cohesionless) or 1.Ø (cohesive).

2 = Lateral yield displacement.

3 = Lateral friction coefficient (cohesionless) or sediment capacity per unit length (cohesive).

4 = Axial yield displacement.

5 - Axial friction coefficient (cohesionless) or sediment capacity per unit length (cohesive).

J: 1-(NNODES - 1) = element number.

C = cohesion

WS = effective sediment unit weight (γ_e).

CN = bearing capacity factor (N_c).

QN = sediment stress factor (N_σ).

WP = effective pipeline weight per unit length.

D = settlement of pipe section into cohesive sediment.

DD = ratio of pipe settlement to pipe diameter.

FD = stress imbalance between pipe weight and supporting sediment.

TD = tangent to the stress imbalance function.

SUBROUTINE DYPIPE refer also to variable lists for AGAPIP and SUBROUTINES STRKIN, INTCAL, GRIDIN, and SOILSM.

Table A.2 (continued)

DYPIPE (cont.)

CSN (I,J,K) = **nodal** and **local** direction cosines for pipeline.

J: 1-NNODES = node or element number.

I: 1 = X direction.

2 = Y direction.

3 = Z direction.

K: 1 = **nodal** $\hat{\tau}$ direction.

2 = **nodal** $\hat{\eta}$ direction.

3 = **nodal** $\hat{\beta}$ direction.

4 = **local** τ direction.

5 = **local** η direction.

6 = **local** β direction.

SCSN (I,J,K) = **local** direction cosines for sediment reference for pipeline.

J: 1-NELEMS = element number

I: 1 = X direction.

2 = Y direction.

3 = Z direction.

K: 1 = **local** τ direction.

2 = **local** η direction.

3 = **local** β direction.

R (I) = RA (I) = force imbalance for each degree of freedom.

I: 1-NDOF

Table A.2 (continued)

DYPIPE (cont.)

TSTIF (I,J) = banded tangent stiffness matrix for entire pipeline.

I: 1-NDOF

J: 1-6 (semi band width)

OFFST (I,J) = hystersis references for sediment model.

I: 1 = axial reference for time step at the element i node.

2 = lateral reference for time step at the element i node.

3 = axial reference for time step at the element j node.

4 = lateral reference for time step at the element j node.

5 = axial reference for iteration at the element i node.

6 = lateral reference for iteration at the element i node.

7 = axial reference for iteration at the element j node.

8 = lateral reference for iteration at the element j node.

Table A.2 (continued)

DYPIPE (cont.)

9 = axial sediment spring constant for the previous iteration at the element i node.

10 = lateral sediment spring constant for the previous iteration at the element i node.

11 = axial sediment spring constant for the previous iteration at the element j node.

12 = lateral sediment spring constant for the previous iteration at the element j node.

J: 1-NELEMS = element number.

ELFRC (I,J) = local element forces.

I: 1-12 = components of generalized force corresponding to the six degrees of freedom at both the i and j nodes of an element

J: 1-NELEMS = element number

U (I) = an incremental correction in position for each degree of freedom.

I: 1-NDOF

UAV (I,J,K) = wave- and current-induced fluid acceleration or velocity at grid points.

Table A.2 (continued)

DYPIPE (cont.)

I: X grid point number (1-64)

J: Y grid point number (1-5)

K: 1 = X component

2 = Y component

UA (I,J) = wave- and current-induced fluid accelerations at pipeline **node** points.

I: 1 = X component.

2 = Y component.

3 = Z component.

J: 1-NNODES = node number.

UV (I,J) = wave- and current-induced fluid velocities at pipeline **node** points.

I: 1 = X component.

2 = Y component.

3 = Z component.

J: 1-NNODES = node number.

VPW (4,8) = statistical covariance estimates for the fluid kinematics

XS (I,J) = reference position of pipeline at the beginning of an episode.

I: 1 = X location.

2 = Y location.

3 = Z location.

J: 1-NNODES = node number.

Table A.2 (continued)

AA (6,6), AB (6,6), AC (6,6), AD (6,6), AE (6,6), AF (6,6), AG (6,6), AH (6,6), AI (6,6) = working space for creating, transforming and assembling tangent stiffness and load imbalance.

Table A.3. PROGRAM AGAPIP INPUT/OUTPUT SPECIFICATION BY UNIT

Unit	Routines	I/O Statement	Variables
1 (READ)	AGAPIP SUB. GRIDIN SUB. SOIL SUB. DYPIPE	READ (1) GS, GX, GY, DT, PKHZ, (ZG (I,1), I = 1,64), ((VPS, (I,J), I = 1,4), J = 1,8), ((VPW (I,J), I = 1,4), J = 1,8)	GS = Grid spacing GX = X location of grid origin GY = Y location of grid origin DT = FFT time increment PKHZ = Peak wave frequency (hertz) ZG(64,5) = Z location of grid points along X grid axis. VPS (4,8) = sediment covariance parameters. VPW (4,8) = fluid kinematic covariance parameters.
2 (READ)	SUB. SOIL	READ (2) (((SOILS (I,J,K), I = 1, 64), J = 1,5) K = 1,4)	SOILS (64, 5,4) = sediment characteristics of grid points I,J (X & Y grid point numbers) K = 1 = cohesion (c) or $\emptyset$. 2 = soil weight (γ_e) or axial friction coefficient (μ_1). 3 = sediment stress factor (N_σ) or lateral friction coefficient (μ_2). 4 = bearing capacity factor (N_c) or $\emptyset$.
3 (WRITE)	SUB. SOIL	WRITE (3) ((SOILN (K,N), K = 1,4), N = 1, NNODES)	SOILN (4, NNODES) = sediment properties at pipe nodes where K = 1,4 and corresponds with SOILS (I,J,K).
3 (READ)	SUB. SOILSM	READ (3) ((SOILN (K,N), K = 1,4) N = 1, NNODES)	

Table A.3. PROGRAM AGAPIP INPUT/OUTPUT SPECIFICATION BY UNIT (Continued)

Unit	Routines	I/O Statement	Variables
3 (WRITE)	SUB. SOILSM	WRITE (3) ((SOYL (M,N), M = 1,5), N = 1, NNODES-1)	SOYL (5,NNODES-1) = sediment spring characteristics N = element number; M = 1 = flag; 1 = cohesive; 0 = cohesionless 2 = lateral yield displacement 3 = lateral friction coefficient (cohesionless) or sediment capacity per unit length (cohesive) 4 = axial yield displacement 5 = axial friction coefficient (cohesionless) or sediment capacity per unit length (cohesive).
3 (READ)	SUB. DYPIPE	READ (3) ((SOYL (M, N) M, = 1,5), N = 1, NNODES-1)	
5 (READ)	AGAPIP	READ (5,*) ETIM, ROEØ, GRAV, PRSS, STEP READ (5,*) VK, STRT, ALPHA, DELL	ETIM = Simulation ending time. ROEØ = Fluid mass density. GRAV = Gravitational coustant. PRSS = Internal pipe pressure. STEP = Time step for simulation. VK = Fluid kinematic viscosity. STRT = Number of initial time substeps for first time increment. ALPHA, DELL = Newmark integration parameters. PINTVL = Number of solution steps between output. NNODES = Number of pipe nodes. NEPR = Number of element property types. NMPR = Number of material property types. RTOL = Force convergence tolerance. ETOL = Energy convergence tolerance.
	SUB. BANNER	READ (5,*) PINTVL	
	AGAPIP	READ (5,*) NNODES, NEPR, NMPR, RTOL, ETOL	

Table A.3. PROGRAM AGAPIP INPUT/OUTPUT SPECIFICATION BY UNIT (Continued)

Unit	Routines	I/O Statement	Variables
5 (READ) (Continued)			ICODE (2, NNODES-1) = Storage array which identifies element and material property selected for each element. ICODE (1,I) = element property number. ICODE (2,I) = material property number.
		READ (5,*) (BRC (I), I = 1,6)	BRC (6) = Boundary restraint codes (1 = free, Ø = fixed). BRC(I); I = 1-3; axial, lateral and rotational codes for node 1. I = 4-6; axial, lateral and rotational codes for node NNODES.
		READ (5,*) (BSC (I), I = 1,4)	BSC (7) = Boundary spring constants and pretension BSC (I); I = 1-3; axial, lateral and rotational springs at beginning of pipe. I = 4; pretension load I = 5-7; axial, lateral and rotational springs at end of pipe.
		READ (5,*) (BSC (I), I = 5,7)	
6 (WRITE)	SUB BANNER SUB STRKIN SUB GRIDIN SUB DUMP SUB DYPIPE SUB OUT	OUPUT FORMATED: Heading, Structural data, Grid data, Solution results, Computation effort, Aborted simulation data.	
7 (WRITE)	SUB STRKIN	WRITE (7) ((XR (I,J), I = 1,6),J=1, NNODES)	

Table A.3. PROGRAM AGAPIP INPUT/OUTPUT SPECIFICATION BY UNIT (Continued)

Unit	Routines	I/O Statement	Variables
7 (READ)	SUB DYPIPE	READ (7) ((XR (I,J), I = 1,6), J=1, NNODES)	
9 (WRITE)	SUB STRKIN	WRITE (9) ((XR (I,J), I = 1,6), J = 1, NNODES) WRITE (9) (BRC (I), I = 1,6) WRITE (9) (BSC (I), I = 1,7) WRITE (9) (EPR (I), I = 1, 6* NEPR) WRITE (9) (MPR (I), I = 1, 4* NMPR) WRITE (9) ((ICODE (I,J), I = 1,2), J = 1, NNODES-1)	
9 (READ)	SUB INTCAL	READ (9) ((XR (I,J), I = 1,6), J = 1, NNODES) READ (9) (BRC (I), I = 1,6) READ (9) (BSC (I), I = 1,7) READ (9) (EPR (I), I = 1, 6* NEPR) READ (9) (MPR (I), I = 1, 4* NMPR) READ (9) ((ICODE (I,J), I = 1,2), J=1, NNODES-1)	
	SUB DYPIPE	READ (9) ((X(I,J), I = 1,6), J=1, NNODES) READ (9) (BRC(I), I=1,6) READ (9) (BSC (I), I = 1,7)	X(6,NNODES) = Current pipeline location X(I,J); I = 1-6; J=1-NNODES; I = 1-3; X,Y,Z position I = 4-6; X,Y,Z rotation.
9 (WRITE)	SUB DYPIPE	WRITE (9) ((X(I,J), I=1,6), J=1, NNODES WRITE (9) (BRC (I), I = 1,6) WRITE (9) (BSC (I), I = 1,7)	
10 (WRITE)	SUB INTCAL	WRITE (10) E,F,S,D1,D2,EM,AS,P,XØ, YØ,ZØ,CD,CL,CM WRITE (10) ((SKII (K,J), K=1,6),	E = Youngs Modulus F = Moment of Inertia S = Element Length

Table A.3. PROGRAM AGAPIP INPUT/OUTPUT SPECIFICATION BY UNIT (Continued)

Unit	Routines	I/O Statement	Variables
		J=1,6), ((SKIJ (K,J),K=1,6),J=1,6) WRITE (10) ((SKJJ (K,J),K=1,6),J=1,6)	D1 = Diameter of load bearing pipe section D2 = Diameter of outer sleeve
10 (READ) (Continued)	SUB FIX	READ (10) E,F,S,D1,D2,EM,AS,P,XØ YØ, ZØ, GD., CL, CM	EM = Mass per unit length of pipe AS = Cross-sectional area supporting load P = Initial axial load
	SUB FIXM	READ (10) ((AA, (K,J), K=1,6), J=1,6) ((AB (K,J), K=1,6), 3=1,6) READ (10) ((AC (K,J), K=1,6), J=1,6)	XØ, YØ, ZØ = X,Y,Z components of element length in reference configuration CD,CL,CM = drag, lift, and inertial coefficients SKII (6,6) = AA (6,6) = upper left 1/4 of elastic stiffness matrix for element. SKJJ (6,6) = AB (6,6) = upper right 1/4 of elastic stiffness matrix for element SKIJ (6,6) = AC (6,6) = lower right 1/4 of elastic stiffness matrix for element
11 (WRITE)	SUB. STRKIN SUB. DYPIPE	WRITE (11) (((WG(I,J,K), I=1,6), J=1, NNODES), K=1,3)	WG (6, NNODES, 3) = Pipeline displacements and kinematics I = 1-6: I = 1-3; X,Y,Z translational components I = 4-6; X,Y,Z rotational components J = 1-NNODES: node number K = 1-3: K = 1; displacements K = 2; velocity K = 3; acceleration
11 (READ)	SUB. DYPIPE	READ (11) (((WG(I,J,K), I=1,6) J=1, NNODES), K=1,3)	

Table A.3. PROGRAM AGAPIP INPUT/OUTPUT SPECIFICATION BY UNIT (Continued)

Unit	Routines	I/O Statement	Variables
12 (READ)	AGAPIP	READ (12) NEVENT	NEVENT = Number of wave episodes
12 (READ)	AGAPIP	READ (12) TØ, T1	TØ = beginning time for an episode
12 (READ)	SUB WAVFLD	READ (12) (((UAV(I,J,K), I=1,64), J=1,5), K=1,2)	T1 = ending time for an episode UAV (64,5,2) = X and Y components of fluid acceleration or velocity at grid points. K = 1 = X K = 2 = Y